UNIVERSITY OF CALIFORNIA
RIVERSIDE

Regulation of the Mechanical Niche to Guide Human Pluripotent Stem Cell Behaviors

A Dissertation submitted in partial satisfaction
of the requirements for the degree of

Doctor of Philosophy

in

Bioengineering

by

Maricela Maldonado

August 2016

Dissertation Committee:
Dr. Jin Nam, Chairperson
Dr. Kaustabh Ghosh
Dr. Prue Talbot

The Dissertation of Maricela Maldonado is approved:

_____

_____

_____
Committee Chairperson

University of California, Riverside

ACKNOWLEDGEMENTS

I would like to acknowledge and thank my mentor and advisor, Dr. Jin Nam. His constant drive to excel and his motivation to succeed pushed me to my limits and significantly contributed to my accomplishments. I will forever cherish our weekly meetings and presentations which prepared me for those critical questions, forced me to look outside of the box and inspired me to broaden our research objectives, and aim high both personally and academically. I would also like to thank my committee members, Dr. Kaustabh Ghosh and Dr. Prue Talbot for their helpful advice and constructive criticism during my graduate studies. Additionally, I would like to thank my oral exam committee members Dr. Frances Sladek and Dr. Hideaki Tsutsui for their suggestions to improve my proposed graduate research.

Next, I would like to thank my colleagues Dr. Karen Low, Dr. Christopher B. Horner, and Dr. Gerardo Ico who always offered a helping hand and quickly became my friends in the Tissue Regenerative Engineering and mechanoTransduction Lab. I will miss our very badly organized lunch and dinner gatherings where half of the conversations always led to research. Additionally, I would like to thank my undergraduate student mentees, Lauren Y. Wong, Rebeccah J. Luu, Mark Perez, Michael E.P. Ramos, Justin Minck, Alex Ospina, and Danielle Myung, which contributed greatly to this project. Overall, I am truly grateful for all of the help and support from both graduate and undergraduate students who were an integral part of my success.

Chapters 2, 3, and 4 of this dissertation are a reprint of the material as it appears in: The effects of electrospun substrate-mediated cell colony morphology on the self-renewal of human induced pluripotent stem cells, *Biomaterials* (5/2015), Enhanced lineage-specific differentiation efficiency of human induced pluripotent stem cells by engineering colony dimensionality using electrospun scaffolds, *Advanced Healthcare Materials* (5/2016), and ROCK inhibitor primes human induced pluripotent stem cells to selectively differentiate towards mesendodermal lineage via epithelial-mesenchymal transition-like modulation, *Stem Cell Research* (8/2016), respectively. The co-author, Professor Jin Nam, listed in these publications directed and supervised the research which forms the basis for this dissertation.

The work included in this dissertation was supported, in part, by the National Science Foundation (NSF) Bridge to the Doctorate Fellowship, the NSF Graduate Research Fellowship Program (DGE-1326120), and start-up funds from the University of California Riverside to Dr. Jin Nam. The work was also supported by the UCR Stem Cell Core Facility, which is a CIRM funded shared facility.

DEDICATION

First and foremost I thank God for allowing me to take advantage of the opportunities brought my way, for giving me the drive to expand my horizons, and for continually blessing me. I would like to dedicate this work to my family and friends who gave me their full support and unconditional love throughout my graduate studies. Although I cannot name each and every one of you, due to space constraints, I hope each of you know that I will be forever grateful for your support. Although I missed many celebrations I do treasure the moments we shared and I know we will have many more opportunities to make great memories.

To my parents Marcelino and Hortencia Maldonado, I cannot thank you enough for all that you have sacrificed for our family. Padre, gracias por enseñarme el valor del trabajo duro. Madre, gracias por enseñarme a ser un mejor ser humano. Espero que estén orgullosos porque mis logros son sus logros y ustedes son la razón por la que estoy aquí el dia de hoy. Los amo hasta el infinito y más allá!

To my sisters Marilyn, Perla, Lorena, and my brother Marcelino Jr., thank you for your help and not letting me go crazy during my time as a graduate student. To my nieces, nephews, godsons and goddaughter I thank you for letting me be a part of your lives and I hope to encourage you to always follow your dreams just like I followed mine. To my aunts and role models Maria del Carmen Maldonado and Lucina Hernandez, desde que era una niña siempre las mire con admiración por que ustedes lograron sus objetivos

académicos y obtuvieron éxito incluso a través de dificultades. Ustedes me inspiraron a dedicar mi tiempo y esfuerzo para sobresalir académicamente y perseguir mis sueños.

Finally, I cannot express enough gratitude to the love of my life, my best friend, my husband Miguel Navarro. You have been there to celebrate with me at my highest point and you have been there to cheer me up during my lowest point. Your constant encouragement, your selfless love, and your humor have kept me from making irrational decisions and making it through all the way to the end. I love you and I believe the best is yet to come!

ABSTRACT OF THE DISSERTATION

Regulation of the Mechanical Niche to Guide Human Pluripotent Stem Cell Behaviors

by

Maricela Maldonado

Doctor of Philosophy, Graduate Program in Bioengineering
University of California, Riverside, August 2016
Dr. Jin Nam, Chairperson

The derivation of human induced pluripotent stem cells (IPSCs) has revolutionized the field of personalized medicine. With their ability to self-renew and differentiate to all cell types of the adult body, their therapeutic potential for multiple diseases is invaluable. Albeit their therapeutic potential is promising, they pose the risk of uncontrolled differentiation or tumorigenesis. Physical forces in the developing embryo have been shown to play a critical role in driving lineage commitment to regulate tissue morphogenesis. In this regard, the current work focused on examining the effects of the mechanical microenvironment, using electrospun scaffolds, on the cellular behaviors of human IPSCs. We examined the role of scaffold stiffness on the (1) self-renewal and (2) directed differentiation of IPSCs. Our findings demonstrate that the mechanical microenvironment contributes to the development of distinct IPSC colony morphology.

Under proliferation conditions, a two-dimensional (2D) colony morphology on stiff scaffolds enhances proliferation and minimizes spontaneous differentiation of IPSCs. In contrast, the development of three-dimensional (3D) colonies on soft scaffolds results in increased spontaneous differentiation towards ectodermal lineage. Additionally, the development of distinct colonies, directed differentiation to mesendodermal lineage is enhanced on stiff scaffolds while ectodermal differentiation is enhanced on soft scaffolds. Furthermore, we demonstrate that modulation of the RhoA signaling pathway by scaffold stiffness or using a ROCK inhibitor can prime IPSCs to differentiate towards a mesendodermal lineage. We further demonstrate that actin and E-cadherin/β-catenin clustering mediates structural pre-stresses imposed on the cells, which may delay activation of the Wnt signaling pathway, as a result of developing 3D colony morphologies. Finally, we demonstrate that modulation of the scaffold stiffness, at each developmental stage of differentiation towards three germ layer derivate cell phenotypes, can enhance the differentiation of IPSCs. Overall, these findings demonstrate that IPSCs are mechano-responsive and that the mechanical niche can be designed to modulate IPSC behaviors for the control of differentiation or to study developmental processes *in vitro*.

TABLE OF CONTENTS

LIST OF FIGURES

LIST OF TABLES

CHAPTER 1 – INTRODUCTION

1.1 – Development and the role of mechanical cues

Embryonic development is a carefully orchestrated process where cells undergo a series of changes governed through biochemical and physical cues to drive tissue morphogenesis [1]. Changes in the basement membrane, which mainly contains extracellular matrix (ECM) proteins laminin, collagen type IV and heparin sulfate proteoglycan, provide structural support within the inner cell mass and the basal side of the trophectoderm layer [2]. Pluripotent stem cells, from the inner cell mass of the developing blastocyst, undergo the process of gastrulation where three distinct germ layers (ectoderm, mesoderm, and endoderm) are formed to give rise to distinct tissues. In this regard, multiple animal models have been used to study early embryonic processes to better understand human development. The mechanical microenvironment due to cell-cell forces or cell-ECM interaction, play an important role during development into organized germ layers or tissues. For example, during drosophila gastrulation movements, the lateral and dorsal cells have stiff and soft mechanical properties which coincide with different cell phenotypes [3]. In a study by Krieg et al., gastrulation in zebrafish was coordinated by cell-cortex tension to direct progenitor cell sorting for germ-layer organization [4]. Such mechanical cues direct organized movements during development where cells shift from having many cell-cell contacts to relying more on the

cell-environment contacts. The regulation or convergence of the RhoA and other signaling pathways maintain cell integrity and cell-cell interaction during self-renewal and differentiation of cells. RhoA has also been demonstrated to play a key role in cell-basement interaction during gastrulation of chick embryos and the regulation of invagination during sea urchin gastrulation where cells undergo a process of epithelial-to-mesenchymal transition [5]. Taken together, these studies demonstrate the critical role of the mechanical microenvironment, through changes in cell-cell or cell-ECM contacts, to regulation cell behaviors during development.

1.1.1 – Embryonic stem cells

With their ability to generate any cell type of the adult body, the derivation of embryonic stem cells (ESCs) is one of the significant milestones for the treatment of a wide range of degenerative diseases, such as diabetes or osteoarthritis [6, 7]. Unlike adult stem cells, such as mesenchymal stem cells which are multipotent and have restricted differentiation potential, ESCs are pluripotent and can differentiate to any germ layer derivate phenotype and they do not undergo senescence during long-term culture *in vitro* [8]. Thus, the use of ESCs offers the advantage that they can be expanded to clinically-relevant cell numbers and given the appropriate culture conditions they will maintain pluripotency. A significant amount of research effort has been placed on defining the culture conditions to regulate the self-renewal and differentiation capacity of ESCs with

various biochemical cues to activate/deactivate specific signaling pathways [9]. Even though progress has been made, standard culture practices still use animal-derived products for their expansion, which hinders their therapeutic application [6]. Traditionally, mouse feeder layers or commercially-available cell-matrix membrane, derived from mouse carcinoma cells are used to maintain pluripotency of the cells. Although embryonic stem cells are a powerful tool to study development and disease processes, their derivation from the inner cell mass of the developing embryo raises multiple ethical concerns which limit their therapeutic potential [10, 11].

1.1.2 – Induced pluripotent stem cells

In 2007, the derivation of human induced pluripotent stem cells (IPSCs) from adult fibroblasts by defined factors revolutionized the field of personalized medicine and overcame the ethical concerns raised with the use of ESCs [12]. With the successful derivation and their ability to behave like ESCs, their therapeutic potential was promising. Since then, multiple somatic cell types have been reprogrammed to study development and diseased-states for patient-specific therapies and drug development. Ongoing research aims to improve the therapeutic potential of IPSCs by developing safe reprogramming techniques where the use of viruses is limited to minimize their genomic integration [13].

A major safety concern of both ESCs and IPSCs is their potential to form teratomas, or uncontrolled differentiation, when they are transplanted *in vivo* [14, 15]. One way to minimize their risk is of spontaneous differentiation is directed differentiation towards target cell phenotypes. Both biochemical and physical factors are being investigated to with the aim to control cellular behavior and govern cell fate [16]. Although significant advances have been made in the development of differentiation protocols to guide the cells towards specific lineages following developmental principles, many protocols are ineffective, relying only on biochemical cues [17, 18]. In this regard, the research objectives of this work aimed to examine the contributions of the mechanical microenvironment on the control of IPSC behavior to regulate self-renewal and directed differentiation.

1.1.3 – Current challenges

Although animals undergo similar processes/movements during development, inherent differences in species make it difficult to directly translate the results for humans [19, 20]. Since ESCs were first derived from mouse, a vast majority of developmental studies are available although there are many key differences between mouse and human ESCs and developmental processes [21]. For example, to maintain pluripotency Activin/Nodal/FGF signaling are necessary while LIF is required for mouse ESCs [22]. Additionally, when cells are dissociated into single cells, human PSCs undergo apoptosis,

likely due to overactivation of the RhoA signaling pathway. In this regard, mouse ESCs can survive as single cells and unlike human PSCs they also form dome-like colony morphologies while human cells exhibit a more epithelial-like behavior. The field of bioengineering and material science has made it possible for researchers to mimic natural ECM for the study of cellular behaviors in 3D as opposed to standard culture practices on rigid tissue culture plastic. Our studies demonstrate that the development of both 2D and 3D platforms can be used to study adult and pluripotent stem cells. With the development of novel, reproducible synthetic substrates, the IPSC and ESC microenvironments can be modulated to examine cellular behaviors in response to physical changes such as substrate stiffness, as explored in the current work.

1.2 – Electrospun scaffolds for pluripotent stem cell culture

1.2.1 – Electrospun scaffolds for pluripotent stem cell culture

In 2007, the derivation of human cell behaviors for a wide range of cell types, including pluripotent stem cells [23-26]. Key studies highlighted here offer insight into the use of synthetic fibrous substrates for pluripotent stem cell culture. Using a wide variety of synthetic polymers, electrospinning can be used to create fibers in the micrometer range to allow for studies of three-dimensional infiltration of cells. Alternatively, scaffolds with a fiber diameter in the nanometer range can be utilized to study stem cell culture in

two-dimensions while cells perceive a degree of three-dimensionality not available with the use of standard tissue culture plates. Although much research remains to be investigated in the effects of electrospun scaffolds on embryonic/pluripotent stem cell functions, some studies have already explored the feasibility of using electrospun scaffolds to support long-term culture or aid in the differentiation process. For example, in some cases the cells have been cultured to examine the effects of self-renewal under proliferation conditions where one polymer substrate can be used to expand mouse ESCs. Alternatively, electrospun scaffolds have been used to examine the effects of surface topography on the induction of differentiation using the traditionally used embryoid body (EB) method.

One distinctive feature of electrospun fibers is their inherent increase in surface area as compared to traditionally used tissue culture plastic flat substrates. The fibrous nature of electrospun scaffolds allows the cells to sense a more 3D microenvironment with a wide variety of cell attachment sites depending on the fiber morphology (i.e. microfibers, nanofibers, or ribbon-morphology). Topographical cues, such as the use of aligned and randomly oriented fibers guide human ESC differentiation towards neuronal lineages [27]. In a study by Mohtaram et al. the changes in surface topography using polycaprolactone (PCL) scaffolds with a smaller diameter loop mesh resulted in higher expression of neuronal differentiation markers [28]. In this regard, the smaller diameter loop meshed allowed for more cell adhesion sites and promoted axon elongation. A

comparative study also demonstrated that electrospun PCL nanofibrous scaffolds supported cell attachment and proliferation, but proliferation was inhibited on the solution-cast PCL film, further demonstrating the significant effects of topographical cues on IPSC behavior [29].

The versatility of the electrospinning technique further allows the functionalization of the fibers to examine the effects of surface chemistry on stem cell behavior [30]. For example, PCL nanofibers can be functionalized with retinoic acid to induce neuronal differentiation [28]. As compared to control scaffolds, ESCs culture on retinoic acid-PCL scaffolds had a significantly higher upregulation of neuronal markers and had more neuronal-like morphologies. Composite electrospun nanofibrous scaffolds composed of poly(d,l-lactide-co-glycolide)/collagen (PLGA/Col) have also been used to enhance differentiation of ESCs to cardiomyocytes as compared to PLGA scaffolds alone [31]. The reinforcement of collagen in these scaffolds promotes the expression of cardiomyocyte marker troponin I suggesting that the surface chemistry also aids in the differentiation process of these cells. In this regard, PCL and chitosan nanofibers have been modified with the arginine-glycine-aspartic acid (RGD) short peptide that is commonly used to promote cell attachment due to its similarly with the binding sites of many ECM proteins. Although these scaffolds have not been used with PSCs they show an increase in attachment and proliferation of NIH3T3 cells as compared to control scaffolds.

Lastly, the development of hybrid scaffolds incorporate other materials to elicit specific cellular responses [23, 32-34]. For example, the use of graphene to enhance conductivity of fibers has been demonstrated to promote neurite growth in neural stem cells. Additionally, cells respond positively by the reinforced fibers as opposed to unstimulated fibers. Many studies also demonstrate that electrospun scaffolds can be combined with hydrogels to promote cell attachment and proliferation [35-37]. Natural polymers, such as collagen and gelatin, can also be blended to enhance cell growth and proliferation since they are typically found within the ECM of developing tissues. Collagen scaffolds also offer the versatility that they can be electrospun to control the fiber diameter or using different combinations they can be synthesized into a gel. Although significant changes in cell attachment sites are inherent these collagen scaffolds provide an avenue to study cellular behaviors. Ultimately, the combinatorial approach of optimizing electrospun scaffold synthesis can be used to analyze the mechanistic details which can enhance self-renewal or differentiation of human PSCs.

1.3 – Aim of Thesis

The objective of this research is to examine how the static mechanical microenvironment of IPSCs affects cellular behaviors. The hypothesis behind this work is that human IPSCs are mechano-responsive and their mechano-modulation can result in enhanced self-renewal or differentiation to specific lineages. To date, many studies focus

on developing biochemical protocols to regulate IPSC behaviors without determining the significant contribution of the physical microenvironment. In our studies we focused on delineating the response of IPSCs to scaffolds with distinct stiffness to elucidate how the mechanical microenvironment regulates cell behaviors.

CHAPTER 2 – THE EFFECTS OF ELECTROSPUN SUBSTRATE-MEDIATED CELL COLONY MORPHOLOGY ON THE SELF-RENEWAL OF HUMAN INDUCED PLURIPOTENT STEM CELLS

2.1 – Abstract

The development of xeno-free, chemically defined stem cell culture systems has been a primary focus in the field of regenerative medicine to enhance the clinical application of pluripotent stem cells (PSCs). In this regard, various electrospun substrates with diverse physiochemical properties were synthesized utilizing various polymer precursors and surface treatments. Human induced pluripotent stem cells (IPSCs) cultured on these substrates were characterized by their gene and protein expression to determine the effects of the substrate physiochemical properties on the cells' self-renewal, i.e., proliferation and the maintenance of pluripotency. The results showed that surface chemistry significantly affected cell colony formation via governing the colony edge propagation. More importantly, when surface chemistry of the substrates was uniformly controlled by collagen conjugation, the stiffness of substrate was inversely related to the sphericity, a degree of three dimensionality in colony morphology. The differences in sphericity subsequently affected spontaneous differentiation of IPSCs during a long-term culture, implicating that the colony morphology is a deciding factor in the lineage commitment of PSCs. Overall, we show that the capability of controlling IPSC colony morphology by electrospun substrates provides a means to modulate IPSC self-renewal.

This chapter has been reproduced from *Maldonado M. et al., 2015, The effects of electrospun substrate-mediated cell colony morphology on the self-renewal of human induced pluripotent stem cells, *Biomaterials*, 59: 207-219, with permission from Biomaterials.

*Adapted from manuscript: Figures: 2.1–2.12

2.2 – Introduction

Induced pluripotent stem cells (IPSCs), derived from patients' somatic cells, hold promising potential in personalized regenerative medicine [38-40]. The capability of PSCs to self-renew and differentiate into multiple lineages makes them an ideal source for cell-based therapies by avoiding genetic mismatch and ethical issues associated with the use of embryonic stem cells (ESCs). Typical culture of IPSCs involves the use of animal-derived products, such as basement extracellular matrix (ECM) extracts from mouse carcinoma cells or mouse feeder cell layers. Because the essential biomolecular components and physiochemical cues for the expansion of human PSCs are not clearly defined, many researchers have depended on the use of animal-derived components, developed by phenomenological approaches, for long-term stem cell culture. However, the presence of possible immunogenic components or contaminants in these xeno-origin products limits the therapeutic use of IPSCs in human [41, 42]. Significant batch-to-batch variability in those products also undermines reproducibility in the phenotypic characteristics of expanded stem cells [43]. Therefore, recent research in the field has focused on developing synthetic substrates for PSC culture [44-47].

Engineered synthetic substrates are advantageous over natural products due to the reproducibility and flexibility of the composition and structure. Their tunable material properties, including surface chemistry, topography, and stiffness, provide an opportunity

to optimize the cellular microenvironment for the maintenance of IPSCs. Among many factors, the mechanical properties of scaffolds have been shown to be one of the main determinants for cellular behaviors in various stem cell types [48-50]. For example, mouse ESCs cultured on substrates with softer stiffnesses, similar to the intrinsic stiffness of the cells, maintain their pluripotency without the addition of exogenous leukemia inhibitory factor [51]. Similarly, mesenchymal stem cells (MSCs) have also been shown to commit to a specific lineage when cultured on matrices with specific elasticity [48]. Changes in cell shape, cell-to-cell contacts, and focal adhesion points, regulated by physical characteristics of substrates, have all been shown to alter stem cell behaviors [52-54].

In this regard, electrospinning is a viable synthesis method to produce physiochemically distinctive substrates for cell culture systems. The advantages of electrospinning include its capability to produce ECM-resembling fibrous structures with controlled fiber dimensions (nanometer to micrometer) and fiber morphology (*e.g.*, cylindrical, ribbon-like, and pores on the fiber surface) using a diverse range of biocompatible polymers [55, 56]. Another advantage is the simplicity of the process enabling scale-up for mass production. For this reason, many have shown the potential of electrospun fiber mats as cell culture substrates for various types of stem cells [57-61]. Surface-aminated polyethersulfone (PES) nanofibers enhanced the proliferation of human umbilical cord blood hematopoetic stem/progenitor cells and induced higher CD34+ expression as compared to cells cultured on commercially available tissue-culture

polystyrene (TCPS) [62]. The versatility of the technique has also allowed for the production of natural extracellular matrix-based electrospun substrates for adipose tissue-derived stem cell culture and expansion [63]. Recently, Hashemi et al. have also demonstrated the feasibility of using collagen-grafted electrospun substrates for maintaining pluripotency in mouse ESCs [61]. Put together, the flexibility of the electrospinning process to synthesize a wide range of fibrous structures provides an opportunity to develop xeno-product free culture systems for the expansion of various stem cell types. However, a more systematic approach is necessary to determine the optimal scaffold characteristics.

In this study, we hypothesized that the mechanical properties of the electrospun substrates would be one of the significant factors regulating stem cell self-renewal. We examined the differential development of IPSC colony on various electrospun fibrous substrates with systematically varied mechanical properties. Such differences in IPSC colony morphology was correlated to the cells' proliferation and the maintenance of pluripotency. Ultimately, we show that electrospun substrates provide an efficient platform for systematically dissecting and optimizing the physiochemical cues that mediate stem cell self-renewal.

2.3 – Materials and Methods

2.3.1 – Substrate fabrication and morphological characterization

All reagents and products were purchased from Sigma-Aldrich (St. Louis, MO) unless otherwise noted. Various fibrous substrates were synthesized by electrospinning using different precursor solutions including 8.5 wt.% poly(ε-caprolactone) (PCL) dissolved in 5:1 trifluoroethanol (TFE)-water, 11 wt.% polyethylene terephthalate (PET, Indorama Ventures, Spartanburg, SC) dissolved in 1:9 trifluoroacetic acid (TFA)-1,1,1,3,3,3-Hexafluoro-2-propanol (HFP) (Oakwood Products Inc., West Columbia, SC), 5 wt.% poly(etherketoneketone) (PEKK, Oxford Performance Materials, South Windsor, CT) dissolved in HFP, or 4 wt.% polycarbonate-urethane (PCU, DSM PTG, Berkeley, CA) dissolved in HFP. A vertical configuration of an electrospinning setup was used with a tip-to-collector distance of 23 cm [64]. The applied voltage and flow rates were adjusted to form a stable Taylor cone for each solution [65, 66]. As-spun samples were plasma-treated at 30 W for 5 minutes to improve the hydrophilicity of the substrates. The microstructure of electrospun fibers was observed under a Philips/FEI XL30 FEG scanning electron microscope (SEM).

2.3.2 – Collagen conjugation and quantification

To examine the effects of biological surface modification, the plasma-treated substrates were further processed with collagen type I conjugation. The plasma-treated samples were subjected to a zero-length crosslinking agent, 100 mM N-hydroxysuccinimide (NHS)/N-(3-Dimethylaminopropyl)-N'-ethylcarbodiimide hydrochloride (EDAC). After the chemical modification to ester linkages of the substrate, the samples were incubated in 1 mg/ml collagen type I in 0.01 M hydrochloric acid (HCl) overnight [67]. The amount of conjugated collagen on the electrospun substrates was quantified with a Sirius red colorimetric assay using a protocol similar to Zhu et al. [68]. Briefly, substrates conjugated with collagen were fixed in Bouin's fluid for 1 h at room temperature, washed with tap water, and air-dried overnight. The samples were then stained with Sirius red dye for 1 h under mild shaking. The dye was removed and each well was washed vigorously with 0.01 m HCl to remove unbound dye. Following washing, the substrate-bound dye was released using 0.1 m sodium hydroxide under mild shaking for 30 min, and optical density of the solution was measured at 490 nm using a plate reader (PerkinElmer, Waltham, MA). Substrates were dried overnight at room temperature and their mass measured. The surface area of the substrates was measured by Brunauer-Emmett-Teller (BET) method [69]. Collagen conjugation on each substrate was quantified to yield the amount of collagen per unit surface area. In addition, the

electrospun fibers were immunofluorescently stained to reveal the uniform localization of collagen on the surface of the fibers.

2.3.3 – Mechanical characterization of electrospun substrates

The mechanical properties of electrospun substrates were determined by atomic force microscopy (AFM) using a MFP-3D AFM (Asylum Research, Santa Barbara, CA). A modified silicon nitride tip (0.6 N/m) attached with a 20 µm diameter borosilicate sphere was used to measure the mechanical responses of electrospun fiber networks. At least three separate measurements were conducted on different locations per substrate at an indentation and retraction speed of 2 µm/s and a set trigger force of 20 nN. The load-displacement data were used to calculate the reduced Young's modulus using the Hertz model for spherical indenters [70].

2.3.4 – IPSC culture

IPSCs were derived from BJ-2522 human neonatal foreskin fibroblast cells (ATCC) by transfecting the cells with OCT4, SOX2 and KLF4 retroviruses as previously described [71]. Additionally, the induced cells were transfected with a GFP-labeled OCT4 reporter [72]. The cells were adapted to Geltrex®-coated cell culture dishes (Life Technologies, Grand Island, NY) in mTeSR1 medium (StemCell Technologies, Vancouver, Canada) at

37 °C and 5% CO2. The genetic stability was confirmed by karyotyping, and pluripotency of this stem cell line was verified by inducing differentiation to ectodermal, endodermal, or mesodermal lineage (**Figure 2.1**). Electrospun substrates were sterilized with 70% ethanol for 1 h, air-dried overnight, and UV-sterilized prior to cell seeding. IPSCs were passaged from a tissue culture flask to electrospun substrates using 0.25% Trypsin-EDTA (Life Technologies) at a seeding density of 125,000 cells/cm^2. Rock inhibitor (10 µm, Reagents Direct, Encinitas, CA) was supplemented 1 h prior to cell harvesting and maintained for a day during substrate culture to improve cell attachment and survival. Cells cultured on Geltrex®-coated 25 cm^2 flasks at the same cell seeding density were used as controls. The IPSCs cultured on the substrates were maintained in mTeSR1, and medium was exchanged daily up to 12 days. To monitor stem cell proliferation and colony formation in situ, an OCT4-GFP transfected cell line was cultured on collagen-conjugated PCL or PCU substrates, and visualized every 4 h during culture using a Nikon BioStation CT with fluorescence and phase imaging.

2.3.5 – Cell proliferation assay

Cell proliferation on different substrates was analyzed using alamarBlue® assay (Life Technologies) according to the manufacturer's protocol. Briefly, alamarBlue® was added directly to cell culture medium at 10 volume% and analyzed after 4 hours.

Fluorescence was measured at an excitation wavelength of 530 nm and an emission reading of 605 nm using a plate reader (PerkinElmer).

2.3.6 – Cell colony morphological observation and image analysis

To examine cell colony morphology by SEM, samples were fixed in 10% formalin overnight and dehydrated as previously described [73]. Briefly, a sequential dehydration of 50%, 70%, 80%, 95%, and 100% ethanol, followed by 3:1, 1:1, and 1:3 Ethanol:Hexamethyldisilazane (HMDS, Ted Pella, Inc., Redding, CA) exchange was performed. After drying overnight, the samples were sputter coated with platinum–palladium prior to imaging under an SEM.

Cell colony morphology was also analyzed using immunofluorescence imaging. Samples were fixed with 4% paraformaldehyde for 30 min. To visualize colony morphology, the fixed cells were subjected to actin and nucleus staining using Alexa569-phalloidin (Life Technologies) and 4’,6-diamidino-2-phenylindole (DAPI, Vector Laboratories, Burlingame, CA), respectively. Alternatively, fixed cells were subjected to PAX6 (Developmental Studies Hybridoma Bank, Iowa City, IA) immunofluorescent staining to determine differentiation towards ectodermal lineage. The samples were observed under an epi-fluorescent microscope (Nikon Eclipse, Melville, NY) or a confocal microscope (Leica SP2, Buffalo Grove, IL).

Quantification and characterization of cell colony morphology were assessed using Imaris Bitplane 7.1.1 (Bitplane, South Windsor, CT). Using a surface area reconstruction, the sphericity (i.e., ratio of the surface area of a sphere to the surface area of the object) was calculated for colonies cultured on different substrates [74]. At least five colonies per condition were analyzed.

2.3.7 – Gene expression analysis

Total RNA from the cells cultured on various substrates for 7 or 12 days was extracted using an RNeasy Micro Kit (Qiagen, Valencia, CA) and cDNA synthesis was performed using iScript cDNA Synthesis Kit (Bio-Rad, Hercules, CA). Real-time PCR was performed to determine gene expression of pluripotency and various differentiation markers using the following custom primers: GAPDH (forward) 5'-ATGGGGAAGGTGAAGGTCG-3' and (reverse) 5'-TAAAAGCAGCCCTGGTGACC-3'; DNMT3B (forward) 5'-GTCGTGCAGGCAGTAGGAAATTAG-3' and (reverse) 5'-GCAATTTGTCTTGAGGCGCTT-3'; NANOG (forward) 5'- GCTTATTCAGGACAGCCCTGA-3' and (reverse) 5'-TTTGCGACACTCTTCTCTGCA-3'; T (forward)5'-GGGTCCACAGCGCATGAT-3' and (reverse) 5'- TGATAAGCAGTCACCGCTATGAA-3'; GSC (forward) 5'-GATGCTGCCCTACATGAACGT-3' and (reverse) 5'- TACTTGGTCTCCTGGAAGAGGTT-3'; PAX6 (forward) 5'- GAGTTCTTCGCAACCTGGCTA-3' and (reverse) 5'-CTGCCCGTTCAACATCCTTAG-3'; NEUROD1 (forward) 5'-AAAGCCCTCTGACTGATTGCA-3'

and (reverse) 5'- GGACGGTTCGTGTTTGAAAGA-3'. Data was analyzed by the comparative threshold cycle (CT) method using GAPDH as an endogenous control [75]. For an ectodermal positive control, ectodermal differentiation of IPSCs was induced by a modified protocol using neurobasal media supplemented with B27, N2, retinoic acid, and dorsomorphin for 8 days [76]. For a mesendodermal positive control, the differentiation was induced using DMEM-F12 (Lonza, Anaheim, CA) supplemented with Wnt3a and Activin-A for 60 hours [77].

2.3.8 – Statistical analysis

All experiments were conducted in at least triplicates, and data is represented as mean ± standard deviation or standard error of means. Data was analyzed using SPSS (v.19.0) to determine significance by one-way ANOVA with Tukey's HSD post-hoc. To correlate substrate properties and cellular behaviors, bivariate correlation was determined by Pearson's correlation coefficients. P value less than 0.05 was regarded as statistically significant.

2.4 – Results

To examine the effects of substrate properties on IPSC behavior, PCL, PET, PEKK and PCU were electrospun to produce various fibrous substrates with distinctive

physiochemical characteristics. These polymer precursors were selected due to their biocompatibility as well as significant differences in bulk elastic modulus to render a large range of stiffness among the substrates after the electrospinning process. Additionally, the ester linkage present in these polymers allowed for the modification of their surface chemistry through collagen conjugation via NHS-EDAC chemistry. We particularly focused on monitoring the colony morphology of IPSCs during a short- and a long-term culture on such substrates and its effects on stem cell self-renewal, including proliferation and maintenance of pluripotency.

The microstructure of electrospun fibrous substrates was characterized using SEM, and fiber diameter was quantitatively measured (**Figure 2.2, A-D**). Typical cylindrical fiber morphology was observed, and the average fiber diameter was 591 ± 402 nm for PCL, 1060 ± 224 nm for PET, 1680 ± 624 nm for PEKK, and 1240 ± 443 nm for PCU. After collagen conjugation all substrates had similar amounts of collagen per substrate surface area at approximately 27 g/m^2 (**Figure 2.2E**). Uniform distribution of collagen on the surface of individual fibers was also visualized by collagen type I immune-staining (**Figure 2.3**). To determine the mechanical properties of electrospun fiber networks, an AFM tip was used to measure the force-displacement relationship, and the reduced Young's modulus of each substrate was calculated. The measured reduced Young's moduli ranged from approximately 19 kPa (PCL) to 193 kPa (PCU) (**Figure 2.2F**).

Regardless of surface treatment (plasma-treated or collagen-conjugated), IPSCs attached on the electrospun substrates and proliferated to form stem cell colonies (**Figure 2.4**). The differences in the morphology of stem cell colonies were distinguishable in approximately 4 days after cell seeding. Darker shades with well-defined boundaries indicated more three-dimensional (3D) cell colonies in comparison to two-dimensional (2D) colonies, which had softer shades with diffused boundaries under optical observation. On day 9 a significant difference in colony morphology was observed (**Figure 2.4**). To compare the effects of surface chemistry on stem cell behavior, the colony morphology of IPSCs cultured on plasma-treated substrates (to improve the hydrophilicity of the polymers without affecting surface chemistry) was compared to collagen-conjugated substrates (**Figure 2.4**). A 3D colony morphology was observed on all plasma-treated substrates regardless of mechanical properties. In contrast, colonies on collagen-conjugated substrates had relatively flattened, spread morphologies on the stiffer substrates while softer substrates induced 3D morphology. Interestingly, the degree of three dimensionality in colony morphology scaled with the stiffness of substrate when the surface chemistry was controlled with collagen conjugation.

To closely monitor the proliferation and development of distinct colony morphologies depending on substrate stiffness, time-lapse imaging of OCT4-GFP transfected IPSCs, cultured on the collagen-conjugated substrates with the lowest (19 kPa) and the highest (193 kPa) reduced Young's modulus, was performed during culture

duration (**Figure 2.5**). Within 4 days, the cells exhibited markedly different colony morphologies; softer substrates limited the edge propagation of IPSC colonies while stiffer substrates induced greater expansion of the colony size resulting in the merge of separate colonies.

To further examine the differences in colony morphology depending on the substrate stiffness, the cellular interaction with the electrospun fibers was observed by SEM following 12 days of culture. The examination showed that plasma-treated substrates, both the softest (19 kPa) and stiffest (193 kPa), induced rounded, 3D colony morphologies (**Figure 2.6, A-B**). In comparison, the collagen-conjugated softest substrates (19 kPa) induced round, 3D IPSC colonies, while the stiffest (193 kPa) induced flat, 2D colony morphologies, confirming the optical observations (**Figure 2.6, C-F**). Interestingly, on the 19 kPa substrates, deformation of fibers was observed around the periphery of the colony toward the center as compared to no deformation on the 193 kPa substrate. The internal structure of 3D cell colonies was revealed by confocal microscopy (**Figure 2.7**). A central pit was observed within the 3D colonies of cells cultured on the collagen-conjugated 19 kPa substrate. The formation of hollow space in the middle of the colony was further confirmed by SEM on the bottom side of a colony that was carefully detached from the substrate (**Figure 2.7C**).

To quantitatively assess colony morphology on different substrates, the sphericity, a degree of shape relative to a perfect sphere, was examined by image analysis (**Figure 2.8**). Initially, z-stack confocal images of DAPI-stained samples were 3D rendered, and contour lines were drawn around the periphery of the IPSC colony to reconstruct a surface representation (**Figure 2.8, A-B**). A linear relationship between the sphericity of colony morphology and the reduced Young's modulus of collagen-conjugated substrates was observed (Pearson's correlation: −0.806, significance: 0.000). As the substrate stiffness increases, the colony sphericity decreases (**Figure 2.8C**). The fiber diameter of the substrates did not exhibit any statistical correlation to the sphericity, indicating that fiber diameter did not directly affect the IPSC colony morphology.

The proliferation of IPSCs was examined in relation to the stiffness of the substrate (**Figure 2.9**). Generally, as the stiffness of the substrate increased, the proliferation also increased, reaching a similar cell number to those cultured on Geltrex®-coated TCPS (a typical IPSC cell culture substrate) at approximately 5 million. Interestingly, the stiffness of collagen-conjugated substrates exhibited greater linear correlation to cell proliferation throughout the culture periods as compared to that of plasma-treated substrates.

To determine if the substrate-modulated colony morphology affected the pluripotency of IPSCs, gene expression analysis was conducted using multiple markers for pluripotency, mesendodermal, or ectodermal differentiation for short- and long-term

culture durations. For short-term culture (7 days), pluripotency was maintained for all substrates (**Figure 2.10, A-B**). Insignificant changes in the expression of differentiation markers with respect to a negative control (i.e., Geltrex®) also demonstrate the maintenance of pluripotency on these substrates (**Figure 2.10, C-F**). IPSCs also maintained expression of pluripotency markers after developing distinct colony morphologies during 12 days of culture (**Figure 2.11, A-B**). However, further investigation using differentiation markers revealed that IPSCs exhibited spontaneous differentiation (**Figure 2.11, C-F**). A slight increase in gene expression of mesendodermal markers, GSC and T, was observed, but these changes were insignificant as compared to a negative control (**Figure 2.11, C-D**). In contrast, a significant degree of spontaneous differentiation toward ectodermal lineage was observed in the cells cultured on 19 kPa substrates, evidenced by a 260-fold increase in PAX6 expression as compared to the negative control (**Figure 2.11E**). This upregulation was even greater than that of the positive control for ectodermal differentiation. The preferential spontaneous differentiation toward ectodermal lineage was further confirmed by the upregulation of NEUROD1 (**Figure 2.11F**). Interestingly, an inverse relationship was observed between the degree of spontaneous differentiation toward ectodermal lineage and the substrate stiffness that controlled colony sphericity (Pearson's correlation for PAX6: −0.640, significance: 0.001; Pearson's correlation for NEUROD1: −0.583, significance: 0.003). To further confirm the spontaneous differentiation toward ectodermal lineage, protein expression of PAX6 was assessed by immunocytochemistry on the colonies cultured on the softest 19 kPa and the stiffest 193

kPa substrates (**Figure 2.12**). The cells on 19 kPa substrates showed significant PAX6 expression especially at the periphery of the colony. However, minimal PAX6 expression was observed in the cells cultured on 193 kPa substrates as compared to the negative control in which cells were cultured on Geltrex®-coated TCPS.

2.5 – Discussion

The development of safe and efficient PSC culture systems has been extensively investigated to redefine optimal laboratory techniques and culture conditions for the expansion of PSCs at clinically relevant numbers. However, typical PSC culture still involves the use of animal-derived products, which significantly prevents the cells' clinical applications. The culture of human PSCs on mouse feeder cell layers or the use of animal-derived 'serum replacements' have been shown to metabolically incorporate substantial amounts of nonhuman sialic acid Neu5Gc into the cells, which invokes an immune response [78]. For this reason, the U.S. Food and Drug Administration (FDA) regards the clinical use of mouse feeder cell-cultured human pluripotent stem cell lines as a xeno-transplantation imposing significant regulatory steps [78, 79]. In this regard, the results presented in this study offer a synthetic alternative for PSC culture. When cultured for a typical cell culture duration in proliferation media, various electrospun substrates supported the self-renewal of IPSCs.

Electrospun scaffolds have been widely studied for the culture and expansion of MSCs [57-59, 80-83]. Jahani et al. have shown that electrospun PCL substrates induce greater proliferation of rat MSCs as compared to those cultured on standard TCPS [84]. Interestingly, MSC culture on electrospun scaffolds with varied protein coatings such as laminin, collagen I, or fibronectin, does not result in significant differences in proliferation, implicating that the physical nature of electrospun fibers is the primary determinant of cellular behaviors [59]. The use of electrospun substrates on PSC culture has been mostly limited to the induction of differentiation by controlling surface chemistry or the alignment of fibers [85-88]. Nonetheless, Zonca et al. recently showed that electrospun PES scaffolds can support the self-renewal of mouse ESCs, demonstrating the feasibility of using electrospun scaffolds as a cell culture substrate for ESCs [60]. Overall, electrospun fibers have shown their potential to support expansion of several types of stem cells. Various electrospun fibrous substrates synthesized in the current study allowed us to systematically dissect the effects of surface chemistry and mechanical properties on PSC behaviors, possibly enabling the optimization of synthetic cell culture systems.

Our results showed that the mechanical properties of substrates are an overarching factor determining PSC colony morphology that subsequently influences cellular behaviors. Similarly, previous studies, including ours, have shown the substrate stiffness-dependent change in the single cell morphology of MSCs [48, 83, 89-91]. Upon attachment, MSCs are immediately influenced by substrate mechanics and exhibit

different morphologies depending on stiffness of the substrates. This difference in the substrate-mediated morphology significantly impacts stem cell behaviors such as proliferation and differentiation. For example, we previously showed that MSCs cultured on stiffer electrospun scaffolds exhibit a more spread morphology whereas softer scaffolds induce a more rounded cell morphology, ultimately determining their preferential differentiation towards either osteoblasts or chondrocytes [83]. In contrast, the current study provides an insight into the effects of substrate mechanics on the colony formation of PSCs which require cell-cell interaction for survival and maintenance of pluripotency, unlike MSCs. IPSCs attached to the substrate as cell aggregates and did not immediately exhibit differences in colony morphology. The substrate-dependent colony morphology (sphericity) arose only after a certain culture duration, due to the deformation of the substrates likely when increased cellular tension (by increased colony size) overcame the substrate stiffness. This hypothesis is further supported by the formation of hollow space within the center of the colony. In spite of vastly different colony-forming behavior between MSCs and PSCs, IPSCs cultured on stiffer substrates exhibited a greater proliferation rate than those on softer substrates similar to previous studies with MSCs.

A prolonged culture of IPSCs after the emergence of substrate-specific colony morphology significantly affected the maintenance of pluripotency. Softer substrates promoted more spherical, 3D colony morphology while stiffer substrates induced a more

spread, 2D colony growth. These notable alterations in colony morphology resulted in differences in the degree of spontaneous differentiation, preferentially towards ectodermal lineage. The significant correlation between colony sphericity and spontaneous differentiation suggests that the colony morphology is likely a deciding factor in lineage commitment of PSCs. These results are also consistent with other studies that showed soft microenvironments promoted neurogenic differentiation in stem cells [48, 92]. Similarly, typical methods for PSC differentiation toward neuroectodermal lineage involve the formation of cell aggregates or embryoid bodies (EBs) which suggest that the formation of aggregated 3D colony morphology, thus, enhanced cell-cell contact can strongly influence PSC fate. A recent study using mouse ESCs demonstrated the formation of embryoid-like colonies with controlled germ layer organization on fibrin gels. [93]. The level of organization was mainly attributed to the mechanical properties of substrates where softer fibrin matrices allowed for a single cell to form a 3D colony as opposed to stiffer substrates. In this regard, the findings in our study present significant implications for controlling stem cell fate by modulating colony morphology. The ability to precisely modulate the colony morphology by controlling the mechanical properties of electrospun fibers could potentially aid in the differentiation of PSCs toward specific lineages. Overall, the mechanical properties of electrospun substrates strongly influence the colony morphology, thus, cellular behaviors by which the optimal cell niche can be designed to induce efficient self-renewal or the differentiation of PSCs toward a specific lineage.

2.6 – Conclusions

We utilized a systematic approach to analyze IPSC behaviors on electrospun fibrous substrates with varied mechanical properties. The mechanical properties of the substrates played a critical role in determining IPSC colony morphology. Specifically, the stiffness of the substrate was inversely correlated with the sphericity of IPSC colony, which, in turn, was linearly related to self-renewal and spontaneous differentiation. We showed that the capability of controlling colony morphology by electrospun substrates provides a means to manipulate stem cell fate either for maintenance of pluripotency (short-term culture) or for lineage-specific differentiation (long-term culture). Therefore, electrospun substrates based on synthetic polymers may promote the clinical application of IPSCs by eliminating the use of animal-derived products and providing suitable culture systems for the use of such cells in patient-specific cell therapies.

2.7 – Figures

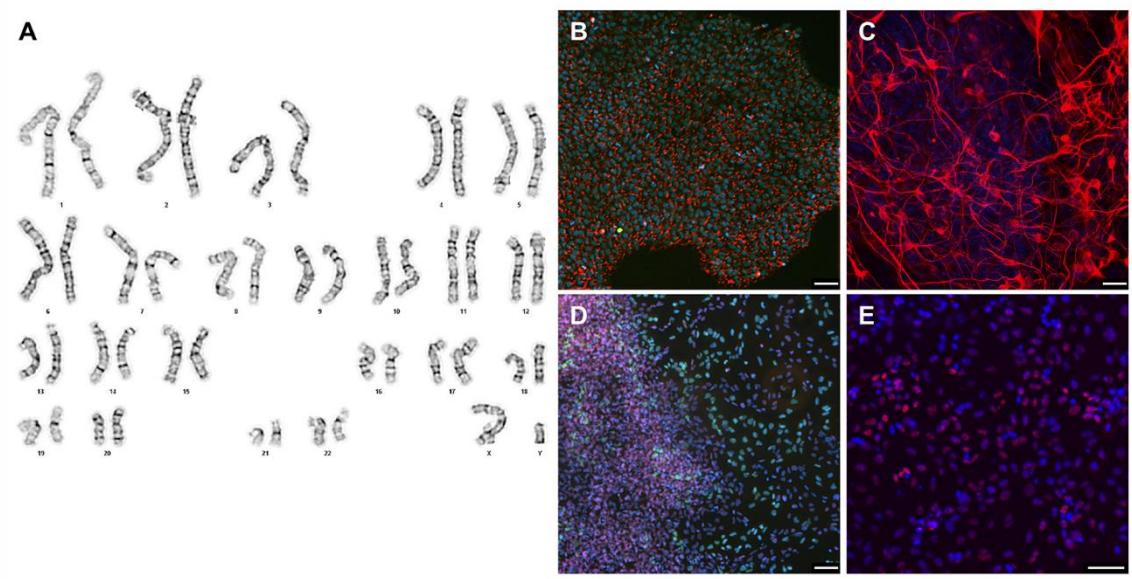

FIGURE 2.1. GENETIC STABILITY AND PLURIPOTENCY OF INDUCED PLURIPOTENT STEM CELLS (IPSCS).

(A) Karyogram of IPSC showing normal human male karyotype. (B-E) Immunofluorescence images of (B) as-induced cells or the cells subjected to lineage specific differentiation to (C) ectodermal lineage, (D) endodermal lineage and (E) mesodermal lineage. Lineage-specific antibodies are used to determine differentiation including (B) SSEA3 (red) and OCT4 (green) (pluripotency marker), (C) TUJ1 (red) (ectoderm marker), (D) FOXA2 (red) (endoderm marker) and OCT4 (green) and (E) BRACHYURY (red) (mesoderm marker), demonstrating multi-lineage differentiation potential of IPSCs (scale bar: 50 µm). To verify pluripotency of the IPSCs, the cells were subjected to various growth factor/cytokine stimulation to induce ecto-/endo-/meso-dermal differentiation: Retinol acid/Dorsomorphin, Activin A/Wnt3A, and Bmp4 for ecto-, endo, and meso-dermal differentiation, respectively [94-96]. The cells were then fixed with paraformaldehyde and immunostained with antibodies for OCT4, TUJ1, FOXA2 or BRACHYURY and appropriate secondary antibodies (all antibodies are from Cell Signaling). The stained samples were imaged using an epi-fluorescent microscope.

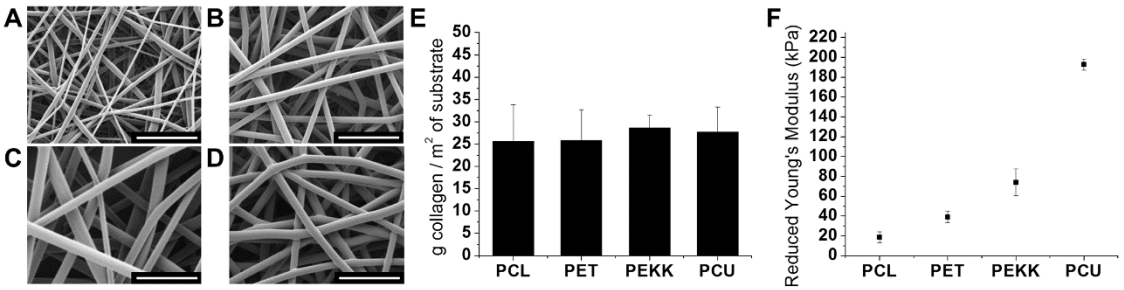

FIGURE 2.2. CHARACTERIZATION OF VARIOUS ELECTROSPUN SUBSTRATES.

Morphological characterization of various electrospun fibers including (A) PCL, (B) PET, (C) PEKK and (D) PCU by scanning electron microscopy (SEM) (scale bar: 10 µm). (E) Quantification of collagen conjugation on various electrospun substrates by spectrophotometry. (F) Reduced Young's modulus of various electrospun substrates determined by atomic force microscopy (AFM).

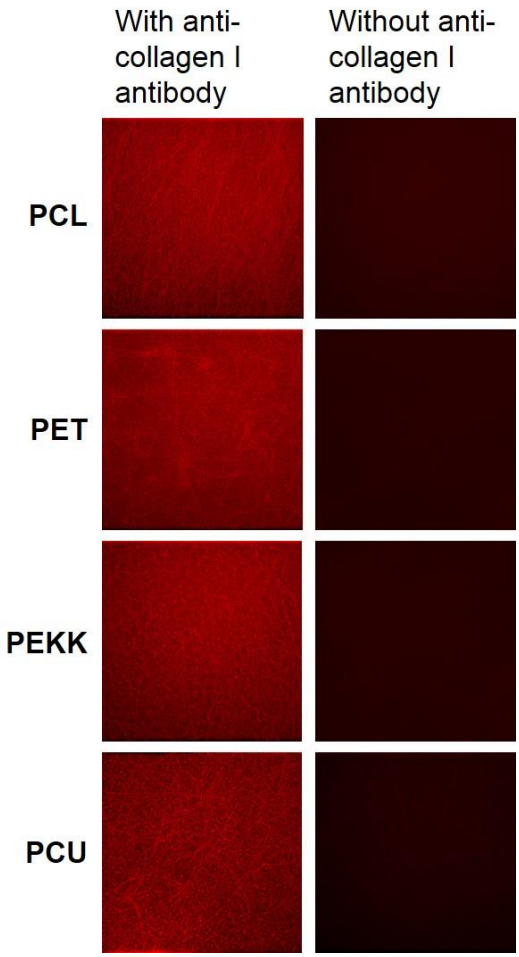

FIGURE 2.3. LOCALIZATION OF COLLAGEN CONJUGATION ON THE SURFACE OF ELECTROSPUN FIBERS

Electrospun substrates were subjected to collagen conjugation, followed by immune-staining with collagen type I antibody to qualitatively visualize the distribution of collagen. Secondary antibody only staining was used as a control for each substrate. Fluorescent images were taken using 40x magnification revealing localization of collagen on the surface of electrospun fibers.

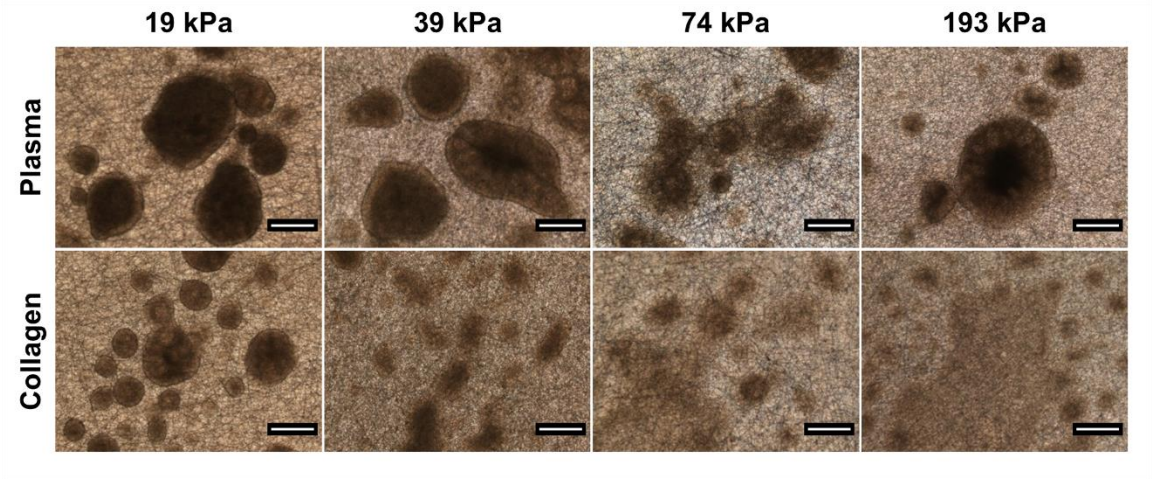

FIGURE 2.4. COLONY MORPHOLOGY OF HUMAN IPSCS ON VARIOUS ELECTROSPUN SUBSTRATES WITH DIFFERENT MECHANICAL PROPERTIES AND SURFACE TREATMENTS.

Optical imaging of IPSCs cultured for 9 days on plasma-treated substrates (top row) in all conditions shows smaller, defined colonies, while cells on collagen-conjugated substrates (bottom row) generally exhibited larger, more spread colonies. Cells on 19 kPa substrates exhibited highly defined, 3D colonies on both plasma-treated and collagen-conjugated substrates (scale bar: 500 μm).

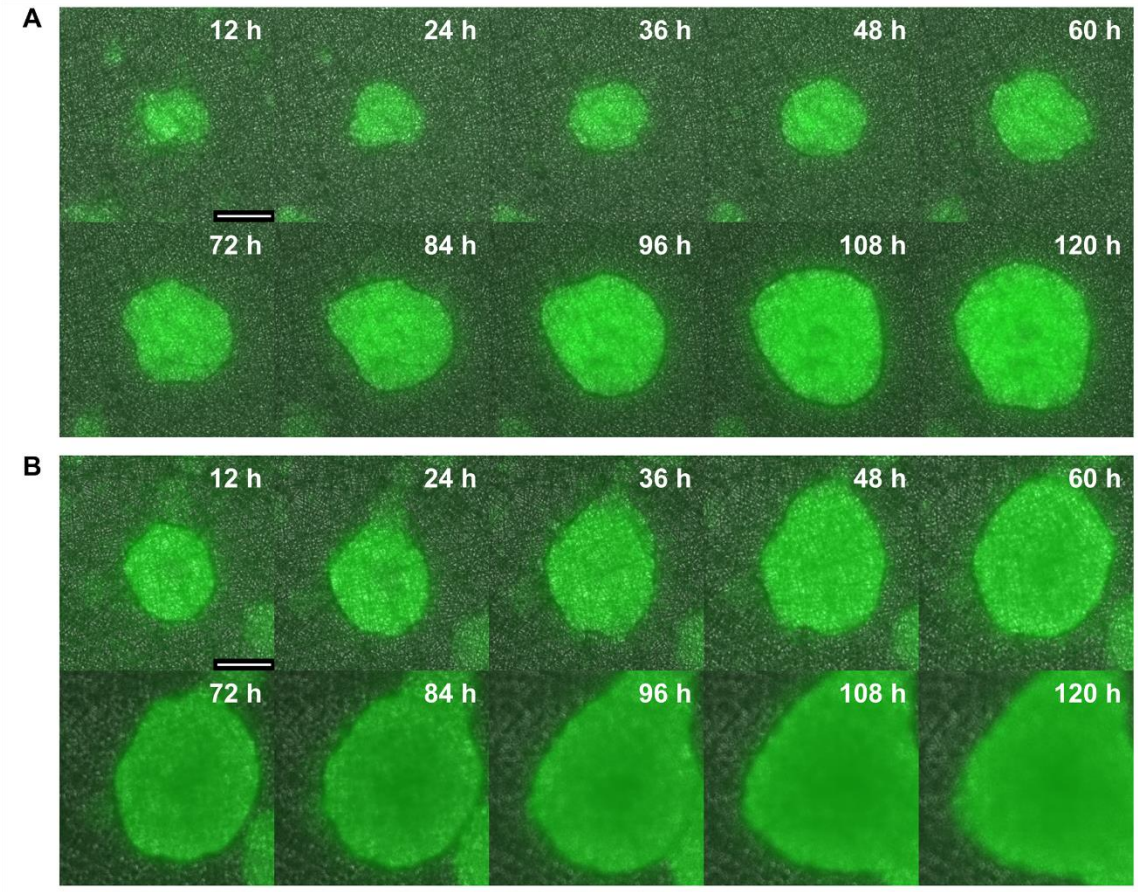

FIGURE 2.5. COLONY FORMATION OF IPSCS ON ELECTROSPUN SUBSTRATES WITH DIFFERENT MECHANICAL PROPERTIES.

Cells transfected with OCT4-GFP were cultured on collagen-conjugated (A) 19 kPa or (B) 193 kPa substrates for 5 days. The colony formation was continuously monitored using a Nikon BioStation CT incubator showing distinctive colony propagations on substrates with different stiffness. Fluorescence and phase time-lapse images were combined at each time point (scale bar: 500 µm).

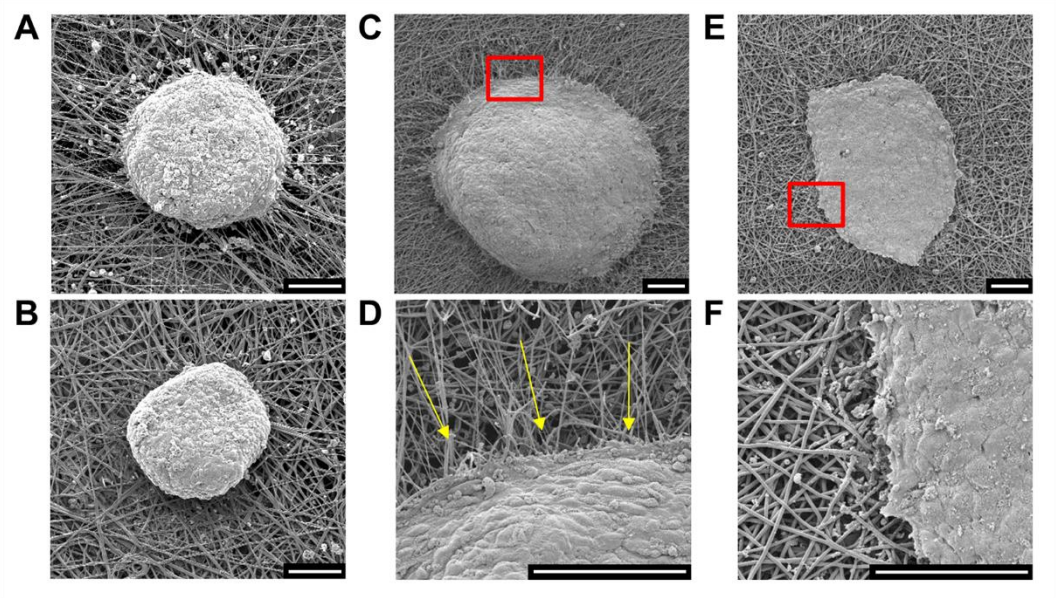

FIGURE 2.6. COLONY MORPHOLOGY OF IPSCS AFTER 12 DAYS OF CULTURE.

SEM images of IPSCs cultured on plasma-treated (A) 19 kPa or (B) 193 kPa substrates, showing a compact 3D colony morphology. (C-D) IPSCs cultured on collagen-conjugated 19 kPa substrates exhibit a round, 3D cell colony morphology while (E-F) cells on 193 kPa substrates exhibit a spread, flattened morphology. At the periphery of the colonies, (D) a deformation of electrospun fibers aligning toward the center of the colony is observed on 19 kPa substrates (arrows), while (F) there is no change in fiber orientation near the periphery of colonies cultured on 193 kPa substrates (scale bar: 50 µm).

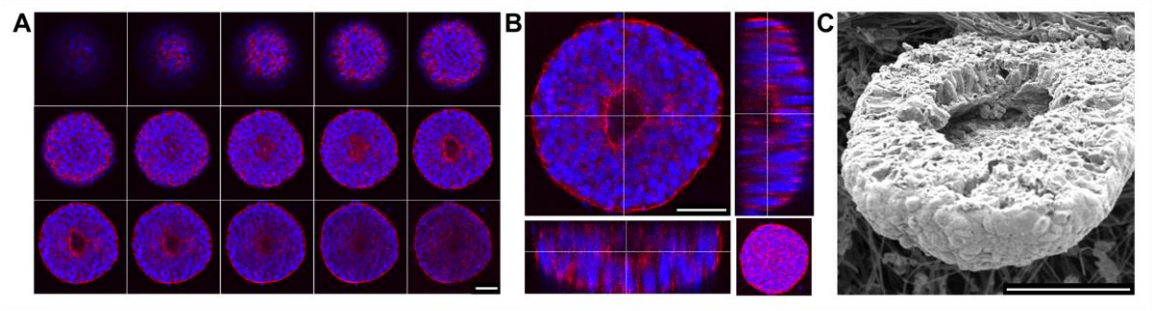

FIGURE 2.7. INTERNAL STRUCTURE OF A THREE DIMENSIONAL IPSC COLONY CULTURED ON A 19 KPA ELECTROSPUN SUBSTRATE.

(A-B) Immunofluorescence images of an IPSC colony cultured on a 19 kPa substrate by confocal microscopy (red: actin, blue: nucleus, scale bar: 50 µm). (A) A series of depth-wise cross-sectional images were acquired at 5 µm distances. (B) A cross-section of the merged images shows a pit in the center of the colony. (C) An SEM image confirmed a central pit formation in the center of a colony of IPSCs (scale bar: 50 µm).

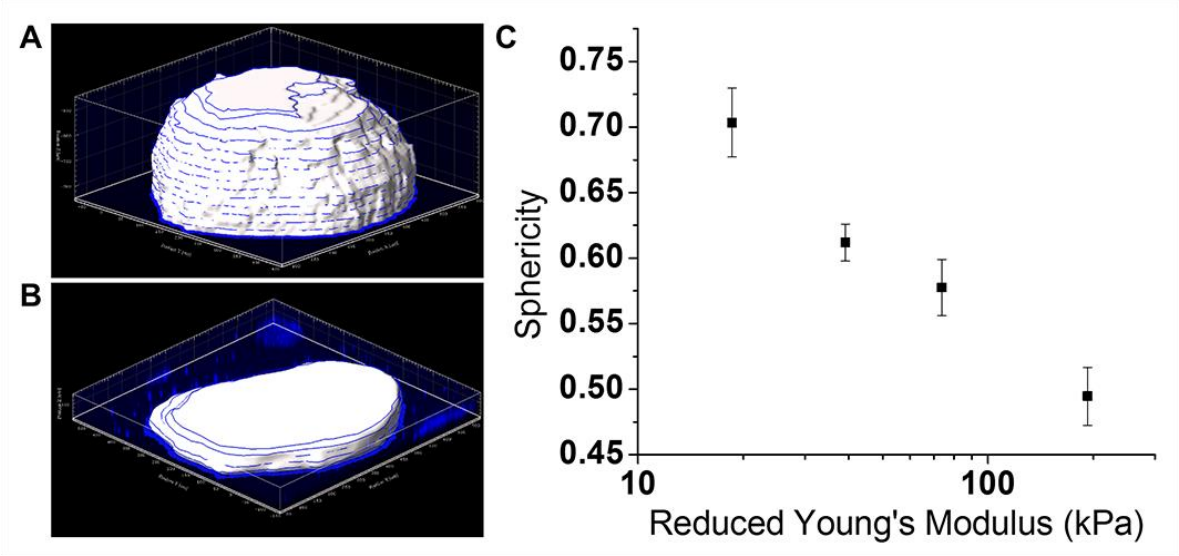

FIGURE 2.8. QUANTITATIVE ANALYSIS OF CELL COLONY MORPHOLOGY BY SPHERICITY MEASUREMENT.

(A-B) Confocal images were reconstructed to render a 3D surface of an IPSC colony by drawing contour lines using Imaris Bitplane software (A and B: representative colony morphologies on 19 kPa and 193 kPa substrates, respectively). (C) colony sphericity of IPSCs cultured on various electrospun substrates having different reduced Young's moduli.

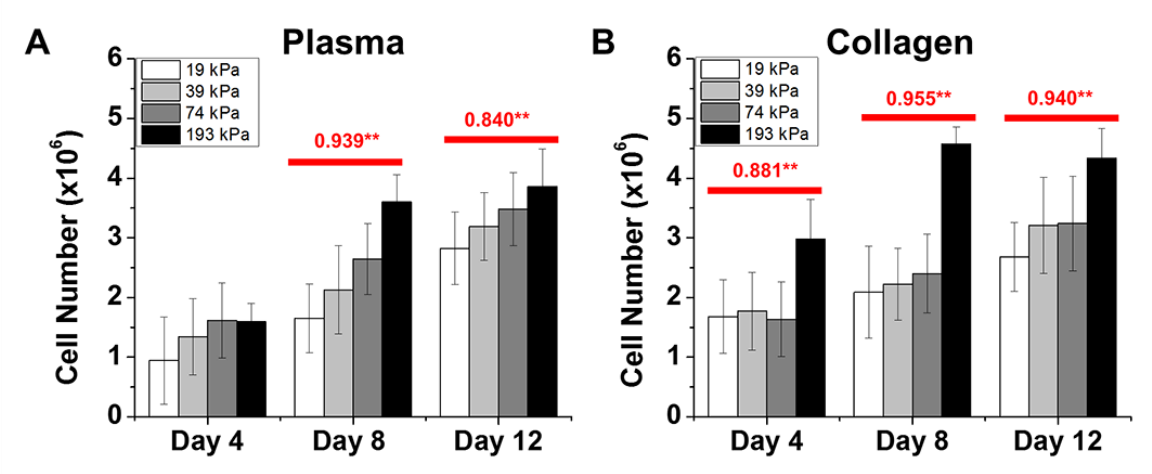

FIGURE 2.9. IPSC PROLIFERATION ON ELECTROSPUN SUBSTRATES WITH DIFFERENT MECHANICAL PROPERTIES.

(A) Plasma-treated substrates exhibited overall lower cell number in the earlier culture period as compared to (B) collagen-conjugated substrates. Generally, the proliferation rate of IPSCs was proportionally related to the reduced Young's modulus of the substrates. The Pearson's correlation coefficient to determine the correlation between substrate's reduced Young's modulus and cell proliferation is noted above the bar graphs for each culture duration (** denotes $p < 0.01$).

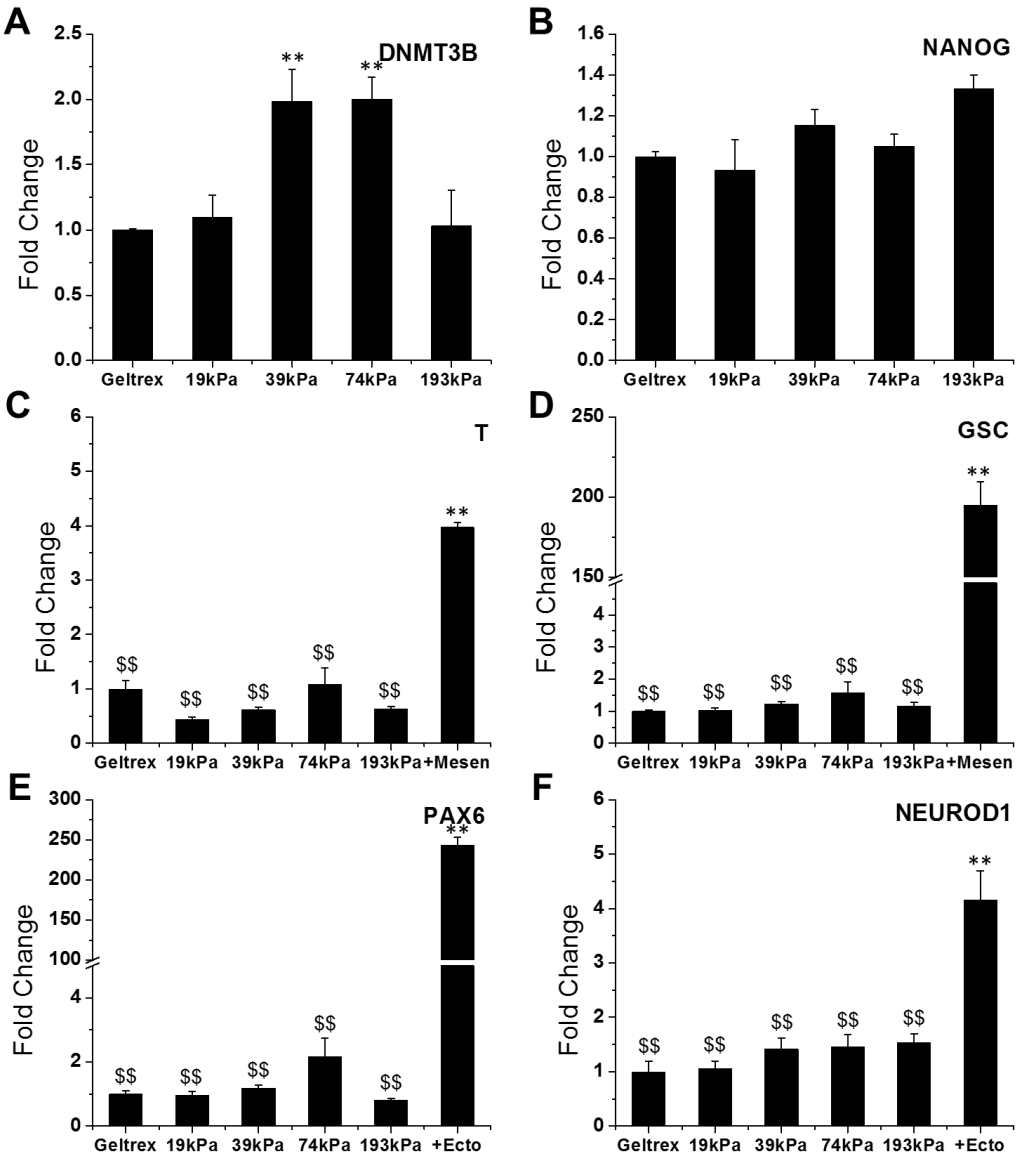

FIGURE 2.10. THE RELATIVE GENE EXPRESSION OF IPSCS CULTURED ON VARIOUS ELECTROSPUN SUBSTRATES FOR 7 DAYS DETERMINED BY QRT-PCR.

IPSCs were cultured in proliferation media for 7 days on electrospun substrates or Geltrex®-coated tissue culture polystyrene (TCPS). (A-B) pluripotency markers: DNMT3B and NANOG; (C-D) mesendodermal cell markers: T and GSC; (E-F) ectodermal cell markers: PAX6 and NEUROD1. The gene expression of cells cultured on Geltrex®-coated TCPS was used as a control. +Mesen and +Ecto denote the gene expression of positive controls for mesendodermal and ectodermal differentiation, respectively (* and ** denote $p < 0.05$ and $p < 0.01$, respectively as compared to Geltrex® controls. $ and $$ denote $p < 0.05$ and $p < 0.01$, respectively as compared to appropriate positive controls).

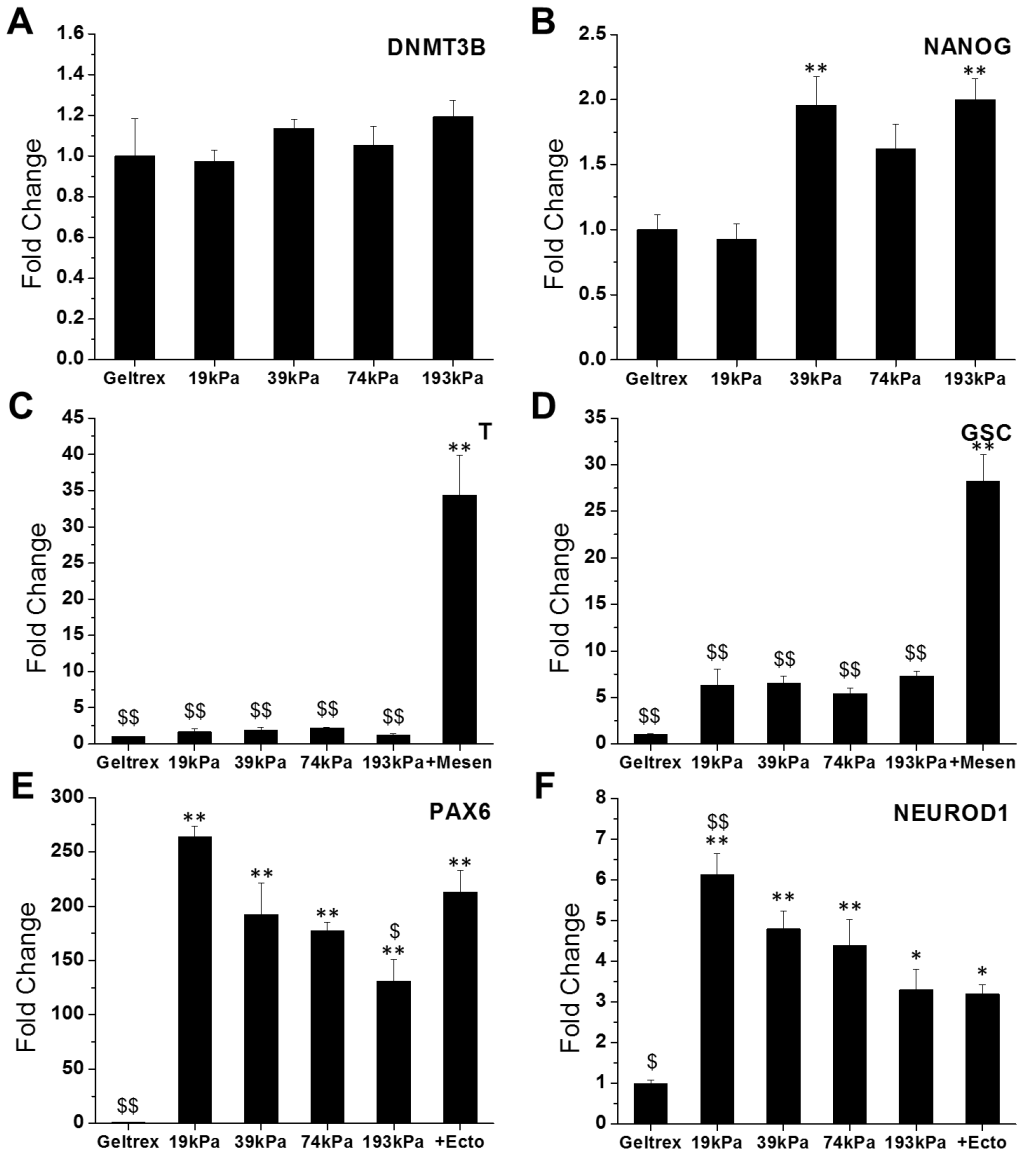

FIGURE 2.11. THE RELATIVE GENE EXPRESSION OF IPSCS CULTURED ON VARIOUS ELECTROSPUN SUBSTRATES FOR 12 DAYS DETERMINED BY QRT-PCR.

IPSCs were cultured in proliferation media for 12 days on electrospun substrates or Geltrex®-coated tissue culture polystyrene (TCPS). (A-B) pluripotency markers: DNMT3B and NANOG; (C-D) mesendodermal cell markers: T and GSC; (E-F) ectodermal cell markers: PAX6 and NEUROD1. The gene expression of cells cultured on Geltrex®-coated TCPS was used as a control. +Mesen and +Ecto denote the gene expression of positive controls for mesendodermal and ectodermal differentiation, respectively (* and ** denote $p < 0.05$ and $p < 0.01$, respectively as compared to Geltrex® controls. $ and $$ denote $p < 0.05$ and $p < 0.01$, respectively as compared to appropriate positive controls).

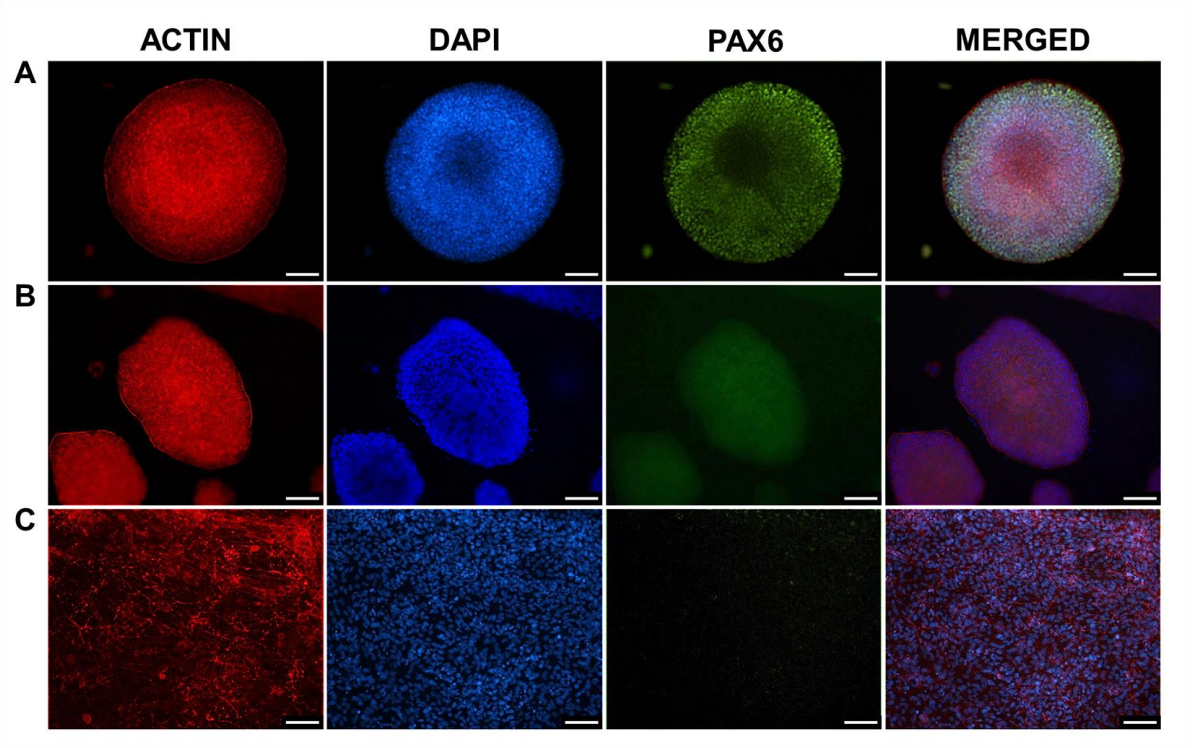

FIGURE 2.12. PAX6 PROTEIN EXPRESSION OF IPSCS CULTURED ON VARIOUS SUBSTRATES FOR 12 DAYS.

(A) Expression of the ectodermal marker PAX6 was observed within the colony, especially around the edges of spherical-3D colonies of IPSCs cultured on 19 kPa substrates. (B) Minimal expression of PAX6 on flat IPSC colony morphology on 193 kPa substrates. (C) No expression of PAX6 on IPSCs cultured on Geltrex®-coated TCPS (green: PAX6, red: actin, blue: nucleus; scale bar: 100 µm).

CHAPTER 3 – ENHANCED LINEAGE-SPECIFIC DIFFERENTIATION EFFICIENCY OF HUMAN INDUCED PLURIPOTENT STEM CELLS BY ENGINEERING COLONY DIMENSIONALITY USING ELECTROSPUN SCAFFOLDS

3.1 – Abstract

A patient-derived stem cell source, i.e., induced pluripotent stem cells (IPSCs), offers great potential for tailored cell therapies and regenerative medicine. IPSCs have the unique ability to duplicate themselves to clinically-relevant cell numbers, as well as, specialize to any adult cell type, a process called differentiation. Nevertheless, the primary concern with the use of IPSCs is their potential to form tumors as a result of uncontrolled differentiation when implanted in the body. To overcome this safety concern researchers have investigated multiple methods to differentiate cells to tissue-specific cell types prior to implantation. The current study uses synthetic polymer meshes with designed mechanics to direct the cellular behaviors of human IPSCs. IPSCs, which typically grow in the form of tight-knit aggregates, develop distinct colony geometries depending on the mechanics of the polymer meshes. Such a differential development of colony morphology critically affected the subsequent differentiation of the cells. These results demonstrate a facile, practical method to enhance the cell type-specific differentiation of IPSCs by culturing cells on the appropriate mechanical microenvironment. Therefore, the optimization of the synthetic polymer meshes for more specialized cell types would significantly advance the clinical translation of IPSCs.

This chapter has been reproduced from *Maldonado M. et al., 2016, Enhanced lineage-specific differentiation efficiency of human induced pluripotent stem cells by engineering colony dimensionality using electrospun scaffolds, *Advanced Healthcare Materials*, 5: 1408-1412, with permission from Advanced Healthcare Materials.

*Adapted from manuscript: Figures: 3.1–3.5

3.2 – Introduction

The guided differentiation of induced pluripotent stem cells (IPSCs) to target cell types holds a promising strategy to produce patient-specific cell sources in regenerative medicine and tissue engineering. Nevertheless, the primary concern with the use of IPSCs is their tumorigenesis or teratoma formation within the body [97]. Therefore, differentiating IPSCs to specific phenotypes prior to implantation is suggested to minimize such a risk of uncontrolled self-renewal/differentiation within the body. A majority of current differentiation protocols require the formation of embryoid bodies (EBs), which produces a three-dimensional (3D) cell colony structure of IPSCs [98, 99]. Albeit elusive mechanistic details, the cell niche in the EBs subjects the cells to complex cell-cell interactions, priming them for subsequent differentiation to various lineages [98, 99]. However, methodologies to form EBs require multiple steps where cells are detached, formed into cell agglomerates by suspension or microwell cultures, and further seeded onto tissue culture plates to induce differentiation [100, 101]. Such complex protocols are time-consuming, and the multistep procedures increase the probability of batch-to-batch variation. Recently, multiple groups have utilized hydrogels to embed stem cells for the formation of EBs and directed differentiation [102]. This method may efficiently position the cells in 3D colonies encapsulated within the matrix, but ultimately retrieval of these cells would be of primary concern due to the necessity of matrix digestion [102]. Therefore, the development of alternative strategies to stimulate 3D colony growth on a

2D-adherent surface is of great interest to maximize the differentiation efficiency of IPSCs. Electrospinning has been demonstrated to produce appropriate microenvironments for various cell types. The versatility of electrospinning permits the incorporation of cells into 3D nanofibrous scaffolds [103, 104]. Interestingly, its 2D format as a cell culture substrate provides a 3D-like topography, which induces cellular behaviors similar to those in 3D hydrogel encapsulation [105]. We have previously demonstrated that the extracellular matrix (ECM)-like morphology of electrospun nanofibers support the self-renewal of IPSCs, depending on the mechanical properties of the scaffolds [106].

The current study makes significant progress by examining how the colony dimensionality, developed by IPSC culture on scaffolds of distinct stiffness, notably affects lineage-specific differentiation. More specifically, we report, herein, a facile method to modulate cell–cell and cell–matrix interactions using a highly tunable cell culture platform to control IPSC colony formation and subsequent differentiation in an efficient and reproducible manner. We demonstrate that our novel technology overcomes the short comings of EB-based differentiation, such as complexity, reproducibility, and cell viability, while substantially improving specification of differentiation towards distinct lineages.

3.3 – Materials and Methods

3.3.1 – Scaffold fabrication

Various nanofibrous scaffolds were synthesized by electrospinning using the precursors of 8 wt.% poly(ε-caprolactone) (PCL, Sigma-Aldrich) dissolved in 5:1 trifluoroethanol:water, 8 wt.% polyethersulfone (PES, Goodfellow USA) in 1,1,1,3,3,3-Hexafluoro-2-propanol (HFP, Oakwood Products), 3 wt.% polycarbonate-urethane (PCU, DSM PTG) in HFP and 5 wt.% poly-ether-ketone-ketone (PEKK, Oxford Performance Materials) in HFP similar to the previous report [106]. The as-spun samples were air-plasma-treated at 30 W for 5 minutes and subsequently subjected to collagen conjugation on the nanofiber surfaces using 100 mM N-hydroxysuccinimide (NHS)/N-(3-Dimethylaminopropyl)-N'-ethylcarbodiimide hydrochloride (EDAC) followed by incubation in 1 mg/ml bovine collagen type I solution in 0.01 M HCl overnight [67]. Scaffolds were sterilized with 70% ethanol, air-dried overnight, and UV-sterilized prior to cell seeding.

3.3.2 – Morphological, surface chemical, and mechanical characterization of scaffolds

The morphology of nanofibrous scaffolds was characterized using a Philips/FEI XL30 FEG SEM as previously described [106]. The surface chemistry of the scaffolds were

characterized by quantifying the amount of conjugated collagen using a Sirius red colorimetric assay as previously described [106, 107]. The mechanical properties of the nanofibrous scaffolds were measured by atomic force microscopy (AFM) using a MFP-3D AFM (Asylum Research). A modified silicon nitride tip (0.6 N/m) attached with a 20 µm-diameter borosilicate sphere was used to measure the mechanical properties of electrospun nanofiber networks. Load-displacement data were collected with an indentation and retraction speed of 2 µm/s, and a set trigger force of 20 nN. The data were used to calculate the reduced Young's moduli by the Hertz model for spherical indenters [70].

3.3.3 – Polyacrylamide gel synthesis

Polyacrylamide (PA) gels with a reduced Young's modulus of approximately 19 kPa were synthesized by a protocol similar to Yeung et al. using a bis-acrylamide solution [108].

3.3.4 – Cell culture

Human induced pluripotent stem cells (IPSCs) were derived as previously described [106] and maintained on Geltrex®-coated (Life Technologies) tissue culture plates in mTeSR™1 medium (Stem Cell Technologies). IPSCs were passaged from a tissue

culture plate to the nanofibrous scaffolds using 0.25% Trypsin-EDTA (Gibco). A ROCK inhibitor (Y-27632, 10 µM, Reagents Direct) was supplemented 1 hour prior to cell harvesting and for a day during scaffold culture to improve cell attachment and survival. Approximately 125,000 cells per cm^2 of scaffold were separately seeded onto PCL, PES, PCU, and PEKK scaffolds. The scaffold-seeded cells were maintained in mTeSR™1 medium for 5 days prior to being subjected to differentiation.

3.3.5 – Differentiation of IPSCs

After the pre-culture period on different scaffolds, the cells were subjected to directed differentiation towards either mesendodermal or ectodermal lineage. Mesendodermal differentiation of IPSCs was induced following a protocol by Oldershaw et al [109]. DMEMF12 was supplemented with the following growth factors: Day 1: WNT3A (25 ng/ml, R&D systems), Activin A (50 ng/ml, Peprotech); Day 2: WNT3A (25 ng/ml), Activin A (25 ng/ml), FGF2 (20 ng/ml, R&D systems); Day 3: WNT3A (25 ng/ml), Activin A (10 ng/ml), FGF2 (20 ng/ml), BMP4 (40 ng/ml, R&D systems). For ectodermal differentiation, a modified protocol from Shi et al. was utilized [76]. Neurobasal media (Gibco) was supplemented with B27 (Gibco), N2 (Gibco), 2 µM dorsomorphin (Compound C, Sigma-Aldrich) and 0.1 µM retinoic acid (Sigma) for 8 days [76]. Media was exchanged daily for both differentiation protocols.

Alternatively, EBs were formed by the hanging drop method using non-treated tissue culture plates and cultured for 5 days, followed by seeding them onto collagen-coated tissue culture plates. The cells spontaneously grew as a monolayer after attachment. After overnight incubation, the cells were exposed to the same differentiation regimen as those cultured on nanofibrous scaffolds.

3.3.6 – IPSC colony morphology and image analysis

To visualize cell colony morphology and the cells' interaction with electrospun scaffolds, IPSCs were fixed with 10% formalin overnight, followed by sequential dehydration prior to SEM imaging, as previously described [73, 106]. Alternatively, cell colony morphology and expression of specific protein markers were analyzed using immunocytochemistry. Briefly, samples were fixed with 4% paraformaldehyde for 30 minutes, and the cell membrane was permeabilized using 0.1% Triton-X in phosphate buffered saline (PBS). The samples were then immuno-stained for lineage-specific protein markers using respective primary (anti-NANOG (Abcam), anti-BRACHYURY (R&D systems), or anti-PAX6 (DSHB)) and secondary (Alexa Fluor 488 IgG or Alexa Fluor 594 IgG, Life Technologies) antibodies. The samples were further subjected to actin and nuclei staining using rhodamine phalloidin (Life Technologies) and 4’,6-diamidino-2-phenylindole (DAPI, Vector Laboratories), respectively. An epi-fluorescent microscope (Nikon Eclipse) or a confocal microscope (Leica SP5) was used to image the stained

samples. Imaris Bitplane 7.1.1 (Bitplane) was used to analyze the colony morphology of IPSCs and measure the sphericity (i.e., ratio of the surface area of a sphere to the surface area of the object) [74].

3.3.7 – Gene expression analysis

Total RNA was extracted using an RNeasy Micro Kit (Qiagen) and cDNA synthesis was performed using an iScript cDNA Synthesis Kit (Bio-Rad). Rt-PCR was performed to determine the gene expression of various differentiation markers using the following custom primers: *GAPDH [5'-*ATGGGGAAGGTGAAGGTCG-*3' (forward) and 5'-*TAAAAGCAGCCCTGGTGACC-*3' (reverse)]; GSC [5'-* GATGCTGCCCTACATGAACGT-*3' (forward) and 5'-*TACTTGGTCTCCTGGAAGAGGTT-*3' (reverse)]; MIXL1 [5'-*CTTTGGCTAGGCCGGAGATTA-*3' (forward) and 5'-*GGCAGGCAGTTCACATCTACCT-*3' (reverse)]; PAX6 [5'-*GAGTTCTTCGCAACCTGGCTA-*3' (forward) and 5'-*CTGCCCGTTCAACATCCTTAG-*3' (reverse)]; NEUROD1 [5'-*AAAGCCCTCTGACTGATTGCA-*3' (forward) and 5'-*GGACGGTTCGTGTTTGAAAGA-*3' (reverse)]*. The data was analyzed using the comparative threshold cycle (C_T) method with *GAPDH* used as an endogenous control [75].

3.3.8 – Statistical analysis

Experiments were conducted in triplicate unless otherwise noted, and data is represented as means ± standard deviation (SD) or standard error of means (SEM). Statistical significance was determined using SPSS (v.22.0) by one-way ANOVA with Tukey's HSD post-hoc. Bivariate correlation of two factors was determined by Pearson's correlation coefficients. Statistical significance was determined when a “p” value was less than 0.05.

3.4 – Results and Discussion

Among many factors within the stem cell niche, the mechanical microenvironment has been shown to significantly affect differentiation of multiple adult stem cell types [89, 110]. The work by Engler et al. pioneered the field by demonstrating that mesenchymal stem cells preferentially differentiate towards a specific lineage based on the substrate stiffness [110]. The substrate stiffness-dependent specification of differentiation is closely related to the cell morphology mediated by cell-ECM interactions, influencing cytoskeletal organization. However, unlike adult stem cells, human pluripotent stem cells require stable cell-cell interactions. Such colony-forming behavior dictates the balance between cell-cell and cell-ECM interactions, which modulates cellular behaviors [16, 111].

To determine how different mechanics of electrospun scaffolds affect the colony formation and differentiation of IPSCs, various scaffolds were synthesized using different polymer precursors such as poly (ε-caprolactone) (PCL), polyethersulfone (PES), polycarbonate-urethane (PCU), and polyether-ketone-ketone (PEKK) to produce nanofibers with distinct mechanical properties. Electrospinning is advantageous for scaffold synthesis since many parameters, including mechanical properties, microstructure, and surface chemistry, can be independently optimized to achieve a desired cellular response [76, 112-114]. Electrospinning parameters such as solution properties (viscosity, conductivity, and surface tension), processing parameters (electrospinning spinneret-to-collector distance, flow rate, and applied voltage) and environmental conditions (ambient temperature and humidity) were tightly controlled for each precursor to synthesize different precursor-based scaffolds with similar fiber diameters. All scaffolds showed randomly oriented nanofibers with typical cylindrical fiber morphology and their average fiber diameters were approximately 450 nm (**Figure 3.1, A-B**). To obtain the same surface chemistry of the polymeric scaffolds, the ester linkage of each polymer precursor was utilized to conjugate collagen type I on the surfaces using NHS-EDAC chemistry. A Sirius Red assay was used to confirm a relatively uniform collagen conjugation among the different nanofibrous scaffolds (**Figure 3.1C**). For mechanical characterization, atomic force microscopy (AFM) was utilized to measure the reduced Young's moduli of the scaffolds ranging from approximately 19 kPa of PCL to 313 kPa of PEKK (**Figure 3.1D**). An IPSC cell line was seeded onto these scaffolds having

distinctive mechanical properties, yet presenting similar morphological and chemical microenvironments for the cells. Their differentiation potentials were then compared to those of EB-formed cells (**Figure 3.1E**).

IPSCs seeded onto the scaffolds proliferated and formed distinct cell colonies depending on the scaffold stiffness (**Figure 3.2A**). After a pre-culture period of 5 days with proliferation media, the colonies on softer scaffolds exhibited round, 3D colony morphologies while cells on stiffer scaffolds displayed more 2D colony development. Regardless of the scaffold stiffness-dependent colony morphology, IPSCs maintained high expression of the pluripotency marker NANOG, indicating that the distinctive colony morphologies did not affect levels of pluripotency during the examined culture period (**Figure 3.2A, 3.3**). The dependency of colony morphology on scaffold stiffness was confirmed by similar cellular behaviors on the nanofibrous scaffolds conjugated with different proteins including fibronectin and Geltrex® (**Figure 3.2, B-C**). Additionally, cells on scaffolds with distinct surface chemistry also maintained high expression of NANOG. This implies that scaffold mechanics, not surface chemistry, is the main determinant for distinct colony formation. Scanning electron microscopy (SEM) clearly revealed the distinct colony morphologies (i.e., dimensionality) of IPSCs cultured on 19 kPa or 313 kPa scaffolds (**Figure 3.2D, top panel**). The differences in colony morphology were quantitatively assessed by measuring its sphericity, a degree of shape relative to the perfect sphere, via confocal microscopy and 3D rendering (**Figure 3.2, D-E**). An inverse

relationship between the IPSC colony sphericity and the reduced Young's modulus of the scaffold was observed (Pearson's correlation: -0.871, significance: 0.000) (**Figure 3.2E**).

To understand the mechanism of developing a 3D colony on 19 kPa nanofibrous scaffolds, we examined the morphological changes in cell-scaffold interactions at various time points using SEM and confocal microscopy (**Figure 3.2F**). A colony size-dependent deformation of nanofibers around the periphery of the colony suggests that IPSCs initially grow in a 2D manner, but after attaining a specific colony size they deform the fibers, resulting in the development of a 3D colony morphology. Confocal imaging confirms this hypothesis by showing the formation of a central cavity as the colony size increases. Additionally, minimal expression of apoptosis marker, Caspase-3, confirms that the formation of a central cavity is not likely due to nutrient/oxygen limitations in 3D colonies of larger sizes (**Figure 3.4**). However, our observation is limited to a colony size of ≈300 μm, and it is possible for the cells in a larger colony to suffer nutrient/oxygen deprivation due to diffusion limits. Nevertheless, to the best of our knowledge, this unique phenomenon of 3D colony formation has only been demonstrated on electrospun scaffolds with specific mechanical properties. When IPSCs were cultured on polyacrylamide gels of similar stiffness at 19 kPa, the cells did not form 3D colonies (**Figure 3.2G**). This is likely due to the combination of the differences in individually pliable networks, topography, available attachment sites and their distribution [89, 115]. Furthermore, unlike the mechanical constraint in our study, micropatterning of cell

adhesion areas did not induce 3D colony formation, indicating the significant role of the mechanical microenvironment on cell–cell and cell–ECM interactions [116, 117]. The three-dimensionality, developed by cell-mediated tension on the soft electrospun scaffolds, results in the formation of a cavity. Unlike large EBs, which form central cavities due to nutrient limitations [118], cells on electrospun scaffolds have the advantage of nutrient diffusion through the porous structure of the nanofibers (**Figure 3.2H**). Considering the fact that the maximization of cell–cell interaction by forming EBs typically results in priming of the cells for subsequent differentiation, the control of colony dimensionality using electrospun scaffolds may provide a more robust and efficient means to control pluripotent stem cell differentiation.

Following the pre-culture period, IPSCs having scaffold-dependent distinct colony morphologies were biochemically induced to differentiate towards either mesendodermal or ectodermal lineage. Under mesendodermal differentiation conditions, the degree of differentiation was positively correlated to the scaffold stiffness, and inversely related to sphericity based on the expression of mesendodermal lineage genes, *e.g.*, *GSC* and *MIXL1* (**Figure 3.5A**). In accordance with the gene expression, a greater protein expression of another mesendodermal lineage marker, BRACHYURY, was present in the cells cultured on stiffer scaffolds as compared to that on softer scaffolds (**Figure 3.5B**). Quantitatively, culture on 313 kPa scaffolds resulted in significantly higher differentiation efficiency than the EB-based method or culture on 19 kPa scaffolds, as

determined by a greater population of BRACHYURY-positive cells (**Figure 3.5C**). In contrast, IPSCs cultured on softer scaffolds (that resulted in higher sphericity) exhibited a greater tendency to differentiate to the ectodermal lineage as evident by the expression of ectodermal genes, *PAX6* and *NEUROD1* (**Figure 3.5D**). These results were also confirmed at the protein level using immunofluorescence imaging of PAX6 where IPSCs on softer scaffolds exhibited greater expression as compared to stiffer scaffolds (**Figure 3.5E**). The IPSCs with spherical colony morphology resulted in a higher percentage of PAX6-positive cells as compared to an EB-based differentiation, a typical cell culture method to enhance ectodermal differentiation (**Figure 3.5F**).

3.5 – Conclusions

Collectively, the results demonstrate that colony dimensionality, which controls cell–cell interactions, can be engineered by electrospun scaffold stiffness due to cellular adaptation to the mechanical microenvironment. The colony dimensionality developed during IPSC self-renewal significantly affects subsequent lineage-specific differentiation efficiency. Therefore, this universal technology provides a novel and facile means to direct cellular behaviors to achieve enhanced differentiation efficiency of IPSCs toward many different target cell types. Furthermore, the synthetic nature of the scaffolds would also facilitate human clinical applications of IPSCs by minimizing the use of animal-derived products to avoid possible xeno-contaminations.

3.6 – Figures

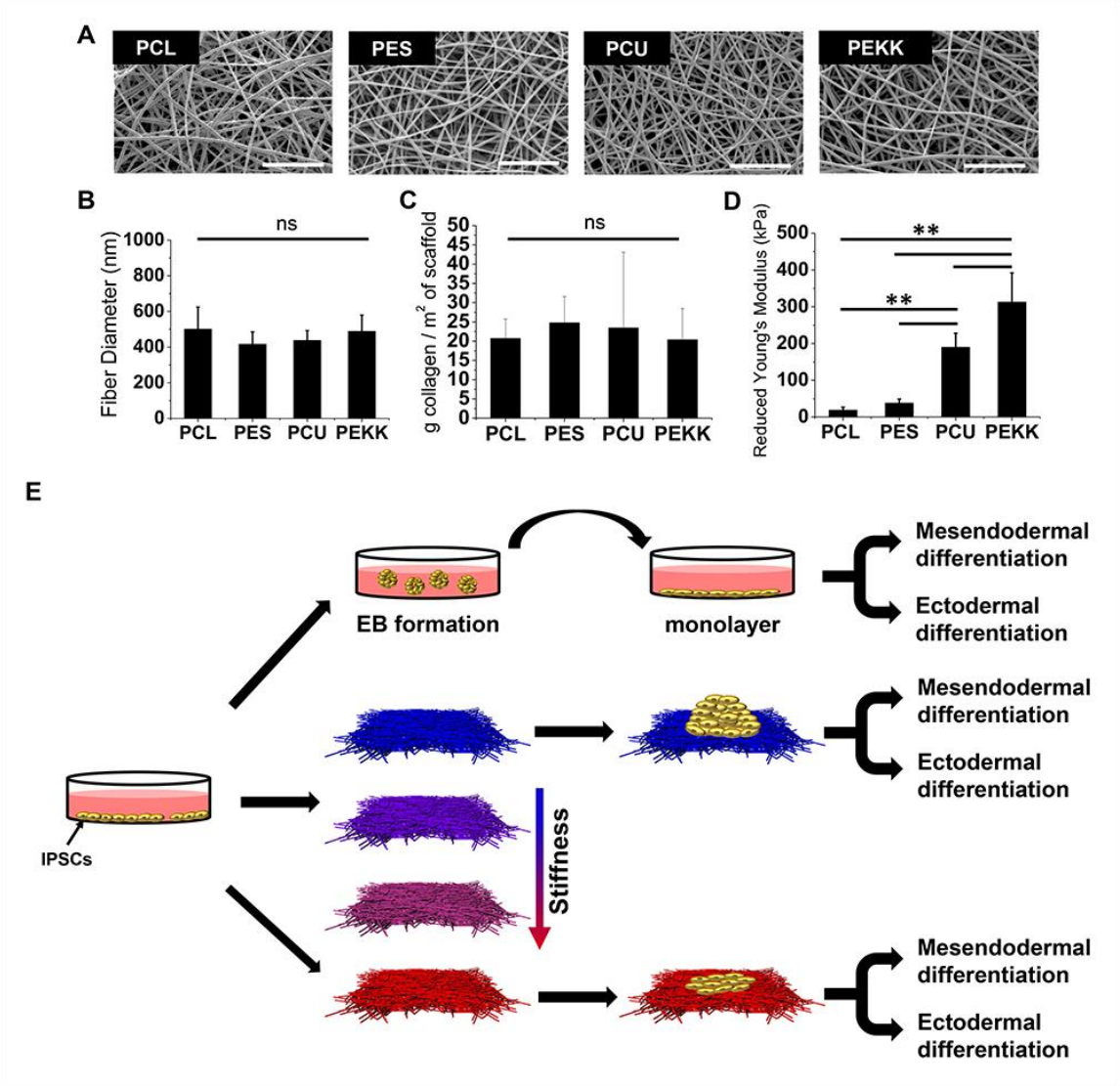
A
PCL
PES
PCU
PEKK
B
Fiber Diameter (nm)
ns
C
g collagen / m² of scaffold
ns
D
Reduced Young's Modulus (kPa)
**
**
E
IPSCs
EB formation
monolayer
Mesendodermal differentiation
Ectodermal differentiation
Stiffness

FIGURE 3.1. MORPHOLOGICAL, SURFACE CHEMICAL, AND MECHANICAL CHARACTERIZATION OF ELECTROSPUN SCAFFOLDS AND AN EXPERIMENTAL DESIGN TO DETERMINE THE EARLY-STAGE DIFFERENTIATION OF HUMAN INDUCED PLURIPOTENT STEM CELLS (IPSCS) ON NANOFIBROUS SCAFFOLDS WITH DISTINCT STIFFNESSES.

(A) SEM images of electrospun poly (ε-caprolactone) (PCL), polyethersulfone (PES), polycarbonate-urethane (PCU), and polyether-ketone-ketone (PEKK) scaffolds displaying similar cylindrical fibrous morphology (scale bar: 10 μm). (B) Average fiber diameters, (C) collagen content conjugated on the nanofiber surfaces, and (D) reduced Young's modulus of the electrospun scaffolds. (E) A schematic depicting an experimental procedure to examine scaffold mechanics-dependent IPSC colony formation and subsequent differentiation towards mesendodermal or ectodermal lineage as compared to traditional embryoid body (EB)-based differentiation. The data are shown as means ± standard deviation (n=6). ** and 'ns' denote $p < 0.01$ and no statistical significance, respectively.

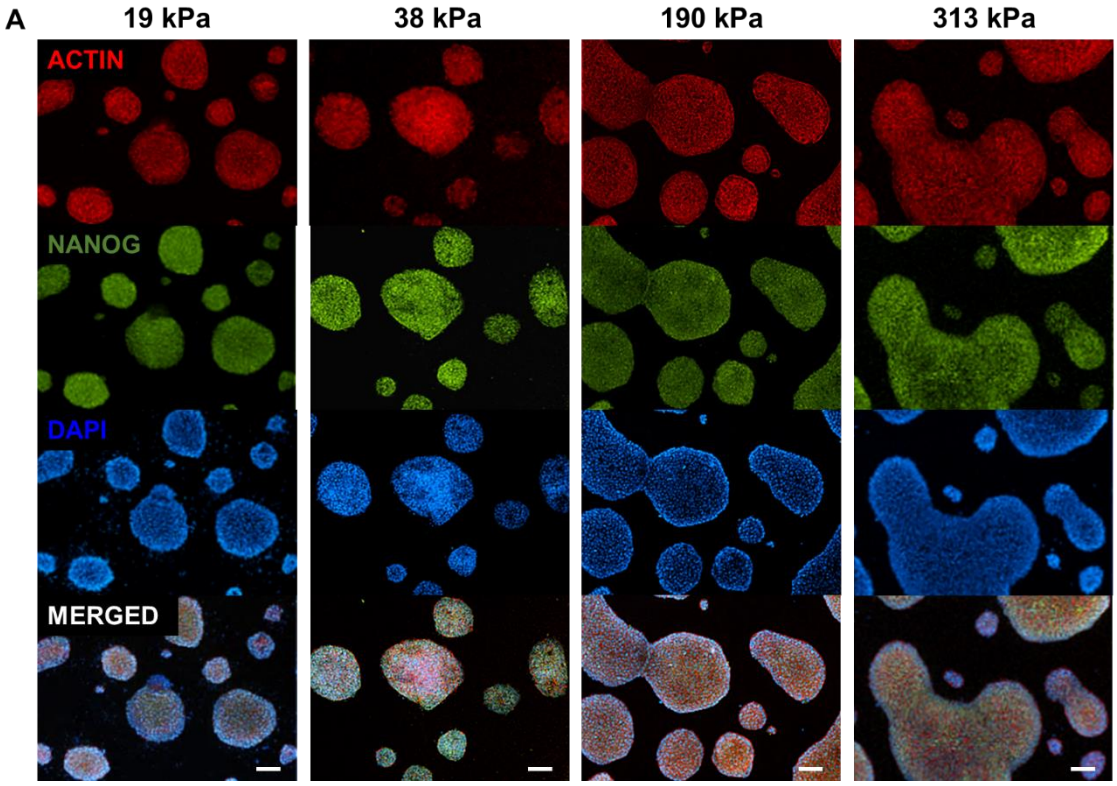

FIGURE 3.2. THE EFFECTS OF SCAFFOLD-STIFFNESS ON THE DIMENSIONALITY OF IPSC COLONY.

(A) IPSCs formed round, 3D colonies on softer scaffolds, while stiffer scaffolds induced a flat, 2D colony morphology after 5 days of culture in proliferation media. IPSCs maintained high expression of pluripotency marker NANOG, independent of the colony morphology (red: actin, green: NANOG, blue: DAPI, scale bar: 100 μm).

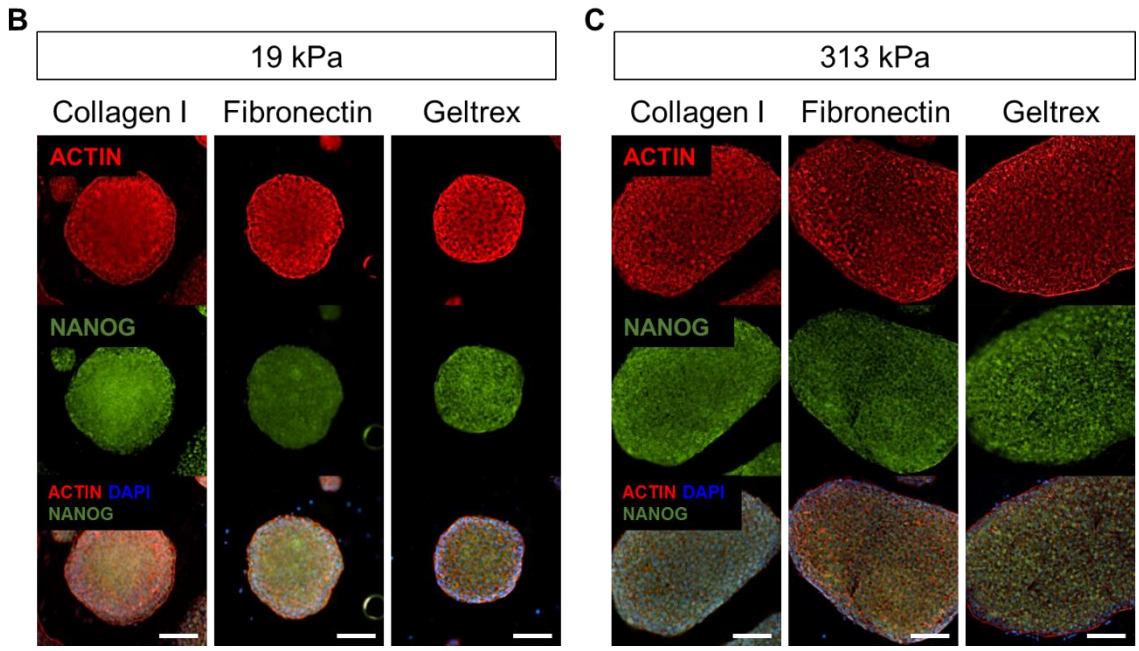

FIGURE 3.3. THE EFFECTS OF SCAFFOLD-STIFFNESS ON THE DIMENSIONALITY OF IPSC COLONY.

(B-C) Regardless of surface chemistry, IPSCs maintained expression of NANOG and formed 3D colonies on 19 kPa scaffolds and 2D colonies on 313 kPa scaffolds (red: actin, green: NANOG, blue: DAPI, scale bar: 100 µm).

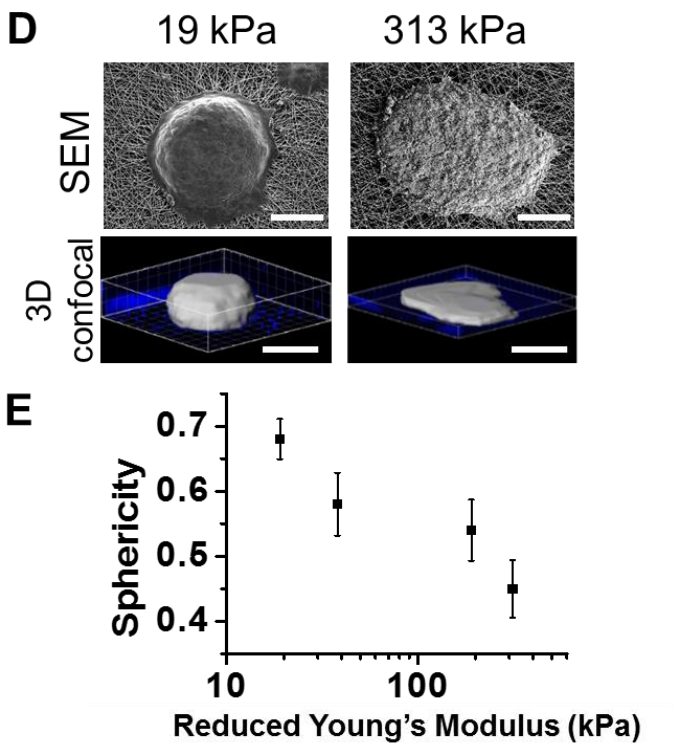

FIGURE 3.4. THE EFFECTS OF SCAFFOLD-STIFFNESS ON THE DIMENSIONALITY OF IPSC COLONY.

(D) SEM images (top) and 3D reconstruction of confocal images (bottom) showing the representative colony morphologies of IPSCs cultured on soft (19 kPa) and stiff (313 kPa) scaffolds (scale bar: 200 μm). (E) The sphericity of IPSC colonies from the 3D reconstruction of confocal imaging exhibits an inverse relationship to the scaffold stiffness. Pearson's correlation: -0.871 and significance: 0.000 (n=5).

F

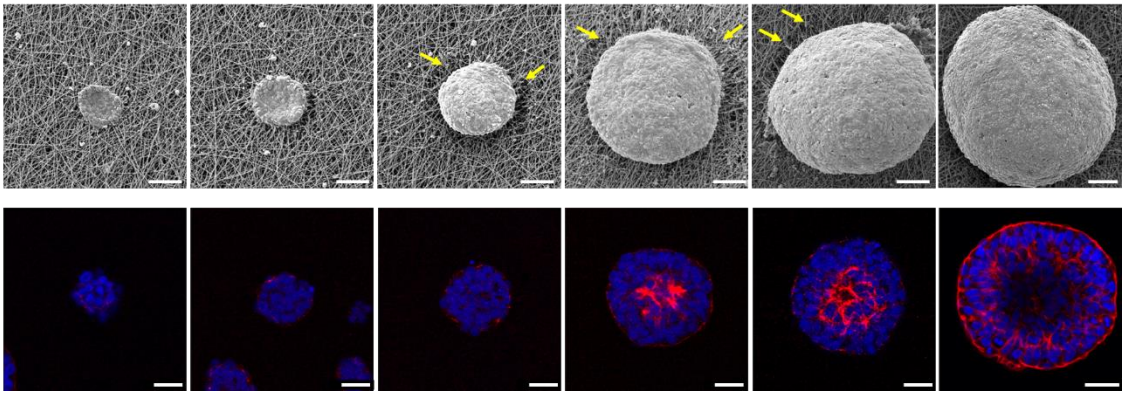

FIGURE 3.5. THE EFFECTS OF SCAFFOLD-STIFFNESS ON THE DIMENSIONALITY OF IPSC COLONY.

(F) The size-dependent development of 3D colony morphology on 19 kPa scaffolds correlated with deformation of fibers (yellow arrows) at the periphery of the colony. Z-cross-sections from confocal imaging, which are depicted at the bottom, revealed a size-dependent cavity formation within the center of the colony (scale bar: 50 µm).

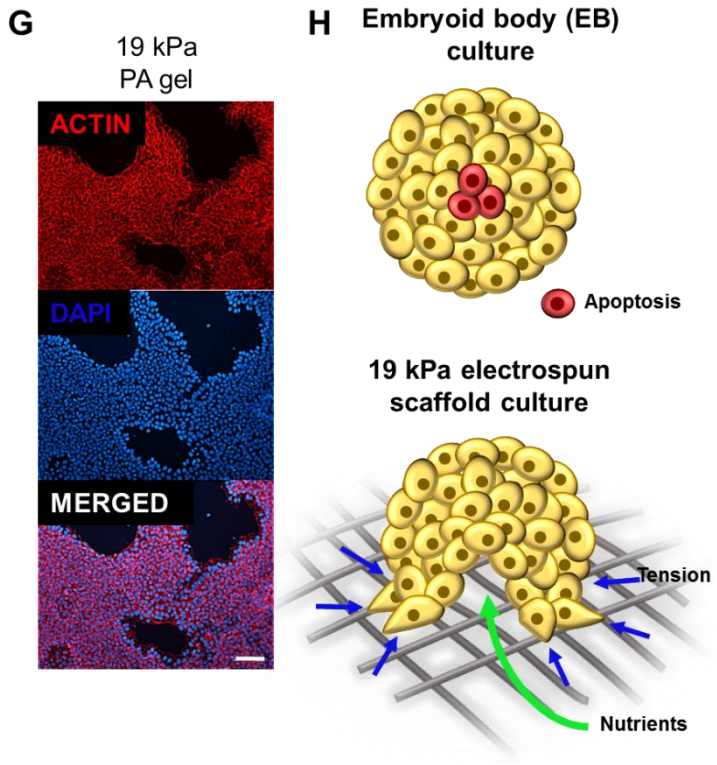

FIGURE 3.6. THE EFFECTS OF SCAFFOLD-STIFFNESS ON THE DIMENSIONALITY OF IPSC COLONY.

(G) IPSCs cultured on a 19 kPa polyacrylamide (PA) gel did not form 3D colonies after 5 days of culture in proliferation media (scale bar: 100 µm). (H) The proposed mechanism of IPSC behaviors in 3D colonies formed by EB vs. electrospun scaffolds.

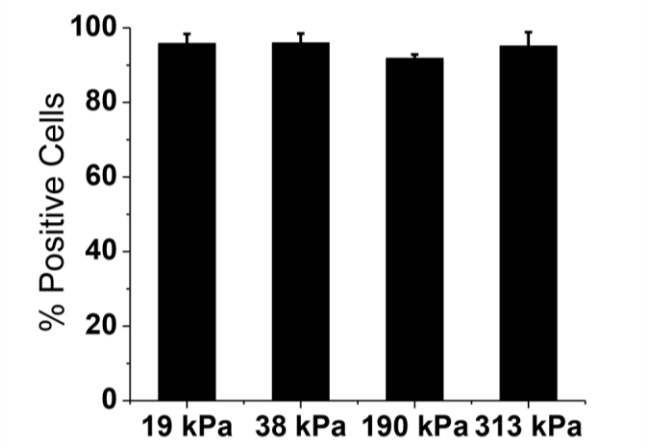

FIGURE 3.3. IPSCS MAINTAIN PLURIPOTENCY REGARDLESS OF SCAFFOLD STIFFNESS.

After 5 days of culture in proliferation media, IPSCs formed distinct colony morphologies depending on scaffold stiffness. Quantitative analysis showed a similar high percentage of NANOG-positive cells, indicating the maintenance of pluripotency regardless of scaffold stiffness. The data are shown as means ± standard deviation (n=10). No significant statistical difference was found.

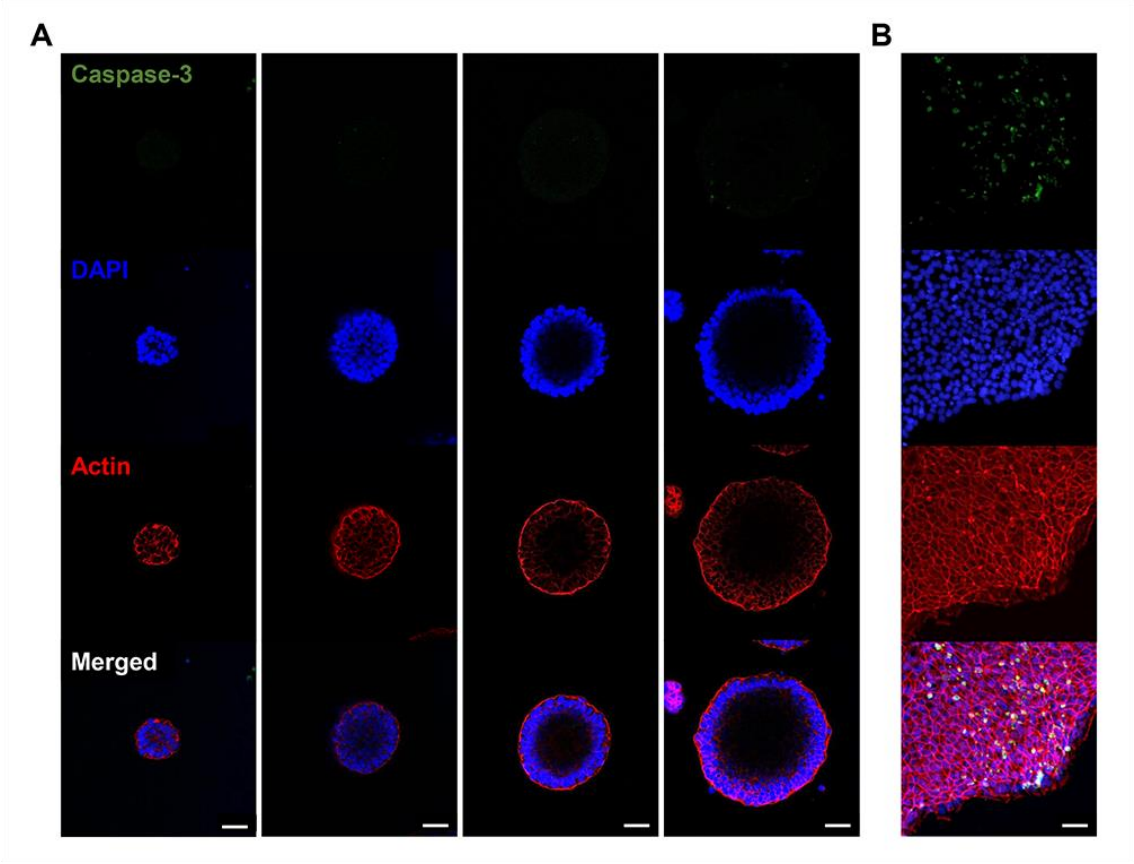

FIGURE 3.7. DEVELOPMENT OF 3D COLONY MORPHOLOGY IS NOT A RESULT OF APOPTOSIS.

The development of 3D colonies on 19 kPa scaffolds results in a size-dependent cavity formation. During this cavity development, no significant expression of apoptosis marker, Caspase-3, was observed in the cells near the cavity (green: Caspase-3, blue: DAPI, red: actin, scale bar: 50 µm).

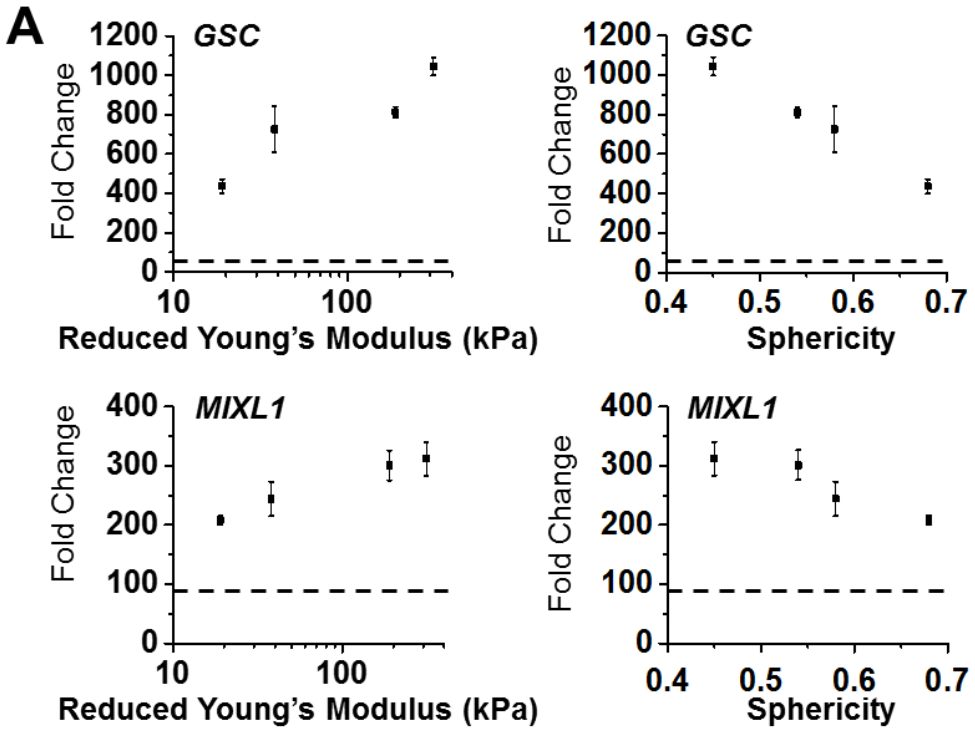

FIGURE 3.8. SCAFFOLD STIFFNESS-DEPENDENT COLONY MORPHOLOGY OF IPSCS MODULATES LINEAGE-SPECIFIC DIFFERENTIATION.

(A) Under directed mesendodermal differentiation by WNT3A and Activin A, the relative gene expression of GSC and MIXL1, mesendodermal lineage markers, are positively related to scaffold stiffness (left) and inversely related to IPSC colony sphericity (right), examined by rt-PCR. IPSCs were pre-cultured in proliferation media for 5 days to obtain distinct colony morphologies, and then subjected to mesendodermal differentiation media for 60 hours. Gene expression was normalized to IPSCs cultured in proliferation media on tissue culture plates. The dashed line denotes the gene expression of the cells subjected to an embryoid body (EB)-based mesendodermal lineage differentiation. The data are shown as means ± standard error of means (n = 6 for rt-PCR).

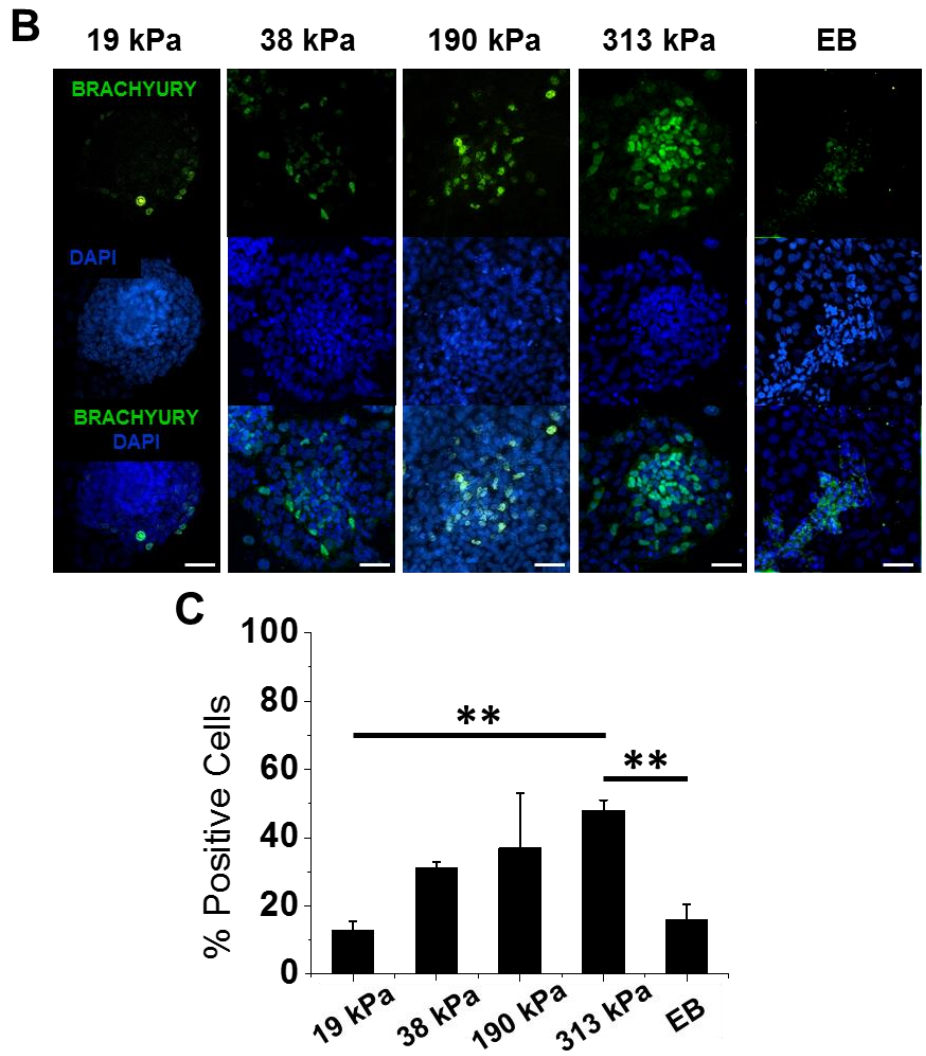

FIGURE 3.9. SCAFFOLD STIFFNESS-DEPENDENT COLONY MORPHOLOGY OF IPSCS MODULATES LINEAGE-SPECIFIC DIFFERENTIATION.

(B) The expression of BRACHYURY, a mesendodermal lineage marker, is positively related to the scaffold stiffness (or inversely to the sphericity) (green: BRACHYURY, blue: DAPI, scale bar: 50 μm), and (C) confirmed by quantification of % positive cells. IPSCs were pre-cultured in proliferation media for 5 days to obtain distinct colony morphologies, and then subjected to mesendodermal differentiation media for 60 hours. Gene expression was normalized to IPSCs cultured in proliferation media on tissue culture plates. The dashed line denotes the gene expression of the cells subjected to an embryoid body (EB)-based mesendodermal lineage differentiation. The data are shown as means ± standard error of means (n = 10 for % positive cell quantification). ** denotes $p < 0.01$.

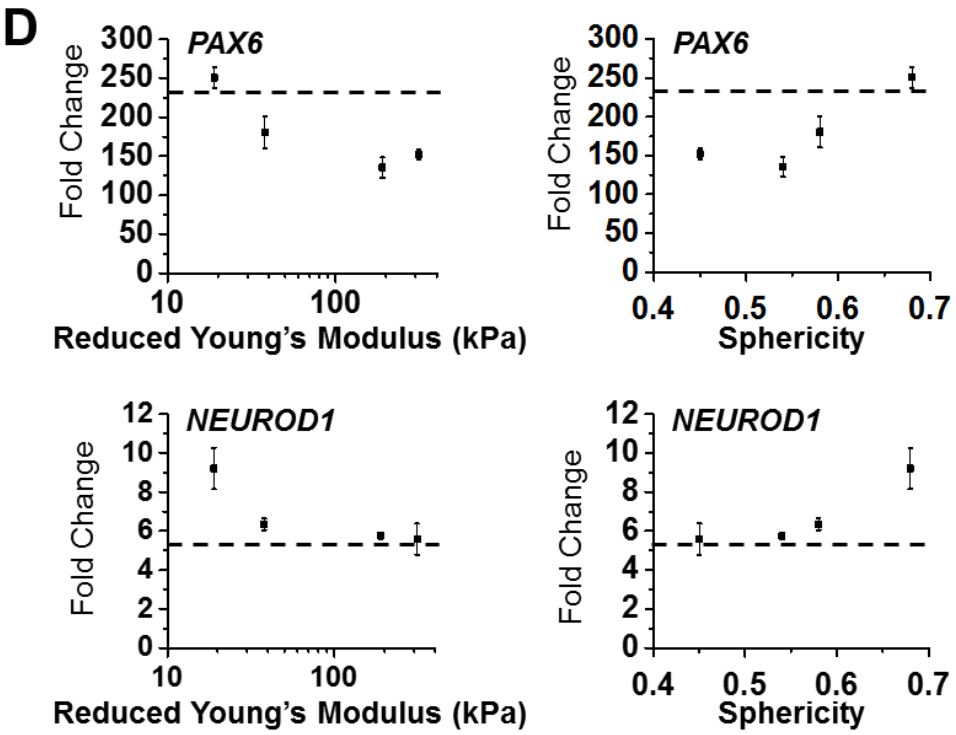

FIGURE 3.10. SCAFFOLD STIFFNESS-DEPENDENT COLONY MORPHOLOGY OF IPSCS MODULATES LINEAGE-SPECIFIC DIFFERENTIATION.

(D) Under directed ectodermal differentiation by retinoic acid and dorsomorphin, the relative gene expression of PAX6 and NEUROD1, ectodermal lineage markers, are inversely related to scaffold stiffness (left) and positively related to IPSC colony sphericity (right), examined by rt-PCR. IPSCs were pre-cultured in proliferation media for 5 days to obtain distinct colony morphologies, and then subjected to ectodermal differentiation media for 8 days. Gene expression was normalized to IPSCs cultured in proliferation media on tissue culture plates. The dashed line denotes the gene expression of the cells subjected to an embryoid body (EB)-based ectodermal lineage differentiation. The data are shown as means ± standard error of means (n = 6 for rt-PCR).

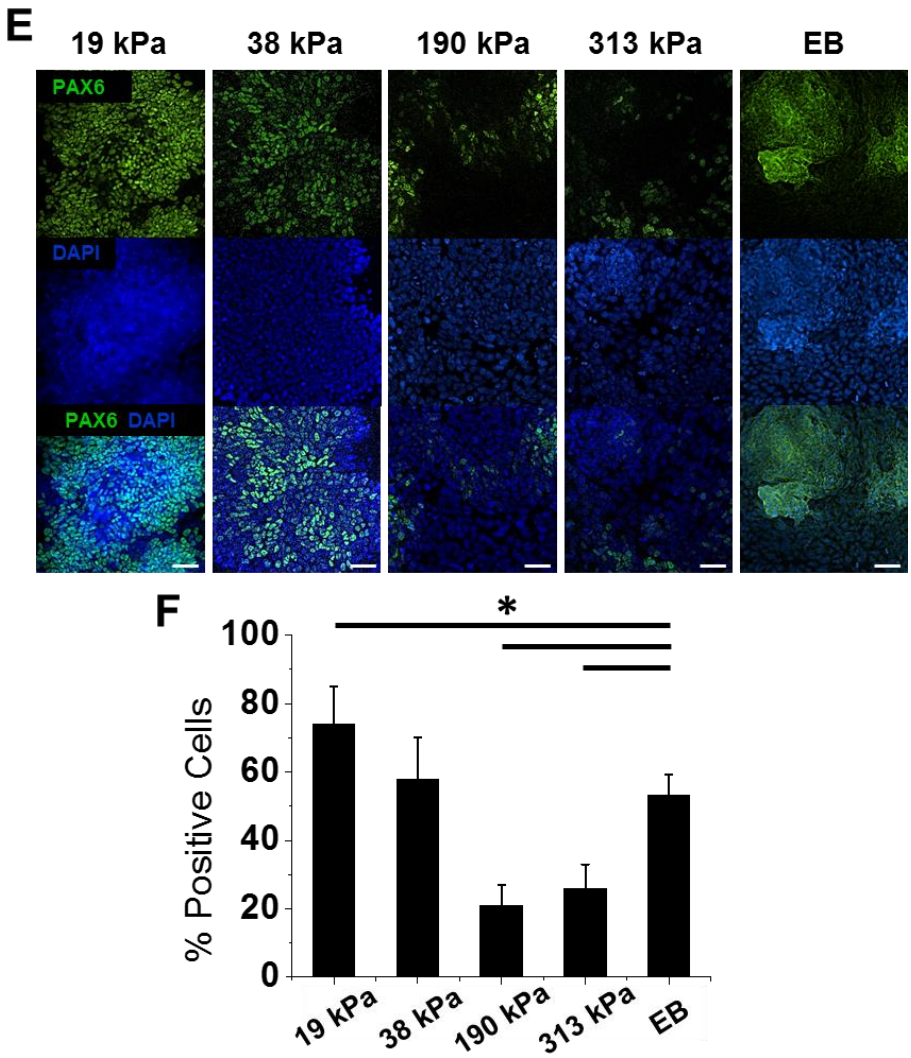

FIGURE 3.11. SCAFFOLD STIFFNESS-DEPENDENT COLONY MORPHOLOGY OF IPSCS MODULATES LINEAGE-SPECIFIC DIFFERENTIATION.

(E) The expression of PAX6 is inversely related to the scaffold stiffness (or positively related to the sphericity) (green: PAX6, blue: DAPI, scale bar: 50 μm), and (F) confirmed by quantification of % positive cells. IPSCs were pre-cultured in proliferation media for 5 days to obtain distinct colony morphologies, and then subjected to ectodermal differentiation media for 8 days. Gene expression was normalized to IPSCs cultured in proliferation media on tissue culture plates. The dashed line denotes the gene expression of the cells subjected to an embryoid body (EB)-based ectodermal lineage differentiation. Note that EB-based differentiation was highly non-uniform and an area displaying a cell aggregate with PAX6 expression is shown. The data are shown as means ± standard error of means (n = 10 for % positive cell quantification). * denotes $p < 0.05$.

CHAPTER 4 – ROCK INHIBITOR PRIMES HUMAN INDUCED PLURIPOTENT STEM CELLS TO SELECTIVELY DIFFERENTIATE TOWARDS MESENDODERMAL LINEAGE VIA EPITHELIAL-MESENCHYMAL TRANSITION-LIKE MODULATION

4.1 – Abstract

Our previous results demonstrated that scaffold stiffness results in the development of distinct IPSC colony morphologies with different cytoskeletal organization. The difference in cytoskeletal organization ultimately led to changes in IPSC behaviors, including self-renewal and lineage-specific differentiation potentials. Such a differential cytoskeletal organization has been associated with the RhoA activity in mesenchymal stem cells. In this context, we hypothesized that modulation of the cell cytoskeleton via Rho-associated protein kinase (ROCK) inhibition would bias the differentiation potential of hIPSCs even in the absence of a physical microenvironment change on tissue culture plastic.

Robust control of human induced pluripotent stem cell (hIPSC) differentiation is essential to realize its patient-tailored therapeutic potential. Here, we demonstrate a novel application of Y-27632, a small molecule Rho-associated protein kinase (ROCK) inhibitor, to significantly influence the differentiation of hIPSCs in a lineage-specific manner. The application of Y-27632 to hIPSCs resulted in a decrease in actin bundling and disruption of colony formation in a concentration and time-dependent manner. Such changes in cell and colony morphology were associated with decreased expression of E-cadherin, a cell-cell junctional protein, proportional to the increased exposure to Y-27632.

Interestingly, gene and protein expression of pluripotency markers such as NANOG and OCT4 were not downregulated by an exposure to Y-27632 up to 36 h. Simultaneously, epithelial-to-mesenchymal (EMT) transition markers were upregulated with an exposure to Y-27632. These EMT-like changes in the cells with longer exposure to Y-27632 resulted in a significant increase in the subsequent differentiation efficiency towards mesendodermal lineage. In contrast, an inhibitory effect was observed when cells were subjected to ectodermal differentiation after prolonged exposure to Y-27632. Collectively, these results present a novel method for priming hIPSCs to modulate their differentiation potential with a simple application of Y-27632.

This chapter has been reproduced from *Maldonado M. et al., 2016, ROCK inhibitor primes human induced pluripotent stem cells to selectively differentiate towards mesendodermal lineage via epithelial-mesenchymal transition-like modulation, *Stem Cell Research*, *in press*.

*Adapted from manuscript: Figures: 4.1–4.8

4.2 – Introduction

The derivation of human induced pluripotent stem cells (hIPSCs) has provided a technological foundation to produce a clinically-relevant, large quantity of cells, potentially offering a solution for cell source limitations in cell therapies and regenerative medicine [119, 120]. Due to the difficulties in controlling behaviors of these cells *in vivo*, however, it is of great interest to develop *in vitro* methods/protocols to direct the differentiation of hIPSCs to specific phenotypes prior to implantation. In this regard, the physiochemical cues to direct lineage/phenotype-specific differentiation have been widely studied to identify the suitable physical and biochemical microenvironment to trigger specific signaling cascades mediating the subsequent differentiation process [76, 109, 120]. Previous work in our lab demonstrated that varying the physical microenvironment, by means of scaffold mechanics, results in the development of distinct hIPSC colony morphologies with different cytoskeletal organization [106]. The difference in cytoskeletal organization ultimately led to changes in IPSC behaviors, including self-renewal and lineage-specific differentiation potentials [106, 121]. Such a differential cytoskeletal organization has been associated with the RhoA activity in mesenchymal stem cells [53]. In this context, we hypothesized that modulation of the cell cytoskeleton via Rho-associated protein kinase (ROCK) inhibition would bias the differentiation potential of hIPSCs even in the absence of a physical microenvironment change.

Previous studies have focused on defining the role of Y-27632, a ROCK inhibitor, in preventing hIPSC dissociation-induced apoptosis of human pluripotent stem cells [122, 123]. Although such efforts have provided an essential means to enhance hIPSC survival during cell expansion, we also observed that cell morphology was significantly affected by Y-27632. Based on this observation, we aimed to examine how pharmacological manipulation of cytoskeletal organization in hIPSCs modulates the self-renewal and differentiation potential of the cells. In this report, we show that a widely used small molecule Y-27632 primes hIPSCs to selectively differentiate towards mesendodermal lineage in an exposure duration-dependent manner. Specifically, the results suggest that the inhibition of ROCK initiates epithelial-mesenchymal transition (EMT)-like changes in hIPSCs to promote mesendodermal differentiation. Overall, we demonstrate a facile method to regulate cell and colony organization, which in turn promotes the early stage differentiation of hIPSCs in a lineage-specific manner.

4.3 – Materials and Methods

4.3.1 – Cell culture

Human induced pluripotent stem cells were derived as previously described [106]. Cells were passaged using 0.25% Trypsin-EDTA (Life Technologies, Grand Island, NY) onto Geltrex®-coated tissue culture plastic or glass coverslips. To enhance initial cell survival,

hIPSCs were seeded in the presence of ROCK inhibitor, Y-27632 (EMD Millipore, Billerica, MA) at 10 μM for 12 hours, and the media was changed to regular maintenance media, mTeSR™1 (STEMCELL Technologies, Vancouver, Canada) for an additional 12 hours to obtain a typical hIPSC cell/colony morphology. During the following pre-culture period, cells were exposed to Y-27632 with various concentrations and exposure durations, and subsequently subjected to gene and protein analyses. Alternatively, the cells after the pre-culture period were subjected to either a mesendodermal or an ectodermal differentiation protocol. For mesendodermal induction, temporally varied concentrations of Activin A (Peprotech, Rocky Hill, NJ), WNT3A (R&D systems, Minneapolis, MN), FGF2 (Invitrogen, Carlsbad, CA), and BMP4 (R&D systems) were used over the course of 60 hours [109]. Specifically, Day 1: WNT3A (25 ng/ml), Activin A (50 ng/ml), Day 2: WNT3A (25 ng/ml), Activin A (25 ng/ml), FGF2 (20 ng/ml), Day 3: WNT3A (25 ng/ml), Activin A (10 ng/ml), FGF2 (20 ng/ml), BMP4 (40 ng/ml). To induce ectodermal differentiation, the cells were subjected to a modified protocol using neurobasal media supplemented with N2 (Life Technologies), B27 (Life Technologies), 2 μM dorsomorphin (Sigma-Aldrich, St. Louis, MO), and 0.1 μM retinoic acid (Sigma-Aldrich) for 72 hours [76]. During the differentiation processes, the cells were optically observed by a BioStation CT (Nikon, Melville, NY) at the indicated time points. Analysis of lineage-specific gene expression was conducted after 60 hours under mesendodermal differentiation condition or 72 hours of ectodermal differentiation. To further confirm the differentiation tendencies of PSCs, a human

embryonic stem cell (hESC) line WA09 (WiCell, Madison, WI) was also exposed to a similar culture regimen to analyze their differentiation tendencies.

4.3.2 – Immunocytochemistry

To analyze hIPSC morphology and expression of lineage specific markers, cells treated with various conditions were fixed with 4% paraformaldehyde for 30 min. After rinsing with phosphate buffered saline (PBS), the fixed cells were permeabilized using a 0.1% Triton-X solution. The cells were then blocked with a 1% BSA in PBS solution for 30 min followed by incubation with respective primary antibodies (mouse anti-NANOG (R&D systems), rabbit anti-E-cadherin (Abcam, San Francisco, CA), goat anti-BRACHYURY (R&D Systems), or mouse anti-PAX6 (DSHB, Iowa City, IA)) at 4 °C overnight. The samples were stained with their respective secondary antibodies (donkey anti-mouse 488, goat anti-mouse 594, goat anti-rabbit 488, or donkey anti-goat 488 (Invitrogen)). Actin and nuclei were counter-stained using rhodamine phalloidin (Life Technologies) and DAPI (4',6-diamidino-2-phenylindole, Vector Laboratories, Burlingame, CA), respectively. Images were acquired using a Nikon Eclipse microscope and Image J software was used to quantitatively assess cell morphology and staining intensity.

4.3.3 – Gene expression analysis

To quantify gene expression, an RNeasy Micro kit was used to extract total RNA from samples (Qiagen, Valencia, CA) and an iScript cDNA Synthesis Kit was used for cDNA synthesis (Bio-Rad, Hercules, CA) as described previously [106]. The following custom primer sequences were used for rt-PCR gene expression analysis: *GAPDH [5'-ATGGGGAAGGTGAAGGTCG-3' (forward) and 5'-TAAAAGCAGCCCTGGTGACC-3' (reverse)]; OCT4 [5'-TCCCAGGACATCAAAGCTCTG-3' (forward) and 5'-CATCGGCCTGTGTATATCCCA-3' (reverse)]; NANOG [5'-GCTTATTCAGGACAGCCCTGA-3' (forward) and 5'-TTTGCGACACTCTTCTCTGCA-3' (reverse)]; FN1 [5'-CCCAATTCCTTGCTGGTATCA-3' (forward) and 5'-TATTCGGTTCCCGGTTCCA-3' (reverse)]; SNAI2 [5'-AGACCCTGGTTGCTTCAAGGA-3' (forward) and 5'-CCTCAGATTTGACCTGTCTGCA-3' (reverse)]; SNAI1 [5'-CTCAGATGTCAAGAAGTACCAGTGC-3' (forward) and 5'-ACTCTTGGTGCTTGTGGAGCAG-3' (reverse)]; LEF1 [5'-GAGCACTTTTCTCCAGGATCACA-3' (forward) and 5'-ATCAGGAGCTGGAGGATGTCTG-3' (reverse)]; T [5'-GGGTCCACAGCGCATGAT-3' (forward) and 5'-TGATAAGCAGTCACCGCTATGAA-3' (reverse)]; MIXL1 [5'-CTTTGGCTAGGCCGGAGATTA-3' (forward) and 5'-GGCAGGCAGTTCACATCTACCT-3' (reverse)]; SOX17 [5'-ACCGCACGGAATTTGAACA-3' (forward) and 5'-AGATTCACACCGGAGTCATGC-3' (reverse)]; FOXA2 [5'-TCCATCAACAACCTCATGTCCT-3' (forward) and 5'-CATCACCTGTTCGTAGGCCTTG-3' (reverse)]; EOMES [5'-GATGGCGTGGAGGACTTGAAT-3' (forward) and 5'-*

CGGTGTTTTGGTAGGCAGTCA-3' (reverse)]; NODAL [5'-CTGGATCATCTACCCCAAGCA-3' (forward) and 5'-ATGAAACTCCTCCCCAACAGG-3' (reverse)]; PAX6 [5'-GAGTTCTTCGCAACCTGGCTA-3' (forward) and 5'-CTGCCCGTTCAACATCCTTAG-3' (reverse)]; SIP1 [5'-TCCACCTCAAAGCGCATTTC-3' (forward) and 5'-GGTATGGTCGTAGCCCAGGAAT-3' (reverse)]; SOX1 [5'-AACGCCTTCATGGTGTGGT-3' (forward) and 5'-TGATCTCCGAGTTGTGCATCTT-3' (reverse)]; OTX2 [5'-AGAGCTAAGTGCCGCCAACAA-3' (forward) and 5'-TTCCCGAGCTGGAGATGTCTT-3' (reverse)]; NCAM1 [5'-GCGAGGTATTTGCCTATCCCA-3' (forward) and 5'-CTGTAATTGGAGCTTGGCAGC-3' (reverse)]. The data was analyzed using the comparative threshold cycle (C_T) method with *GAPDH* used as an endogenous control [75].

4.3.4 – Statistical Analysis

All experiments were conducted at least in triplicate biological samples and data is represented as means ± standard error of means (SEM). SPSS (v.23.0) software was used to determine statistical significance using either one-way ANOVA with Tukey's post-hoc or one sample student t-test. Pearson's correlation coefficient was determined to reveal bivariate correlation between two factors. The difference was considered significant when a 'p' value was < 0.05.

4.4 – Results and Discussion

4.4.1 – ROCK inhibitor modulates the colony and cellular morphologies of human induced pluripotent stem cells

A ROCK inhibitor, Y-27632, has been conventionally utilized on hIPSCs for its pro-survival effect after dissociation from their typical colony formation to single cells during culture [122, 123]. The application of Y-27632, even at lower concentrations, e.g., 10 μM Y-27632, accommodates cell attachment after dissociation and subsequent survival. However, such cellular behaviors are associated with the development of distinct cell morphologies, which is known to affect differentiation in adult stem cells [115]. Thus, we first examined how different concentrations of Y-27632 affect the cell morphology and colony formation of hIPSCs. During culture in maintenance media (mTeSR^{TM}1) for 36 hours with various concentrations of Y-27632, up to 50 μM, noticeable differences in cell detachment/apoptosis were not observed throughout the culture period regardless of the concentration (**Figure 4.1, A-B**). Significant changes in cell colony morphology, however, were observed with the application of Y-27632 (**Figure 4.1, A-B**). As the concentration of Y-27632 increased, the cells dispersed, forming loosely populated colonies. Albeit Y-27632 effectively disrupted hIPSC colony formation, the cells maintained expression of pluripotency marker NANOG for the examined duration. The changes in individual cell morphology were also observed by immunofluorescence

imaging (**Figure 4.1C**). Quantitative analysis of cell morphology based on the projected cytoplasmic area revealed greater cell spreading with the increased Y-27632 concentration (Pearson's correlation coefficient: 0.740, significance; 0.000) (**Figure 4.1D**). The changes in cell shape were associated with cytoskeletal reorganization as evident from actin bundling changes, which was significantly decreased with the increased Y-27632 concentration (Pearson's correlation coefficient: -0.423, significance: 0.000) (**Figure 4.1E**). Based on these observations, we utilized 40 μM Y-27632 for the subsequent experiments, which was the minimum concentration eliciting significant effects on the colony and cell morphologies of hIPSCs without altering their protein expression of pluripotency marker NANOG.

4.4.2 – ROCK inhibitor affects hIPSC morphology and gene expression of EMT markers in an exposure duration-dependent manner

To explore the exposure duration-dependent changes in cell and colony morphologies, hIPSCs were cultured in the maintenance media supplemented with 40 μM Y-27632 for either 0, 2, 12, 24, or 36 hours during the pre-culture period prior to the start of differentiation (**Figure 4.3A**). Similar to our concentration study, cell and colony morphologies were significantly disrupted with the addition of Y-27632 as compared to the control (**Figure 4.3B**). Before the supplementation with Y-27632, cells developed colonies with well-defined boundaries, but within 2 hours after the addition of Y-27632

the cells at the periphery of the colonies developed extensions and exhibited an elongated, spread morphology (**Figure 4.2**).

A longer exposure to Y-27632 had more significant effects on cell morphology evident by a decrease in actin bundling (**Figure 4.3B**). Such distinguishable differences in cell/colony morphology led us to examine differences in cell-cell junction protein E-cadherin (**Figure 4.3C**). Increasing exposure to Y-27632 resulted in a remarkable disruption of E-cadherin expression at the cell junctions (**Figure 4.3, C-D**). For shorter exposure durations, the effects of Y-27632 were primarily localized to cells at the periphery of the hIPSC colonies. These findings were also confirmed with a human ESC line where a noticeable decrease in E-cadherin expression and actin bundling within the cytoplasm were observed (**Figure 4.5A**).

Because E-cadherin expression is one of the markers typically used to determine pluripotency in hIPSCs, we also examined the expression of pluripotency marker NANOG. No significant differences in NANOG expression were observed for the examined durations (**Figure 4.3, C-D**). Additionally, gene expression of *OCT4* and *NANOG*, pluripotent genes, were not significantly downregulated after 36 hours of exposure to Y-27632 in both the hIPSC and hESC cell lines (**Figure 4.3E, 4.5B**). A similar observation was noted in a study where the upregulation/maintenance of pluripotency markers was shown at the early stage of pluripotent stem cell differentiation to mesendodermal

lineage [109]. Although we observed sustained expression of pluripotency markers, further analysis is required to determine if the cells truly maintain pluripotency. The cell-cell interaction changes in pluripotent stem cells are often associated with an EMT, which results in a loss of E-cadherin expression at the cell-cell junctions similar to our observation in the current study [21].

To determine if the application of ROCK inhibitor induces such a transition, we next examined the gene expression of EMT markers in the cells stimulated by Y-27632 (**Figure 4.3F, 4.4**). Increases in gene expression of EMT markers, *FN1*, *SNAI2*, *SNAI1*, and *LEF1*, were detected with increased exposure to Y-27632 (**Figure 4.3F, 4.4**). These observations collectively suggest that the application of the ROCK inhibitor, in an exposure duration-dependent manner, primes the cells for EMT. In this regard, Richter et al. demonstrated the importance of EMT-related genes in mediating BMP4-stimulated mesendodermal differentiation of human embryonic stem cells; it was shown that differentiation was primarily localized in the cells at the edges of colonies, which displayed disrupted E-cadherin organization with enhanced cell migration [124].

In comparison, our results demonstrate that Y-27632 effectively modulates the cell/colony morphology of hIPSCs similar to the migrating cells during EMT, which maintain a more spread morphology and exhibit a decrease in cell-cell junctional E-cadherin. Additionally, similar behaviors were observed in the hESC line (**Figure 4.5**).

Therefore, the morphological control of PSCs by Y-27632 may provide a means to prime the cells for subsequent differentiation.

4.4.3 – Morphological modulation of hIPSCs with Y-27632 enhances mesendodermal differentiation, but not ectodermal differentiation, in an exposure duration-dependent manner

Based on the observed close relationship between cell morphology and the specification of differentiation in various adult stem cells types [53], we hypothesized that the morphological changes of hIPSCs by Y-27632 would bias the differentiation potential of the cells. To examine the effects of Y-27632 on the differentiation potential of hIPSCs, cells were pre-cultured for 36 hours with various exposure durations to Y-27632 prior to the start of mesendodermal differentiation by Activin A and WNT3A (**Figure 4.3A**). No significant differences in expression of mesendodermal markers *T* and *MIXL1* were observed for the 2 hour pre-culture with Y-27632 (**Figure 4.6A**). In contrast, *T* and *MIXL1* were significantly enhanced by pre-culture with Y-27632 for longer exposure times of 12, 24, and 36 hours. Markers of both endodermal (*SOX17* and *FOXA2*) and mesodermal (*EOMES* and *NODAL*) lineage were also significantly upregulated with 36 hour exposure to Y-27632. Similarly, the expression of BRACHYURY at the protein level was also significantly increased with longer Y-27632 exposure durations (**Figure 4.6B**). Quantitative analysis of protein expression revealed a 61% increase with 12 hour-long

application of Y-27632 and up to a 63% increase with 36 hours. Surprisingly, the opposite trend was revealed when the cells were subjected to dorsomorphin and retinoic acid-mediated ectodermal differentiation; a decrease in expression of ectodermal markers *PAX6*, *SIP1, SOX1, OTX2,* and *NCAM1* were observed with increasing exposure duration of Y-27632 (**Figure 4.7A**). Protein expression of PAX6 was also significantly decreased by longer exposure to Y-27632 with the 36H exposure samples exhibiting a 66% decrease in percent-positive cells (**Figure 4.7B**). Similarly, the differentiation potential of hESCs followed similar trends to hIPSCs where mesendodermal differentiation was significantly enhanced with 36H Y-27632 exposure while ectodermal differentiation was inhibited (**Figure 4.8**). Overall, the morphological modulation of human PSCs, by ROCK inhibitor, primes the cells to preferentially differentiate towards mesendodermal lineage.

Many labs utilize differentiation protocols which require the formation of embryoid bodies (EBs) to enhance differentiation of pluripotent stem cells via increased cell-cell contacts [125]. Although it can simulate natural embryonic development, the formation of EBs to promote differentiation can be time and labor intensive. More significantly, it often results in heterogeneous and inefficient differentiation due to growth factor/nutrient diffusion limitations in EBs. Monolayer culture-based differentiation, such as protocols used in this study, has its own limitations resulting in relatively decreased efficiency in some cases, but it improves many technical problems associated with the EB-based differentiation process. In this regard, our results

demonstrate a novel use of a small molecule like Y-27632 to differentially regulate cell cytoskeletal and cell-cell junctional protein organization in hIPSC monolayer culture. More importantly, such a morphological modulation provides a means to effectively enhance lineage-specific differentiation. Future studies will focus on defining the mechanistic details by which Y-27632 switches the self-renewal state of pluripotent stem cells to the primed state.

4.5 – Conclusions

In this study, we report a previously unexplored field of interest where Y-27632 is identified as a potent small molecule to prime hIPSCs to selectively differentiate towards mesendodermal lineage. By effectively regulating the cell cytoskeleton and cell-cell junction proteins, Y-27632 induces hIPSCs to undergo EMT-like changes which predispose the cells to differentiate towards mesendodermal lineage. Simultaneously, such a disruption of actin and E-cadherin organization results in an inhibition of ectodermal differentiation. These results present a new methodology to enhance the directed differentiation of human PSCs towards mesendodermal target cell types.

4.6 – Figures

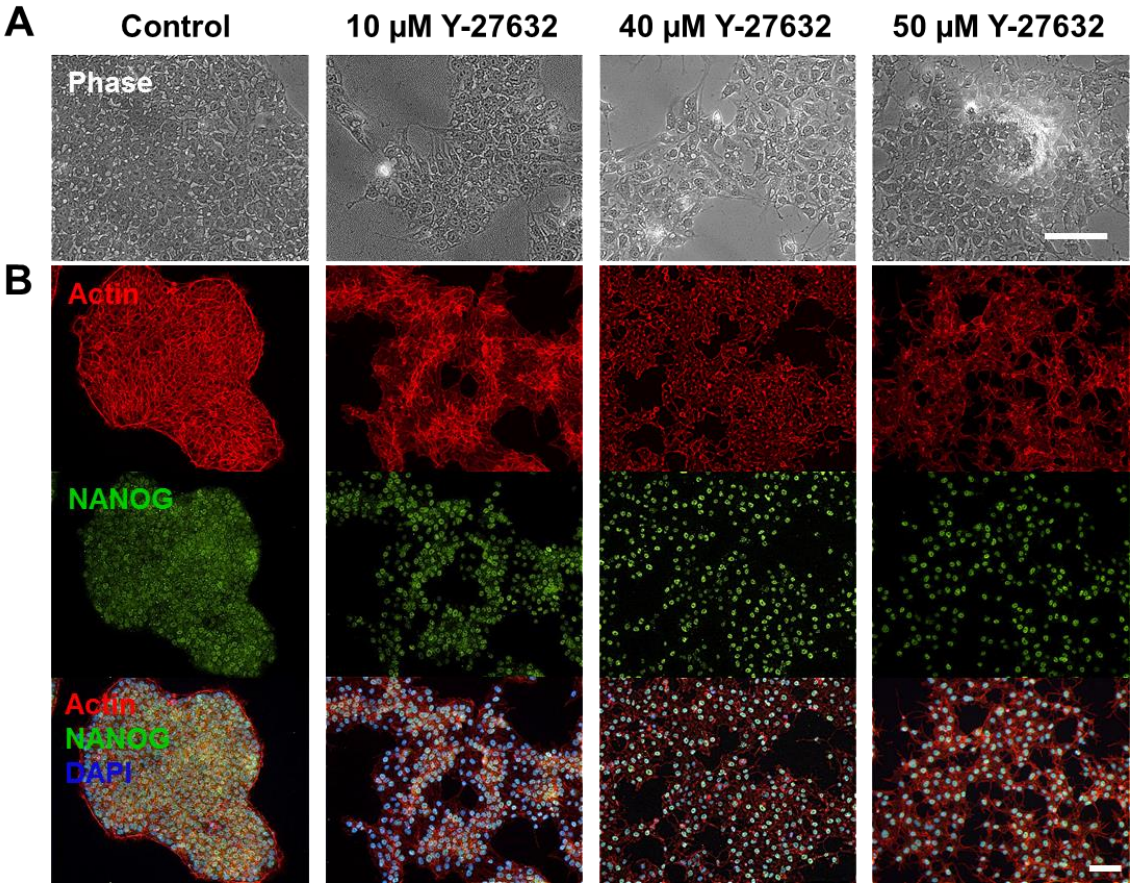

FIGURE 4.1. Y-27632 MODULATES COLONY AND CELL MORPHOLOGIES OF HIPSCS IN A CONCENTRATION-DEPENDENT MANNER.

(A) Phase contrast and (B) immunofluorescent images showing that colony morphologies of hIPSCs were differentially regulated by the application of Y-27632 at various concentrations. Regardless of colony morphologies the cells maintained expression of pluripotency marker NANOG (red: actin, green: NANOG, blue: DAPI, scale bar: 100 μm). Cells were pre-cultured in mTeSR™1 media with various concentrations of Y-27632 for 36 h before analysis.

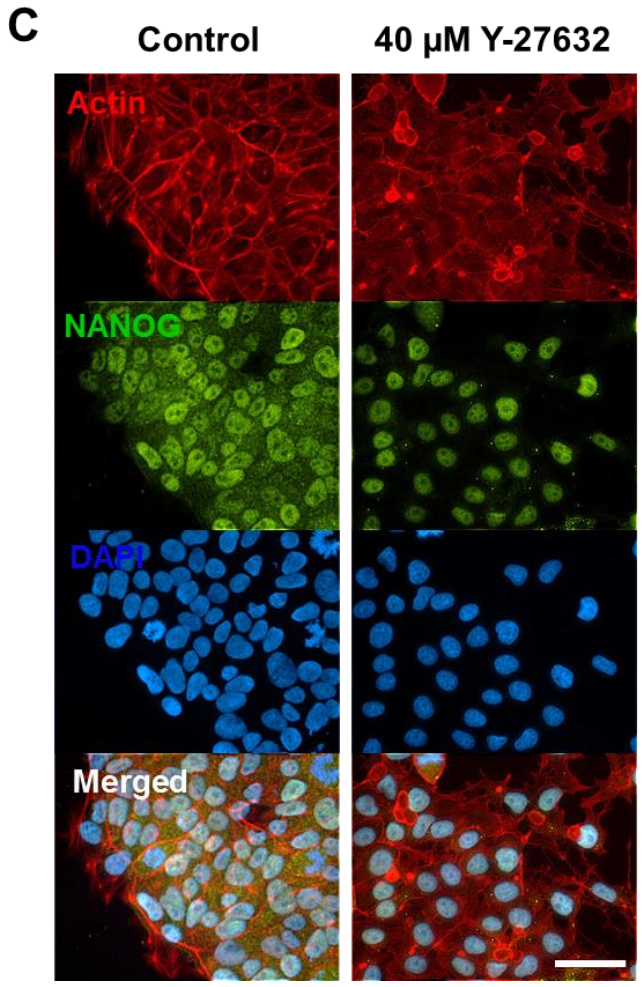

FIGURE 4.2. Y-27632 MODULATES COLONY AND CELL MORPHOLOGIES OF HIPSCS IN A CONCENTRATION-DEPENDENT MANNER.

(C) High magnification fluorescent images of the actin cytoskeleton and NANOG expression revealed changes in cell spreading and cytoskeletal organization by Y-27632 (red: actin, green: NANOG, blue: DAPI, scale bar: 50 μm). Cells were pre-cultured in mTeSR™1 media with various concentrations of Y-27632 for 36 h before analysis.

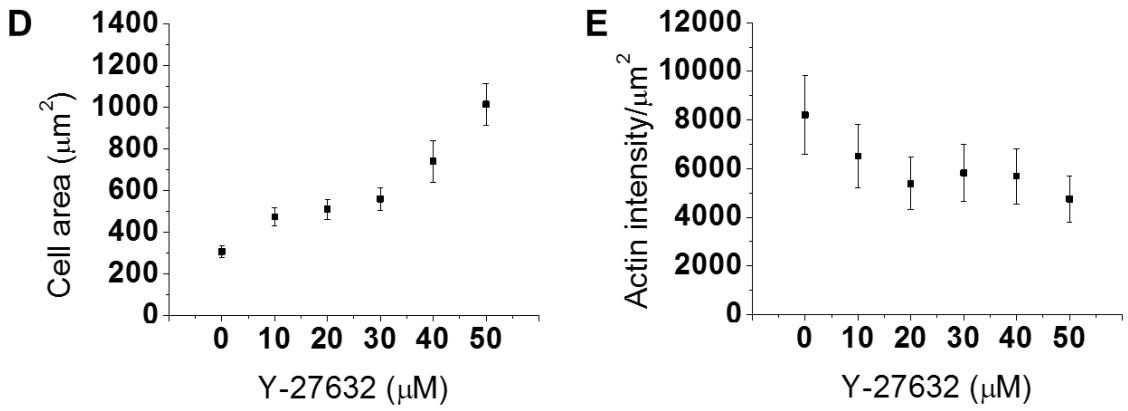

FIGURE 4.3. Y-27632 MODULATES COLONY AND CELL MORPHOLOGIES OF HIPSCS IN A CONCENTRATION-DEPENDENT MANNER.

(D) An increase in cell spreading was positively related to the concentration of Y-27632 (n = 100 cells, Pearson's correlation: 0.740, significance: 0.000). (E) Actin bundling in hIPSCs was inversely related to the concentration of Y-27632 (n = 100 cells, Pearson's correlation: − 0.423, significance: 0.000). Cells were pre-cultured in mTeSR™1 media with various concentrations of Y-27632 for 36 h before analysis.

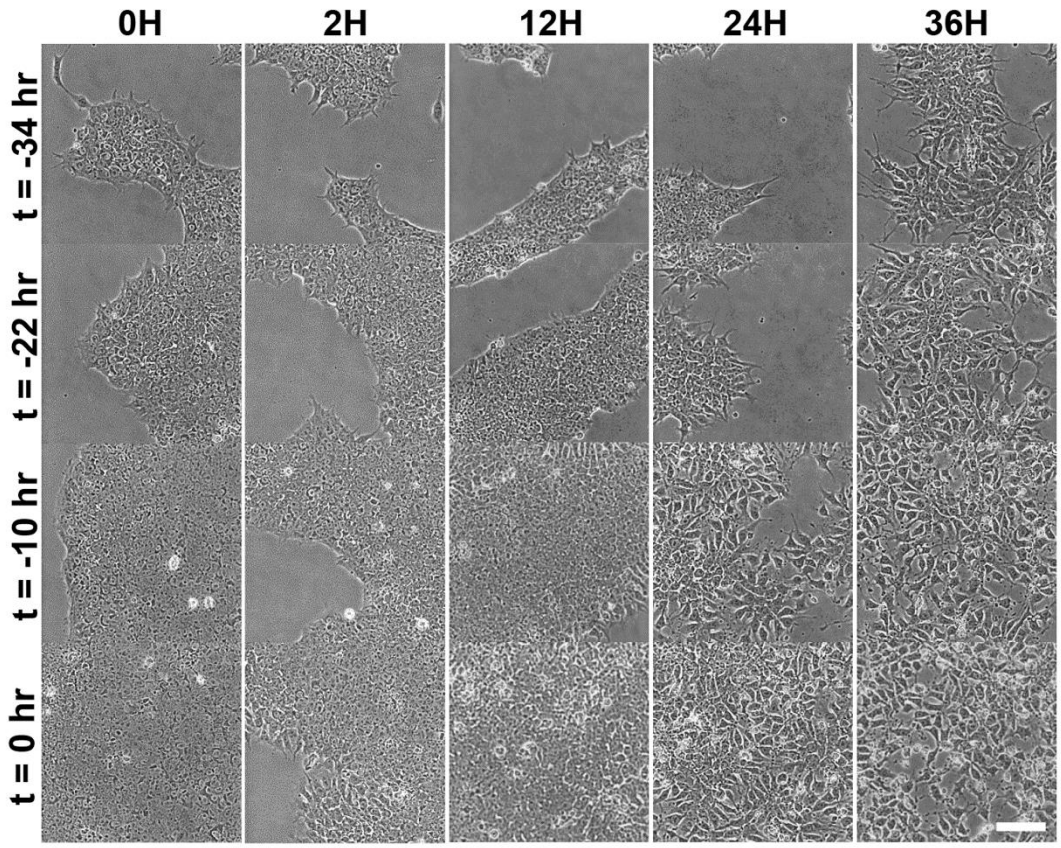

FIGURE 4.4. Y-27632 INDUCES CELL SPREADING OF HIPSCS.

The addition of Y-27632, during the pre-culture of hIPSCs with mTeSRTM1 media up to 36 hours, induced cell spreading with longer exposure to Y-27632 resulting in disruption of colony formation (scale bar: 100 µm). Optical images were taken using a BioStation CT at various time points prior to the start of differentiation at t=0 hr. Time t = -34 hr indicates 34 hrs before the induction time point of differentiation (the time point at the start of the pre-culture period) and 0 hr indicates hIPSC morphology at the induction time point of differentiation. Column titles indicate the culture duration with Y-27632 (i.e. 12H indicates the addition of Y-27632 for 12 hours prior to the start of differentiation).

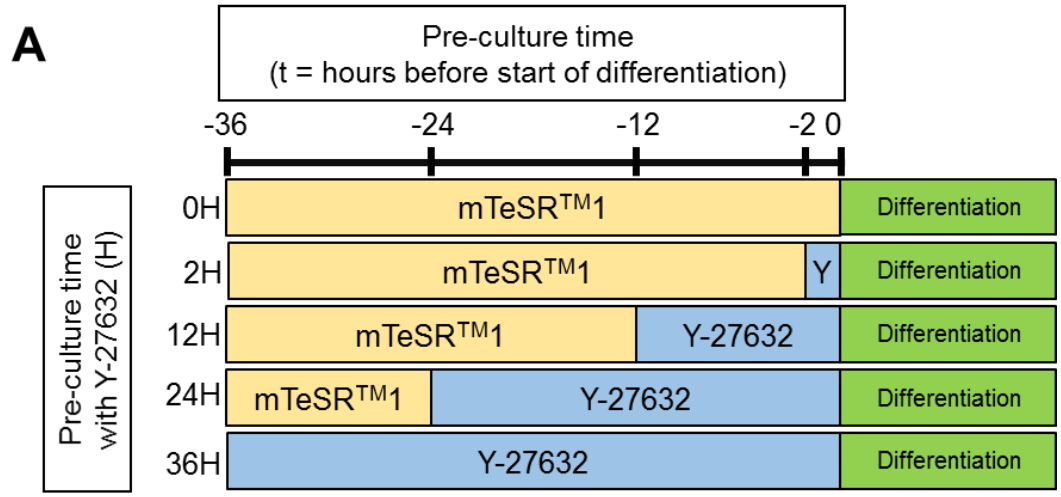

FIGURE 4.5. Y-27632 INDUCES CELL SPREADING OF HIPSCS, WHICH INCREASES EXPRESSION OF EMT MARKERS, IN AN EXPOSURE DURATION-DEPENDENT MANNER.

(A) A schematic of experimental design to examine the exposure duration-dependent effects of Y-27632 on hIPSCs. Cells were maintained in mTeSR™1 media supplemented with 40 µM Y-27632 for the indicated durations prior to being subjected to differentiation at t = 0. (B) Actin bundling decreased as the exposure duration to Y-27632 increased at t = 0 (red: actin, blue: DAPI, scale bar: 100 µm). (C) While longer exposure to Y-27632 decreased E-cadherin expression, hIPSCs maintained expression of pluripotency marker NANOG up to 36 h of the Y-27632 exposure at t = 0 (green: E-cadherin, red: NANOG, blue: DAPI, scale bar: 100 µm). (D) Quantification of E-cadherin and NANOG expression confirmed a decrease

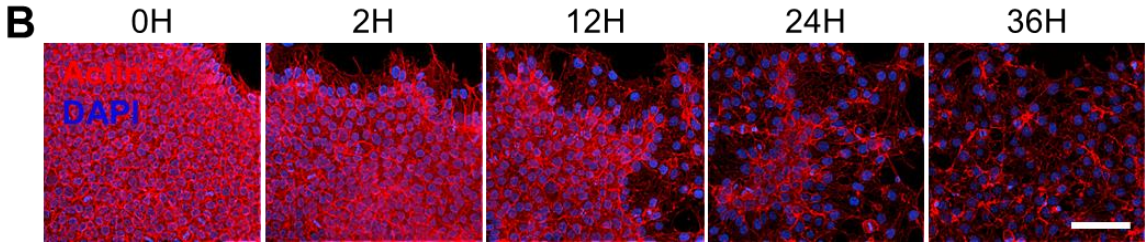

FIGURE 4.6. Y-27632 INDUCES CELL SPREADING OF HIPSCS, WHICH INCREASES EXPRESSION OF EMT MARKERS, IN AN EXPOSURE DURATION-DEPENDENT MANNER.

(A) A schematic of experimental design to examine the exposure duration-dependent effects of Y-27632 on hIPSCs. Cells were maintained in mTeSR™1 media supplemented with 40 µM Y-27632 for the indicated durations prior to being subjected to differentiation at t = 0. (B) Actin bundling decreased as the exposure duration to Y-27632 increased at t = 0 (red: actin, blue: DAPI, scale bar: 100 µm). (C) While longer exposure to Y-27632 decreased E-cadherin expression, hIPSCs maintained expression of pluripotency marker NANOG up to 36 h of the Y-27632 exposure at t = 0 (green: E-cadherin, red: NANOG, blue: DAPI, scale bar: 100 µm). (D) Quantification of E-cadherin and NANOG expression confirmed a decrease

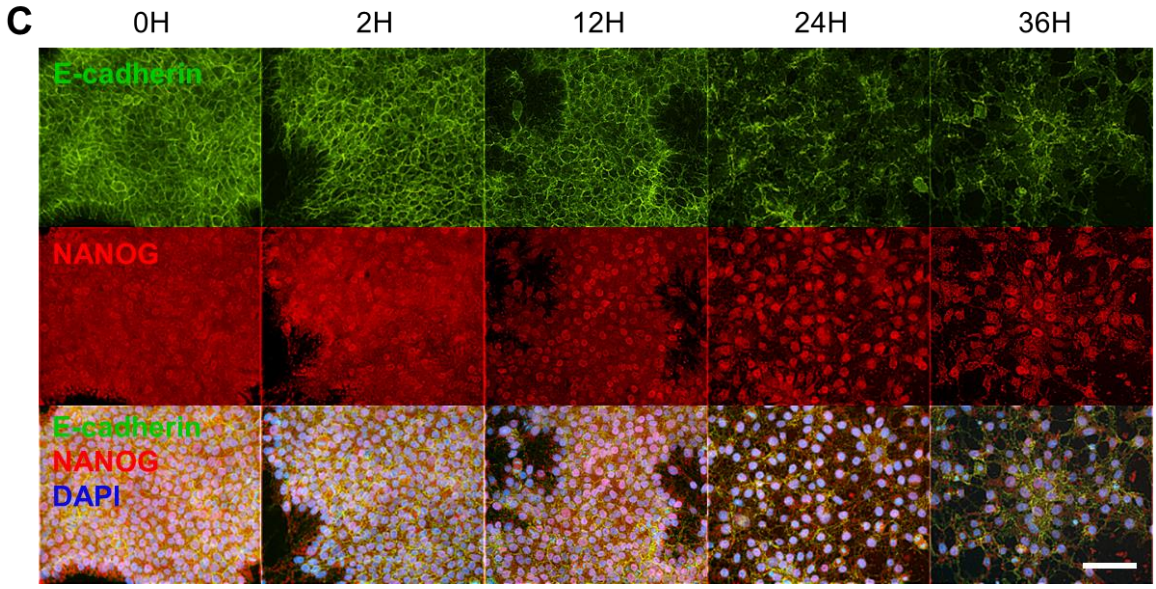

FIGURE 4.7. Y-27632 INDUCES CELL SPREADING OF HIPSCS, WHICH INCREASES EXPRESSION OF EMT MARKERS, IN AN EXPOSURE DURATION-DEPENDENT MANNER.

(A) A schematic of experimental design to examine the exposure duration-dependent effects of Y-27632 on hIPSCs. Cells were maintained in mTeSR™1 media supplemented with 40 µM Y-27632 for the indicated durations prior to being subjected to differentiation at t = 0. (B) Actin bundling decreased as the exposure duration to Y-27632 increased at t = 0 (red: actin, blue: DAPI, scale bar: 100 µm). (C) While longer exposure to Y-27632 decreased E-cadherin expression, hIPSCs maintained expression of pluripotency marker NANOG up to 36 h of the Y-27632 exposure at t = 0 (green: E-cadherin, red: NANOG, blue: DAPI, scale bar: 100 µm). (D) Quantification of E-cadherin and NANOG expression confirmed a decrease

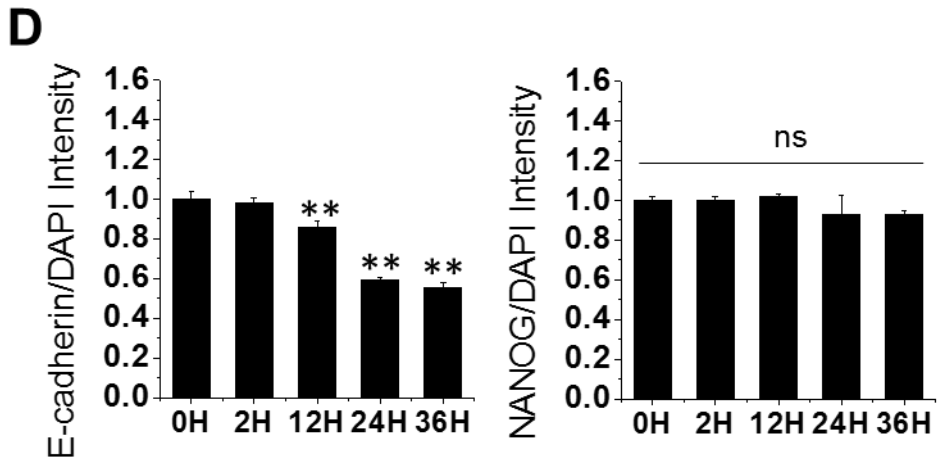

FIGURE 4.8. Y-27632 INDUCES CELL SPREADING OF HIPSCS, WHICH INCREASES EXPRESSION OF EMT MARKERS, IN AN EXPOSURE DURATION-DEPENDENT MANNER.

(A) A schematic of experimental design to examine the exposure duration-dependent effects of Y-27632 on hIPSCs. Cells were maintained in mTeSR™1 media supplemented with 40 µM Y-27632 for the indicated durations prior to being subjected to differentiation at t = 0. (B) Actin bundling decreased as the exposure duration to Y-27632 increased at t = 0 (red: actin, blue: DAPI, scale bar: 100 µm). (C) While longer exposure to Y-27632 decreased E-cadherin expression, hIPSCs maintained expression of pluripotency marker NANOG up to 36 h of the Y-27632 exposure at t = 0 (green: E-cadherin, red: NANOG, blue: DAPI, scale bar: 100 µm). (D) Quantification of E-cadherin and NANOG expression confirmed a decrease

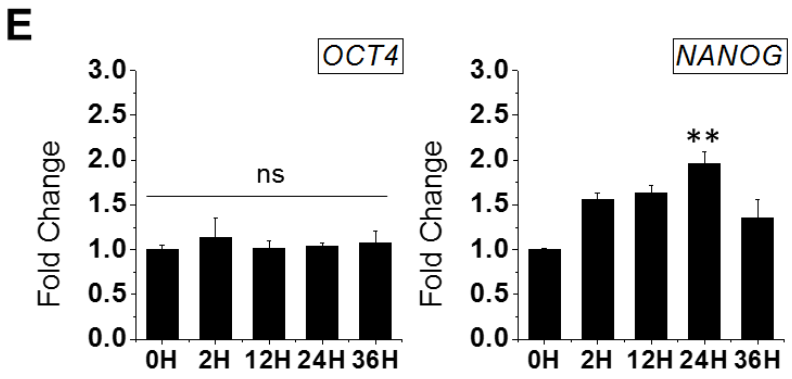

FIGURE 4.9. Y-27632 INDUCES CELL SPREADING OF HIPSCS, WHICH INCREASES EXPRESSION OF EMT MARKERS, IN AN EXPOSURE DURATION-DEPENDENT MANNER.

(A) A schematic of experimental design to examine the exposure duration-dependent effects of Y-27632 on hIPSCs. Cells were maintained in mTeSR™1 media supplemented with 40 µM Y-27632 for the indicated durations prior to being subjected to differentiation at t = 0. (B) Actin bundling decreased as the exposure duration to Y-27632 increased at t = 0 (red: actin, blue: DAPI, scale bar: 100 µm). (C) While longer exposure to Y-27632 decreased E-cadherin expression, hIPSCs maintained expression of pluripotency marker NANOG up to 36 h of the Y-27632 exposure at t = 0 (green: E-cadherin, red: NANOG, blue: DAPI, scale bar: 100 µm). (D) Quantification of E-cadherin and NANOG expression confirmed a decrease

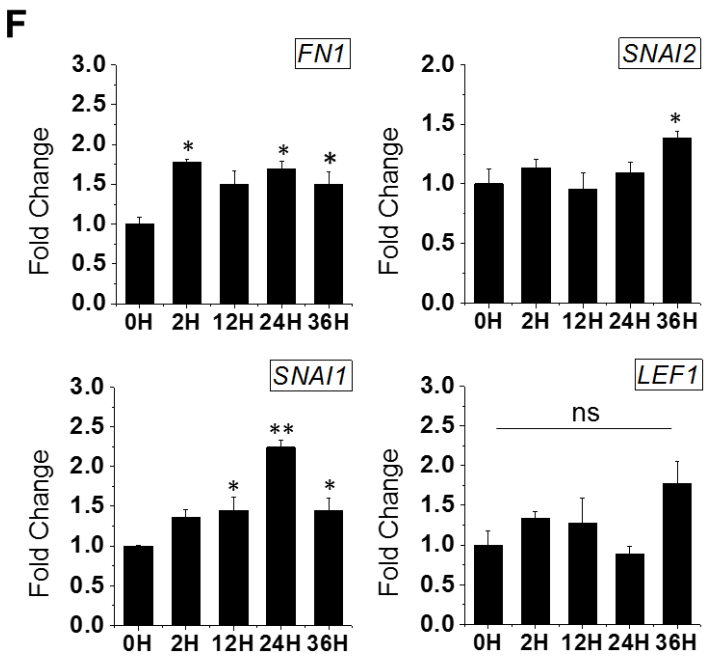

FIGURE 4.10. EXPRESSION OF EMT GENES AFTER THE PRE-CULTURE OF HIPSCS WITH Y-27632 UP TO 36 HOURS PRIOR TO THE INDUCTION OF DIFFERENTIATION.

Exposure of hIPSCs to Y-27632, during the pre-culture period, resulted in the upregulation of EMT marker SNAI (statistically significant) and LEF1 (statistically non-significant, yet notable increase in 36H, in a duration-dependent manner (n=6, 3 biological samples with 2 technical duplicates, *: $p<0.05$ and **: $p<0.01$ as compared to 0H, 'ns' indicates no significance). Gene expression was analyzed after 36 hours of pre-culture in mTeSRTM1 media, before the start of differentiation, and fold change values were normalized to 0H controls.

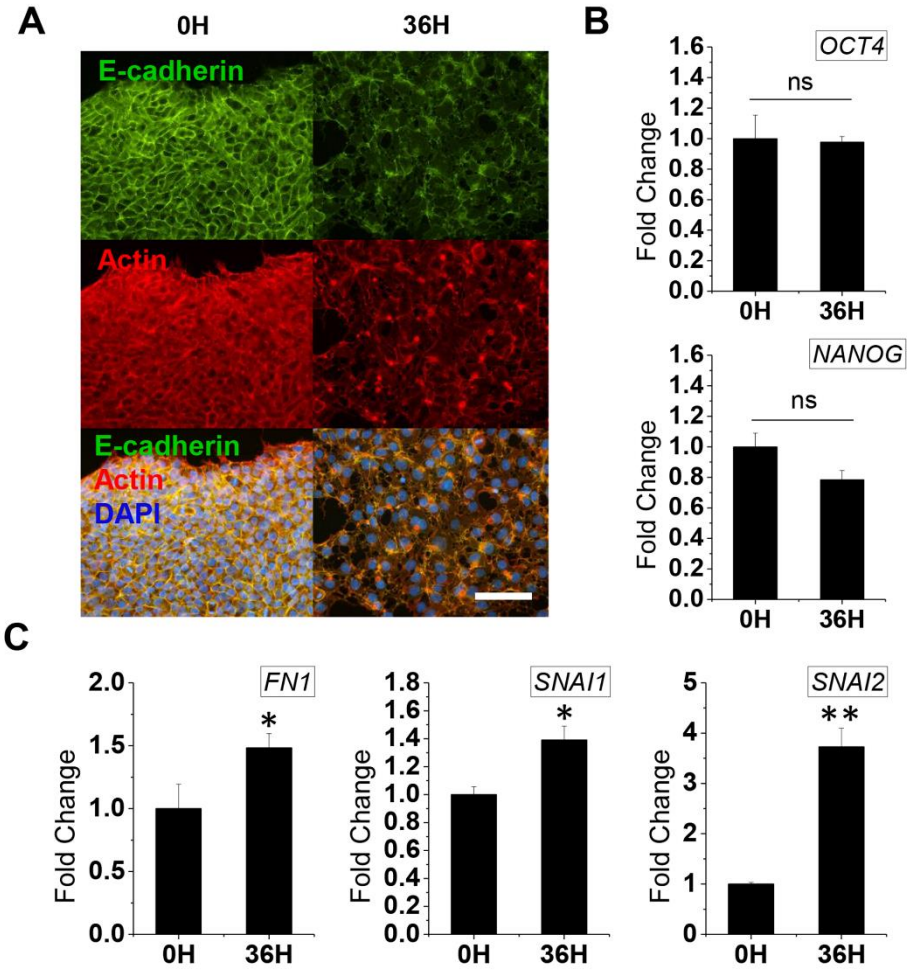

FIGURE 4.11. Y-27632 INDUCES MORPHOLOGICAL CHANGES AND INCREASES EXPRESSION OF EMT MARKERS IN A HUMAN EMBRYONIC STEM CELL (HESC) LINE.

(A) The addition of Y-27632 during the pre-culture of WA09 cells induced cell spreading and disruption of E-cadherin and actin organization (green: E-cadherin, red: actin, blue: DAPI, scale bar: 100 µm). (B) No significant changes in the gene expression of pluripotency markers OCT4 or NANOG were detected after culture with or without Y-27632 for 36 hours. (C) The gene expression of EMT markers FN1, SNAI1, and SNAI2 was significantly increased with exposure to Y-27632, similar to hIPSCs. Cells were maintained in mTeSRTM1 media with or without 40 µM Y-27632 for 36 hours prior to analysis of gene and protein expression. Gene expression fold change values were normalized to 0H controls. n=6, 3 biological samples with 2 technical duplicates, *: $p<0.05$ and **: $p<0.01$ as compared to 0H, 'ns' indicates no significance.

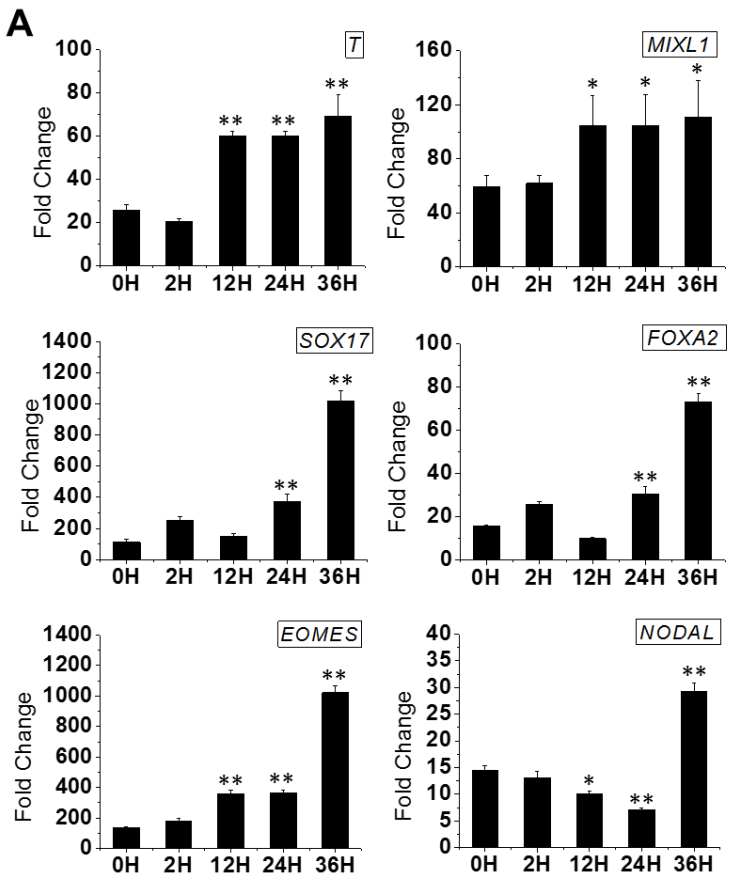

FIGURE 4.12. MESENDODERMAL DIFFERENTIATION IS ENHANCED BY THE APPLICATION OF Y-27632 DURING THE PRE-CULTURE PERIOD IN AN EXPOSURE DURATION-DEPENDENT MANNER.

Human IPSCs were pre-cultured for 36 h in mTeSR™1 media (supplemented with 40 µM Y-27632 for the designated durations such as 0, 2, 12, 24 and 36 h (Fig. 4.3A)) followed by subsequent WNT3A and Activin A-mediated mesendodermal differentiation for 60 h. (A) Gene expression of mesendodermal markers T and MIXL1 was positively correlated to Y-27632 exposure duration. Endodermal markers (SOX17 and FOXA2) and mesodermal markers (EOMES and NODAL) were also significantly affected by exposure to Y-27632 before the induction of differentiation (n = 6, 3 biological samples with 2 technical duplicates, *: $p < 0.05$ and **: $p < 0.01$ as compared to 0H control. Gene expression fold change values were normalized to that of hIPSCs not subjected to either Y-27632 or differentiation).

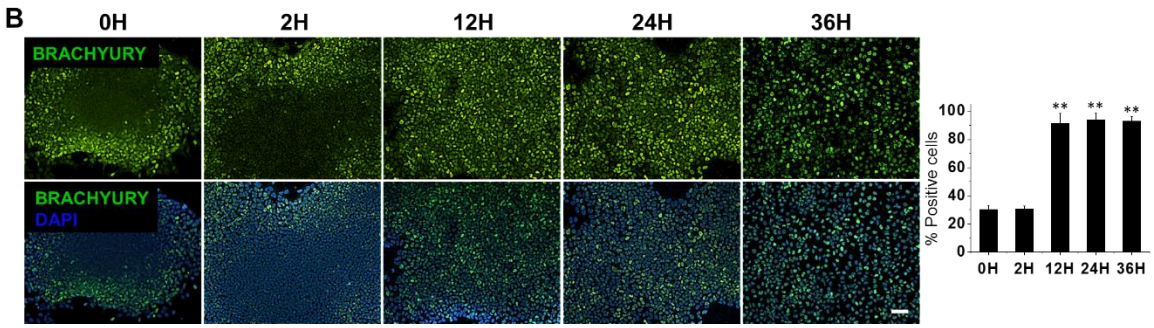

FIGURE 4.13. MESENDODERMAL DIFFERENTIATION IS ENHANCED BY THE APPLICATION OF Y-27632 DURING THE PRE-CULTURE PERIOD IN AN EXPOSURE DURATION-DEPENDENT MANNER.

Human IPSCs were pre-cultured for 36 h in mTeSR™1 media (supplemented with 40 µM Y-27632 for the designated durations such as 0, 2, 12, 24 and 36 h (Fig. 4.3A)) followed by subsequent WNT3A and Activin A-mediated mesendodermal differentiation for 60 h. (B) Immunofluorescent imaging and its quantitative analysis showed that expression of mesendodermal marker BRACHYURY is positively correlated to Y-27632 exposure duration (green: BRACHYURY, blue: DAPI, scale bar: 100 µm; n = 6000 cells, **: $p < 0.01$ as compared to 0H control).

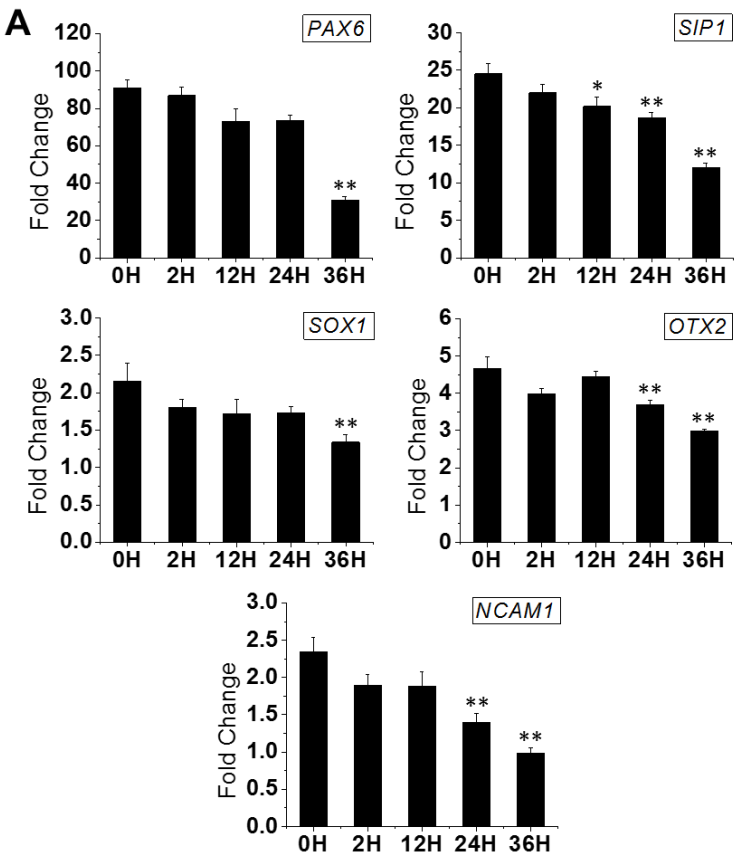

FIGURE 4.14. ECTODERMAL DIFFERENTIATION IS INHIBITED BY THE APPLICATION OF Y-27632 DURING THE PRE-CULTURE PERIOD IN AN EXPOSURE DURATION-DEPENDENT MANNER.

Human IPSCs were pre-cultured for 36 h in mTeSR™1 media (supplemented with 40 µM Y-27632 for the designated durations such as 0, 2, 12, 24 and 36 h (Fig. 4.3A)) followed by subsequent dorsomorphin and retinoic acid-mediated ectodermal differentiation for 72 h. (A) Gene expression of ectodermal markers PAX6, SIP1, SOX1, OTX2, and NCAM1 was inversely correlated to Y-27632 exposure duration (n = 6, 3 biological samples with 2 technical duplicates, *: $p < 0.05$ and **: $p < 0.01$ as compared to 0H control. Gene expression fold change values were normalized to that of hIPSCs not subjected to either Y-27632 or differentiation).

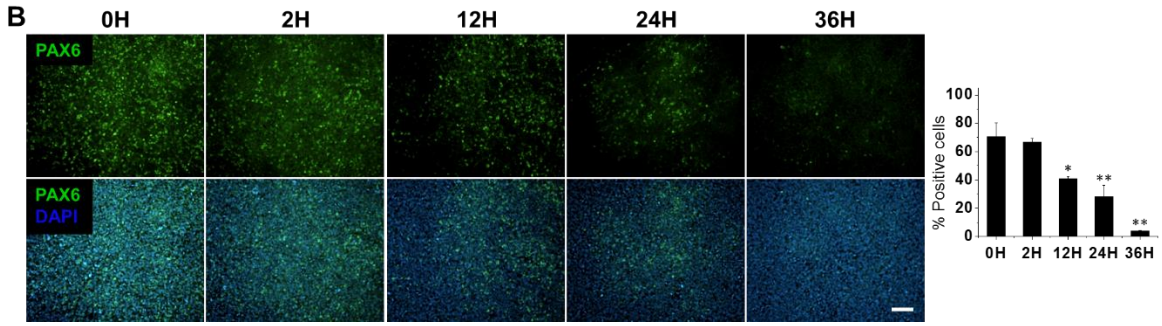

FIGURE 4.15. ECTODERMAL DIFFERENTIATION IS INHIBITED BY THE APPLICATION OF Y-27632 DURING THE PRE-CULTURE PERIOD IN AN EXPOSURE DURATION-DEPENDENT MANNER.

Human IPSCs were pre-cultured for 36 h in mTeSR™1 media (supplemented with 40 µM Y-27632 for the designated durations such as 0, 2, 12, 24 and 36 h (Fig. 4.3A)) followed by subsequent dorsomorphin and retinoic acid-mediated ectodermal differentiation for 72 h. (B) Immunofluorescent imaging and its quantitative analysis showed that PAX6 expression is inversely correlated to Y-27632 exposure duration (green: PAX6, blue: DAPI, scale bar: 100 µm; n = 6000 cells, *: $p < 0.05$ and **: $p < 0.01$ as compared to 0H control).

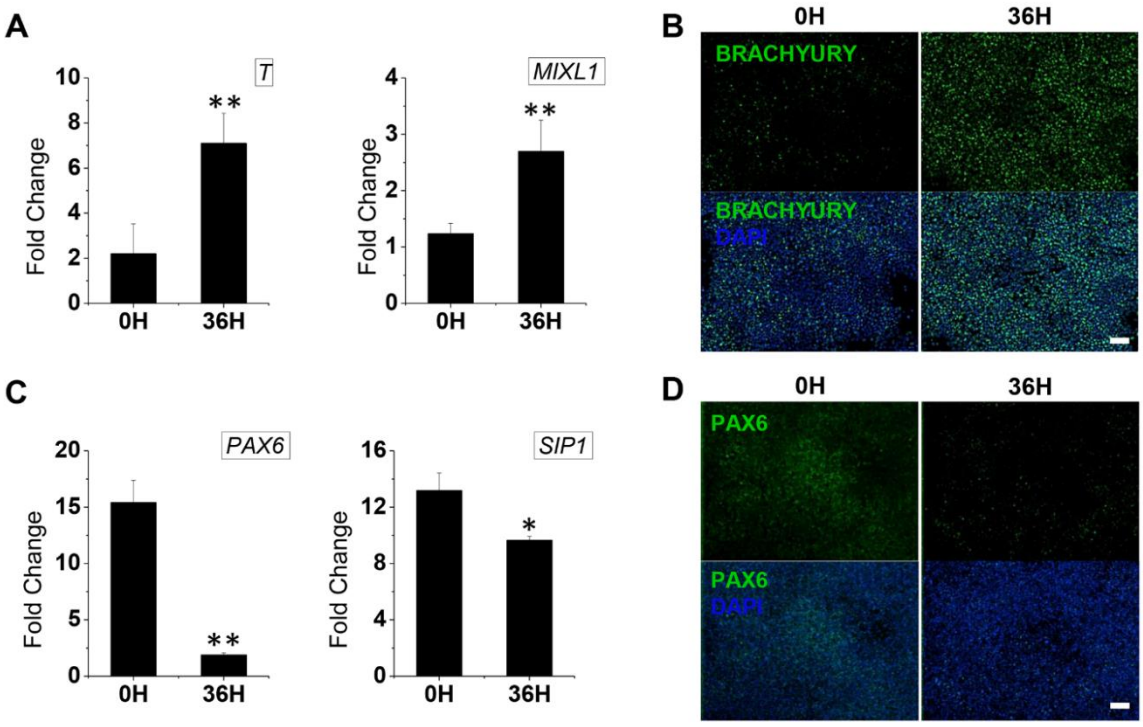

FIGURE 4.16. PRE-CULTURE OF HESCS WITH Y-27632 ENHANCES SUBSEQUENT MESENDODERMAL BUT INHIBITS ECTODERMAL DIFFERENTIATION.

Human ESCs (WA09) were pre-cultured in mTeSRTM1 media (supplemented with or without 40 µM Y-27632) for 36 hours followed by the induction of (A-B) mesendodermal differentiation for 60 hours or (C-D) ectodermal differentiation for 72 hours. (A) Gene expression of mesendodermal markers T and MIXL1 was significantly enhanced by the Y-27632 pre-culture before the induction of differentiation. (B) Similarly, protein expression of BRACHYURY was enhanced by the Y-27632 incubation. (C) In contrast, gene expression of ectodermal markers PAX6 and SIP1 was significantly downregulated with exposure to Y-27632 prior to the induction of differentiation. (D) Protein expression of PAX6 was also inhibited with exposure to Y-27632. Gene expression was analyzed after 36 hours of pre-culture in mTeSRTM1 media (with or without Y-27632) followed by defined mesendodermal or ectodermal differentiation. All fold change values were normalized to that of hESCs not subjected to either Y-27632 or differentiation. n=6, 3 biological samples with 2 technical duplicates, *: $p<0.05$ and **: $p<0.01$ as compared to 0H.

CHAPTER 5 – MECHANO-MODULATION OF E-CADHERIN CLUSTERING REGULATES EARLY-STAGE DIFFERENTIATION OF HUMAN PLURIPOTENT STEM CELLS ON ELECTROSPUN NANOFIBROUS SCAFFOLDS

5.1 – Abstract

Considering significant effects of the cell niche on stem cell behaviors, a tightly controlled microenvironment may provide a means to maximize the differentiation efficiency by modulation of cell-cell and cell-matrix interactions. In this study, nanofibrous scaffolds with designed mechanical properties were utilized to engineer distinct colony formation of human induced pluripotent stem cells (IPSCs) to analyze how structural differences affect early-lineage commitment. No significant difference in the expression of focal adhesion marker, vinculin, was observed regardless of colony morphology. Colony dimensionality was strongly associated with the organization of actin and E-cadherin, likely developed by structural pre-stresses within the colonies as predicted by computational modeling. The formation of an actin ring and clustering of E-cadherin within the 3D colony in a radially-aligned manner, indicative of greater cell-cell interactions, were accompanied by higher RhoA activity. The inhibition of downstream effector ROCK during the pre-culture of IPSCs was sufficient to abolish the 3D colony formation, resulting in the elimination of the scaffold-dependent differentiation tendency. These results offer a novel strategy to regulate cell-cell interaction by modulating IPSC colony morphology to enhance early lineage-specific differentiation.

5.2 – Introduction

Human induced pluripotent stem cells (IPSCs) are a promising cell source for regenerative medicine because of their derivation from a patient, the capability of expansion to clinically-relevant numbers, and their ability to differentiation towards any somatic cell type [97]. Nonetheless, their therapeutical potential remains limited due to their inefficient derivation, unregulated differentiation, and their ability to form teratomas in the body [126]. In this regard, significant progress has been made over the past 10 years to address the safety issues with their derivation and develop differentiation protocols to enhance their induction towards multiple adult cell types. A majority of the protocols are based on the sequential application of the cytokine/growth factor milieu adapted from embryogenesis to direct differentiation of PSCs into specific lineages/phenotypes [76, 77, 127]. However, the efficiency of such directed differentiation remains a major limitation.

A common method for differentiation of PSCs is the formation of embryoid bodies (EBs) which result in non-homogeneous differentiation [98, 99]. The lack of specificity by prepositioning the cells to a state for differentiation into all three germ layers limits the final yield efficiency. In this regard, we have previously demonstrated that electrospun scaffolds with distinct mechanics can be used to significantly change IPSC colony morphology which affects self-renewal and directed lineage-specific differentiation [106,

121]. Unlike EB-based differentiation technologies, distinct colony morphologies on electrospun scaffolds are developed under proliferation conditions making it a beneficial tool to study the early induction of differentiation from the pluripotent state. Additionally, the advantage of electrospinning as a scaffold synthesis technique permits the change of multiple topographical features, with minimal changes to processing parameters, to study the effects on cellular behaviors [76, 112-114]. Although the effects of substrate mechanics on adult stem cell behaviors has been widely studied, little is known about the mechanism by which PSC behavior is regulated by the mechanical microenvironment. One significant feature of PSCs is their colony-forming nature which relies on cell-cell interaction for maintenance of pluripotency and survival after dissociation. Therefore, the investigation of how the mechanical microenvironment affects cell-cell interaction is necessary to understand how the physical microenvironment can result in disruption of the self-renewal state of pluripotent stem cells. Nonetheless, it is critical to understand the mechano-responsive pathways which can regulate early differentiation events of IPSCs to develop the proper culture platform to elicit specific cellular responses.

Our observation of colony morphology-dependent self-renewal and differentiation efficiency of IPSCs on electrospun scaffold stiffness, led us to hypothesize that a mechano-responsive pathway pre-disposes the cells to preferentially differentiate towards a specific lineage. We previously determined that changes in the cell

cytoskeleton and colony formation of IPSCs were significantly affected by ROCK inhibitor Y-27632 resulting in expression of epithelial-to-mesenchymal transition markers in an exposure-dependent manner. These results suggested that the RhoA signaling pathway is a key target to manipulating cellular behavior. In the current study we examined how differences in the colony morphology, RhoA activity, and its associated changes in cytoskeletal organization impact subsequent guided differentiation. To determine the shift in differentiation potential, cells were pre-cultured on electrospun scaffolds with designed mechanics to develop distinct colony morphologies and cytoskeletal, cell-cell, and cell-matrix markers were analyzed using immunocytochemistry. Additionally, computational modeling was used to predict the cell pre-stresses imposed by the development of distinct colony morphologies. Actin and E-cadherin organization correlated to the 3D colony hoop stress and thus implicated these components as mediators of the structural stresses imposed by the development of a 3D colony formation. Scaffold stiffness-dependent RhoA activity was responsible for differential colony formation and subsequent differentiation potential. This was evident from ROCK inhibition resulting in the desensitization of the cells to scaffold mechanics, which led to scaffold-independent differentiation tendency. Therefore, we demonstrate that engineering the colony dimensionality of IPSCs differentially controls cell-cell interaction to selectively enhance the differentiation towards various lineages.

5.3 – Materials and Methods

5.3.1 – Scaffold synthesis

Poly(ε-caprolactone) (PCL) and poly-ether-ketone-ketone (PEKK) electrospun nanofibrous scaffolds were synthesized and characterized as previously described [121]. The precursor solutions of 8 wt.% PCL dissolved in 5:1 trifluoroethanol-water (Sigma, St. Louis, MO) and 5 wt.% PEKK (Oxford Performance Materials, South Windsor, CT) dissolved in 1,1,1,3,3,3-Hexafluoro-2-propanol (HFP) were electrospun using a vertical setup. The examine the effects of scaffolds stiffness on IPSC behavior, the processing parameters for the scaffold synthesis were optimized to achieve approximately 450 nm average fiber diameter which results in a Reduced Young's Modulus of 19 kPa for PCL and 313 kPa for PEKK as our previous report characterized [121]. To examine the effects of scaffold mechanics while maintaining similar surface chemistry, the electrospun scaffolds were conjugated with bovine collagen type I. Briefly, the samples were air-plasma-treated at 30 W for 5 minutes, treated with 100 mM N-hydroxysuccinimide (NHS)/N-(3-Dimethylaminopropyl)-N'-ethylcarbodiimide hydrochloride (EDAC) for 1 hour at room temperature, and incubated with 1 mg/ml collagen type I in 0.01 M HCl overnight [67]. Prior to cell seeding, the scaffolds were sterilized with 70% ethanol for 1 hour, air-dried overnight, and UV-sterilized for at least 30 minutes prior to cell seeding.

5.3.2 – Cell culture

A human induced pluripotent stem cell line was derived as previously described [106]. Stock cells were maintained on Geltrex®-coated (Life Technologies, Grand Island, NY) tissue culture plates in proliferation media mTeSR™1 (StemCell Technologies, Vancouver, BC, Canada) at 37 °C and 5% CO_2. Stock IPSCs were passaged to the collagen-conjugated scaffolds using 0.25% Trypsin-EDTA (Gibco, Grand Island, NY) at approximately 125,000 cells per cm^2 of scaffold. ROCK inhibitor, Y-27632 (10 μM, Reagents Direct, Encinitas, CA), was supplemented to the proliferation media to improve initial cell attachment and survival. The following day, Y-27632 was removed from the media unless otherwise noted. IPSCs were pre-cultured in mTeSR1 medium for 5 days to allow for the development of distinct colony morphologies depending on scaffold stiffness. Alternatively, the proliferation media was supplemented with 40 μM Y-27632 during the 5 day pre-culture period to prevent scaffold-dependent colony formation. After the pre-culture period the proliferation media was exchanged to either defined mesendodermal or ectodermal differentiation media.

5.3.3 – Differentiation of IPSCs

The cells pre-cultured in proliferation media on 19 kPa or 313 kPa electrospun scaffolds for 5 days, with or without Y-27632, were subjected to defined differentiation

protocols as previously described [121]. Mesendodermal differentiation was induced using an adapted protocol by Oldershaw et al. consisting of DMEM:F12 basal media with sequential supplementation of Activin A (Peprotech, Rocky Hill, NJ), WNT3A (R&D systems, Minneapolis, MN), FGF2 (R&D systems), and BMP4 (R&D systems) for 60 hours [109, 121]. Ectodermal differentiation was induced using a modified protocol from Shi et al. consisting of neurobasal media (Gibco) supplemented with B27 (Gibco), N2 (Gibco), 2 μM dorsomorphin (Compound C, Sigma) and 0.1 μM retinoic acid (Sigma) for 8 days [76, 121]. Cells were maintained in an incubator at 37 °C and 5% CO_2 with daily media exchanges.

5.3.4 – Immunocytochemistry

Standard immunocytochemistry protocols were utilized to determine differences in protein expression of IPSCs cultured on electrospun scaffolds. Samples were fixed for 30 minutes with 4% paraformaldehyde at room temperature followed by permeabilization using 0.1% Triton-X in phosphate buffered saline (PBS). After blocking the samples with a 1% bovine serum albumin (BSA) in PBS solution for 30 minutes at room temperature, the following primary antibodies were utilized: mouse anti-Vinculin (R&D systems, Minneapolis, MN), rabbit anti-E-cadherin (Abcam, Cambridge, MA), mouse anti-β-catenin (Invitrogen, Waltham, MA), mouse anti-NANOG (Abcam), goat anti-BRACHYURY (R&D systems), or mouse anti-PAX6 (Developmental Studies Hybridoma

Bank, Iowa City, IA). After overnight incubation at 4 °C the respective secondary antibodies were used: Alexa Fluor 488 donkey anti-mouse IgG (H+L), Alexa Fluor 488 goat anti-rabbit IgG (H+L), Alexa Fluor 594 goat anti-mouse IgG (H+L), or Alexa Fluor 488 donkey anti-goat IgG (H+L) (Invitrogen). Unless a sequential stain for two protein markers was performed, the samples were subjected for actin using rhodamine phalloidin (Life Technologies). Samples were mounted onto glass slides using a mounting medium containing 4',6-diamidino-2-phenylindole (DAPI, Vector Laboratories, Burlingame, CA) to stain the nuclei. Fluorescence imaging was conducted using an epi-fluorescent microscope (Nikon Eclipse, Melville, NY) or a confocal microscope (Leica SP5, Buffalo Grove, IL).

5.3.5 – Protein quantification by western blot

To analyze the protein expression of F-actin and E-cadherin, total protein were extracted from cells cultured in proliferation media on 19 kPa or 313 kPa nanofibrous scaffolds for 5 days. Approximately 20 μg of total proteins were loaded onto a precast gel for electrophoresis and proteins were separated at 200 V for 45 minutes (Bio-Rad, Hercules, CA). Proteins were transferred to a nitrocellulose membrane at 100 V for 30 minutes. The membrane was blocked using 5% nonfat milk in PBS with Tween-20. The membrane was probed using a primary (mouse anti-beta actin (Sigma), rabbit anti-E-cadherin (Abcam), rabbit anti-GAPDH (Sigma)) and secondary (Alexa Fluor 594 donkey

anti-mouse IgG (H+L), Alexa Fluor 594 goat anti-rabbit IgG (H+L)) antibody for the specific detection of F-actin, E-cadherin, or GAPDH as an internal control. After fluorescence detection, the lanes were quantified using ImageJ software.

5.3.6 – Computational modeling of pre-stresses in IPSC colonies

The pre-stress distribution within IPSC colonies was modeled by finite element analysis using COMSOL Multiphysics. To observe the pre-stress distribution of both 3D and 2D cell colonies, a finite element analysis of structural mechanics was conducted using COMSOL Multiphysics. Colony dimensions of IPSCs cultured on 19 kPa (3D morphology) and 313 kPa (2D morphology) were measured from immunofluorescent images to determine the values used for modeling. A spherical representative 3D colony was modeled after the average dimensions of a 3D colony having a radius of 95 µm with a central pit radius of 65 µm. The 2D colony had an average radius of 134 µm without the presence of a pit, with a height of 5 µm. The cell colony density of 1.1 g/ml, Young's Modulus of 0.9 kPa, and a Poisson's ratio of 0.5 were set as the model parameters based on available literature [128, 129]. Both colonies were fixed at the bottom faces of the model and applied forces of -1.3 µN and -2.6 µN, representative of the hydrostatic pressure present in a typical volume of a well of a 24-well plate, were assigned to the top of the 3D and 2D colony, respectively. Hoop stresses were analyzed as the 3rd principal stresses.

5.3.7 – RhoA analysis

To analyze the effect of substrate stiffness on RhoA activity, IPSCs were pre-cultured on 19 kPa or 313 kPa nanofibrous scaffolds or tissue culture plate controls for either 3 or 5 days. The presence of active RhoA was quantified using a G-LISA quantification assay using manufacturer's instructions (Cytoskeleton, Inc., Denver, CO). Additionally, the amount of total RhoA was quantified using a Total RhoA ELISA kit (Cytoskeleton, Inc.).

5.3.8 – IPSC colony morphology analysis

To examine the changes in IPSC colony morphology after the pre-culture period in proliferation media, with or without Y-27632, DAPI-stained samples were imaged using a confocal microscope. Imaris Bitplane 7.1.1 (Bitplane, South Windsor, CT) software was used to create a surface representation of the colonies to quantify the differences in sphericity as previously described [106, 121]. By definition, the sphericity of an object is determined as the ratio of the surface area of a sphere to the surface area of the object, in this case, the IPSC colony [74].

5.3.9 – Gene expression analysis

To examine gene expression of lineage-specific markers, cells were lysed and total RNA was purified using an RNeasy Micro Kit (Qiagen, Valencia, CA) followed by cDNA synthesis using an iScript cDNA Synthesis Kit (Bio-Rad) as previously described [106]. Quantitative real-time PCR was performed using the following custom primers: *GAPDH [5'*-ATGGGGAAGGTGAAGGTCG-*3' (forward) and 5'*-TAAAAGCAGCCCTGGTGACC-*3' (reverse)]; GSC [5'-* GATGCTGCCCTACATGAACGT-*3' (forward) and 5'-* TACTTGGTCTCCTGGAAGAGGTT-*3' (reverse)]; MIXL1 [5'-* CTTTGGCTAGGCCGGAGATTA *-3' (forward) and 5'-* GGCAGGCAGTTCACATCTACCT *-3' (reverse)]; PAX6 [5'-* GAGTTCTTCGCAACCTGGCTA-*3' (forward) and 5'*-CTGCCCGTTCAACATCCTTAG-*3' (reverse)]; NEUROD1 [5'*-AAAGCCCTCTGACTGATTGCA-*3' (forward) and 5'-* GGACGGTTCGTGTTTGAAAGA-*3' (reverse)]*. The comparative threshold cycle (C_T) method was used to analyze the fold change differences with *GAPDH* used as an endogenous control [75].

5.3.10 – Statistical analysis

All experiments were conducted with a minimum of triplicate biological samples and data is represented as mean ± standard deviation (SD) or standard error of means (SEM). Comparison of groups for statistical significance was determined using SPSS

(v.23.0) software with either one-way ANOVA with Tukey's HSD post-hoc or one sample student T-test. Pearson's correlation coefficient was determined to reveal bivariate correlation between two factors. Statistical significance was reported when a 'p' value was less than 0.05.

5.4 – Results

5.4.1 – Distinct mechanics of electrospun scaffolds mediate differential IPSC colony formation.

Our previous studies demonstrated the significant role of the cellular microenvironment on human IPSC colony morphology (dimensionality) [106, 121]. Nanofibrous poly(ε-caprolactone) (PCL) scaffolds having a reduced Young's modulus of 19 kPa promote a three-dimensional colony development. In contrast, polyether-ketone-ketone (PEKK) scaffolds, having a 313 kPa reduced Young's modulus, promoted a two-dimensional colony development. Although IPSCs with distinct colony dimensionalities maintained expression of pluripotency marker NANOG, the directed differentiation to ectodermal lineage was enhanced on soft scaffolds (3D colonies) while mesendodermal differentiation was enhanced on stiff scaffolds (2D colonies) [121]. The objective of the current study was to determine a possible mechanism by which IPSCs on distinct scaffold

stiffness, which have developed significantly different colony dimensionalities, regulate the mechanobiology of IPSCs.

5.4.2 – Development of distinct colony dimensionality results in the reorganization of actin and E-cadherin, but no significant changes in focal adhesion marker vinculin.

Initially, to determine the colony morphology-dependent changes in cell-ECM and cell-cell interactions the protein expression of vinculin, actin, and E-cadherin were evaluated using immunocytochemistry (**Figure 5.1, 5.2, A-B**). No significant differences in vinculin expression were observed for cells cultured on soft or stiff scaffolds while a notable difference in actin organization was determined (**Figure 5.1**). In contrast, a notable difference in cell-cell junction marker E-cadherin was observed between IPSCs on soft and stiff scaffolds (**Figure 5.2, A-B**). IPSCs on 19 kPa scaffolds exhibited increased bundling of actin at the colony periphery and clustering of E-cadherin at the cell junctions (**Figure 5.2A**). In contrast, cells cultured on 313 kPa scaffolds had evenly distributed organization of both actin and E-cadherin (**Figure 5.2B**). To determine if changes in clustering were attributed to increased protein levels, actin and E-cadherin expression were quantified, and insignificant changes were observed between IPSCs having distinct colony morphologies on soft and stiff scaffolds (**Figure 5.2, C-D**). Beta-catenin is a known Wnt signaling mediator that controls early stages of differentiation in pluripotent stem cells [130]. To investigate if the colony-morphology-dependent E-cadherin clustering

affects the localization of beta-catenin, the cells having different colony morphologies were co-immunostained with beta-catenin and E-cadherin. Beta-catenin was primarily localized with E-cadherin at the cell-cell junctions (**Figure 5.2, E-F**). Greater expression of beta-catenin co-localized with E-cadherin clusters, were observed in 3D colonies on 19 kPa scaffolds (**Figure 5.2E**).

5.4.3 – Reorganization of actin and E-cadherin mediates colony morphology-dependent structural stresses.

To examine possible mechanisms which induce scaffold stiffness-dependent colony formation, we investigated the pre-stresses of IPSC colonies having different morphologies by computational simulation (**Figure 5.3A**). Under a hydrostatic pressure, the tensional hoop stress is distributed on the surface of the 3D colony towards the top portion. The tensile stress changes to compression near the bottom of the colony (**Figure 5.3A, left panel**). In contrast, purely compressive hoop stress is present in the 2D colony from the center of the colony out to the periphery (**Figure 5.3A, right panel**). To validate the hypothesis that actin and E-cadherin mediate structural stress imposed by the 3D colony formation, the hoop stress was quantified along the periphery of the simulated colony (**Figure 5.3B**). Due to observable differences in the predicted hoop stresses within a 3D colony, fluorescent confocal images, of the 3D colony with the same dimensions as the COMSOL simulation, were taken at 5 µm z-values and the intensity of actin was

quantified at the colony periphery with respect to the colony height (**Figure 5.3C**). A significant correlation was determined for actin intensity and hoop stress (Pearson's correlation: 0.803, significance: 0.000) (**Figure 5.3D**). Similarly, E-cadherin intensity was greater near the top of the 3D colony (**Figure 5.3E**) and a significant correlation with the predicted hoop stress was determined (Pearson's correlation: 0.618, significance: 0.008) (**Figure 5.3F**).

5.4.4 – RhoA-ROCK signaling regulates colony morphology of IPSCs and subsequent differentiation.

The major signaling pathway involved in cytoskeletal organization including actin and cadherins, is the RhoA signaling pathway. To determine if the observed differential actin and E-cadherin organization in a colony morphology-dependent manner is due to the RhoA signaling, the RhoA activities of the cells cultured on soft or stiff scaffolds were quantified (**Figure 5.4A**). IPSCs cultured on soft or stiff scaffolds for a shorter culture duration (3 days), which did not induce fully distinctive IPSC colony formation, exhibited an insignificant difference in RhoA activity. However, further development of distinctive 3D colony morphologies on soft scaffolds was accompanied with significantly greater RhoA activity at Day 5. In addition, a greater RhoA activity was observed in the cells cultured on nanofibrous scaffolds, regardless of scaffold stiffness, as compared to IPSCs cultured on tissue culture plate control (**Figure 5.4A**).

To further examine if the RhoA-mediated cell contractility modulated colony morphology, a ROCK inhibitor, Y-27632, commonly used in IPSC passaging, was utilized. To determine the effects of RhoA-mediated cell contractility on scaffold stiffness-induced colony morphology, IPSCs were pre-cultured in the presence of Y-27632 on soft 19 kPa or stiff 313 kPa scaffolds for 5 days. A more distinctive change was observed in the cells on 19 kPa scaffolds where Y-27632 abolished the formation of 3D colonies (**Figure 5.4B**). In the presence of the ROCK inhibitor, the colonies on both soft and stiff scaffolds showed a similar flat, 2D morphology. In spite of changes in colony morphology by the application of ROCK inhibitor, all the colonies maintained pluripotency, evident by NANOG expression (**Figure 5.4B**). A statistically significant change in colony sphericity was observed with the supplementation of Y-27632 regardless of the scaffold stiffness (**Figure 5.4C**). To determine how Y-27632 supplementation affects cytoskeletal organization, the structure of actin and E-cadherin was investigated in the cells cultured on soft and stiff scaffolds (**Figure 5.4, D-E**). Bundling of actin and clustering of E-cadherin in the IPSCs cultured on 19 kPa scaffolds (**Figure 5.2A**) were eliminated by Y-27632 (**Figure 5.4D**). Both actin and E-cadherin organization were similar for the cells cultured on 19 kPa and 313 kPa scaffolds with Y-27632. Notably, E-cadherin was diffused throughout the cell cytoplasm instead of localizing to cell-cell contacts as observed in control samples (**Figure 5.2, A-B**).

To examine the effects of colony morphology on IPSC differentiation tendency, the cells cultured on soft or stiff scaffolds in the presence or absence of ROCK inhibitor

were biochemically induced to differentiate towards mesendodermal or ectodermal lineage. The pre-culture with Y-27632, which prevented 3D colony formation, induced a greater expression of *GSC* and *MIXL1* under mesendodermal differentiation conditions (**Figure 5.5A**). Similarly, the application of Y-27632 enhanced the protein expression of BRACHYURY as compared to the minimal expression in the IPSCs pre-cultured on the soft scaffolds, which had formed 3D colony morphologies (**Figure 5.5B**). In contrast, the application of Y-27632 during pre-culture significantly reduced the ectodermal differentiation tendency of the cells, evident by downregulated *PAX6* and *NEUROD1* expression (**Figure 5.5C**). PAX6 protein expression was highest in cells which had formed 3D colonies on 19 kPa scaffolds, but minimal in the cells which had developed 2D colonies via culture on 313 kPa scaffolds or Y-27632 treatment regardless of scaffold stiffness (**Figure 5.5D**).

5.5 – Discussion

Colony morphology change strongly depends on cytoskeletal reorganization due to the cellular adaptation to their microenvironment. Initially, cells form focal adhesions and these binding sites are changed so that the cells adapt to the substrate mechanics or in response to externally applied force. In our study, cell-ECM interaction was not highly influenced by the development of colony dimensionality, whereas the organization of actin and cell-cell junctional protein, E-cadherin, was a key feature distinguished from

different colony morphologies. 3D colonies developed radially-aligned actin rings, or actomyosin cables, with greater E-cadherin clustering at the neighboring cell-cell junctions as opposed to 2D colonies. Such differences in cytoskeletal organization are likely due to the differential pre-stresses imposed on the cells by different colony structure, as predicted by the simulation in our study. A significant correlation between actin or E-cadherin with hoop stress implicates these components as force mediators in the development of colony dimensionality. Actin and cadherins have been shown to act as force sensors regulating cellular behaviors under mechanical stresses [131-133]. The force balance is critical for the homeostasis of the cells as shown by a study demonstrating that disruption of a single component in the myosin – p120-catenin - E-cadherin axis results in disruption of the cell colony morphology, inhibiting the self-renewal of ESCs [134].

The RhoA signaling pathway is responsible for cytoskeletal reorganization. Adult stem cells have shown to exhibit greater RhoA activity on a stiffer substrate upon seeding due to tensional force from an individual cell to its surroundings [110, 135, 136]. In contrast, our results showed greater activation of RhoA in IPSCs cultured on electrospun scaffolds as compared to much stiffer glass controls. Furthermore, once IPSC colonies developed to a specific size the intracolonial tension was enough to overcome the stiffness of scaffolds, resulting in the fiber deformation to form 3D colonies. This coincided with the hyper-activation of RhoA in the cells on softer 19 kPa scaffolds. The

intracolonial forces by high RhoA activity in 3D IPSC colonies appear to be mediated through cell-cell interactions in addition to the cell-ECM interactions. Considering the fact that the RhoA signaling pathway and its regulation of cytoskeleton modulate phenotypic commitment of MSC differentiation, similar observations in PSCs may pre-dispose the cells to differentiate into a specific lineage. The mechanisms pertaining to the effects of RhoA regulation on stem cell behaviors in human PSCs remain elusive. Dissociation of human PSC colonies into single cells results in the hyperactivation of RhoA, typically leading to apoptosis [137]. However, hyperactivation of RhoA in the 3D colonies appears to be mediated by E-cadherin clustering. The spatial rearrangement of E-cadherin, which is involved in many signaling cascades including the Wnt pathway, may be responsible for priming of the cells to differentiate towards specific lineages. Inhibition of ROCK remarkably affects E-cadherin and junctional actin localization similar to ROCK1 depleted carcinoma cells where junctional contacts are weakened and the cadherin complex and F-actin at cell-cell junctions are displaced [138].

E-cadherin has been implicated in the maintenance of pluripotency, the differentiation of PSCs during gastrulation, and the development of ectodermal lineage [139, 140]. In our previous study, we demonstrated that an extended culture duration of IPSCs in 3D colonies resulted in the spontaneous differentiation towards ectodermal lineage [106]. Similarly, upon biochemical induction, the cells in the 3D colonies exhibited even greater tendency to differentiate towards ectodermal lineage as opposed to their

2D counterparts. During this process, the clustering of E-cadherin may, in part, play a role in the predisposition of the cells by downregulating Wnt signaling. Beta-catenin, a major mediator of the Wnt signaling pathway, has been shown to be sequestered by E-cadherin [141]. Clustering of E-cadherin increases its association with beta-catenin and decreases their dissociation rate, ultimately inhibiting the translocation of beta-catenin to the nucleus for activation of Wnt signaling [142, 143]. Our results show that Wnt signaling may be downregulated in 3D colonies due to the co-localization of beta-catenin with E-cadherin clusters which explains, in part, the decreased efficiency for mesendodermal differentiation. The inhibition of Wnt signaling cascades by its inhibitor, Dickkopf-1, has been also shown to enhance the induction of neural differentiation [144, 145]. Therefore, the observed clustering of E-cadherin in 3D colonies likely suppresses the Wnt signaling pathway by the detainment of beta-catenin at the cell membrane, resulting in the preferential differentiation towards ectodermal lineage. Further investigation is required to determine the localization of beta-catenin after mesendodermal induction in 2D or 3D colonies and manipulation of beta-catenin clustering and its effects on Wnt signaling are also necessary to validate the current implications.

5.6 – Conclusions

Overall, we have demonstrated that IPSC colony morphology can be directly modulated by the mechanics of electrospun scaffolds to alter lineage-specific

differentiation. The colony morphology-dependent differentiation efficiency is likely due to the reorganization of cytoskeletal and junctional proteins, regulated by the RhoA-ROCK-E-cadherin axis. This observation demonstrates that control of cell-cell interaction by modulating stem cell colony morphology with scaffolding provides a novel means to direct stem cell differentiation. Such results would also enable the development of robust protocols to enhance differentiation efficiency of IPSCs towards downstream target cell types.

5.7 – Figures

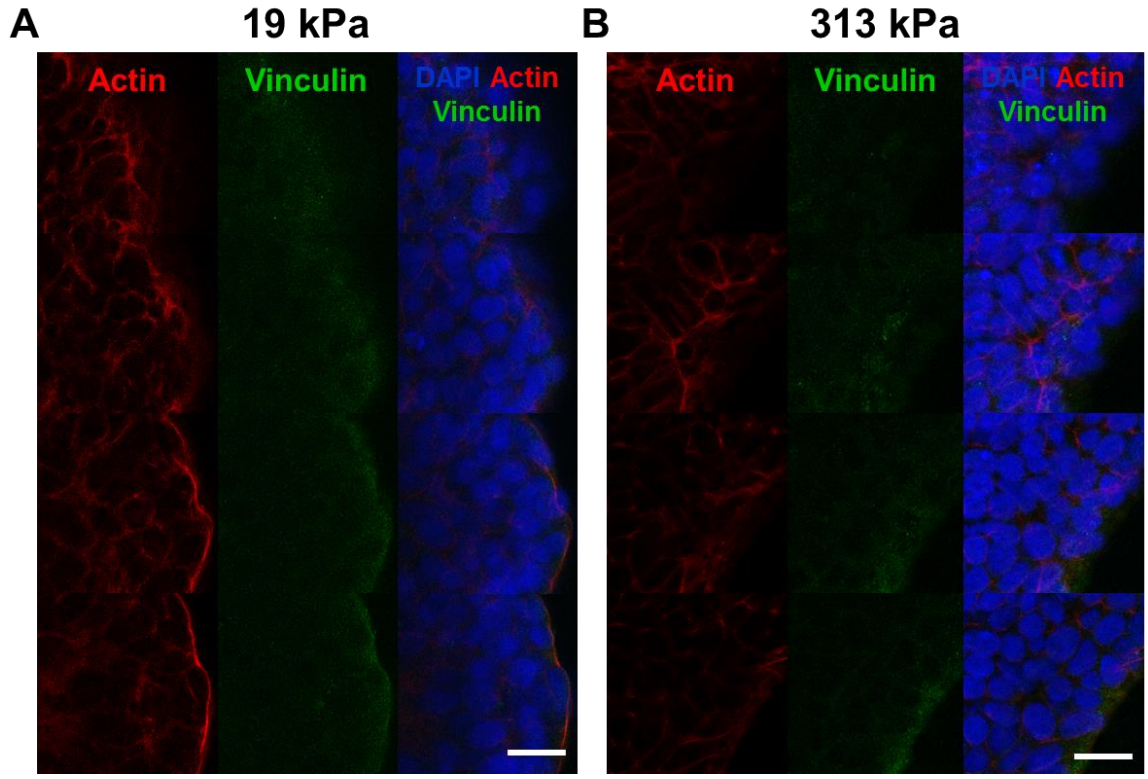

FIGURE 5.1. IPSC COLONY MORPHOLOGY DOES NOT SIGNIFICANTLY CHANGE FOCAL ADHESION PROTEIN, VINCULIN.

(A-B) Confocal images of representative IPSC colonies cultured on soft (19 kPa) or stiff (313 kPa) scaffolds revealing no significant differences in the organization of vinculin (red: actin, green: vinculin, blue: DAPI, scale bar: 25 µm). IPSCs were pre-cultured in proliferation media for 5 days on 19 kPa and 313 kPa scaffolds prior to analysis of protein expression by immunocytochemistry.

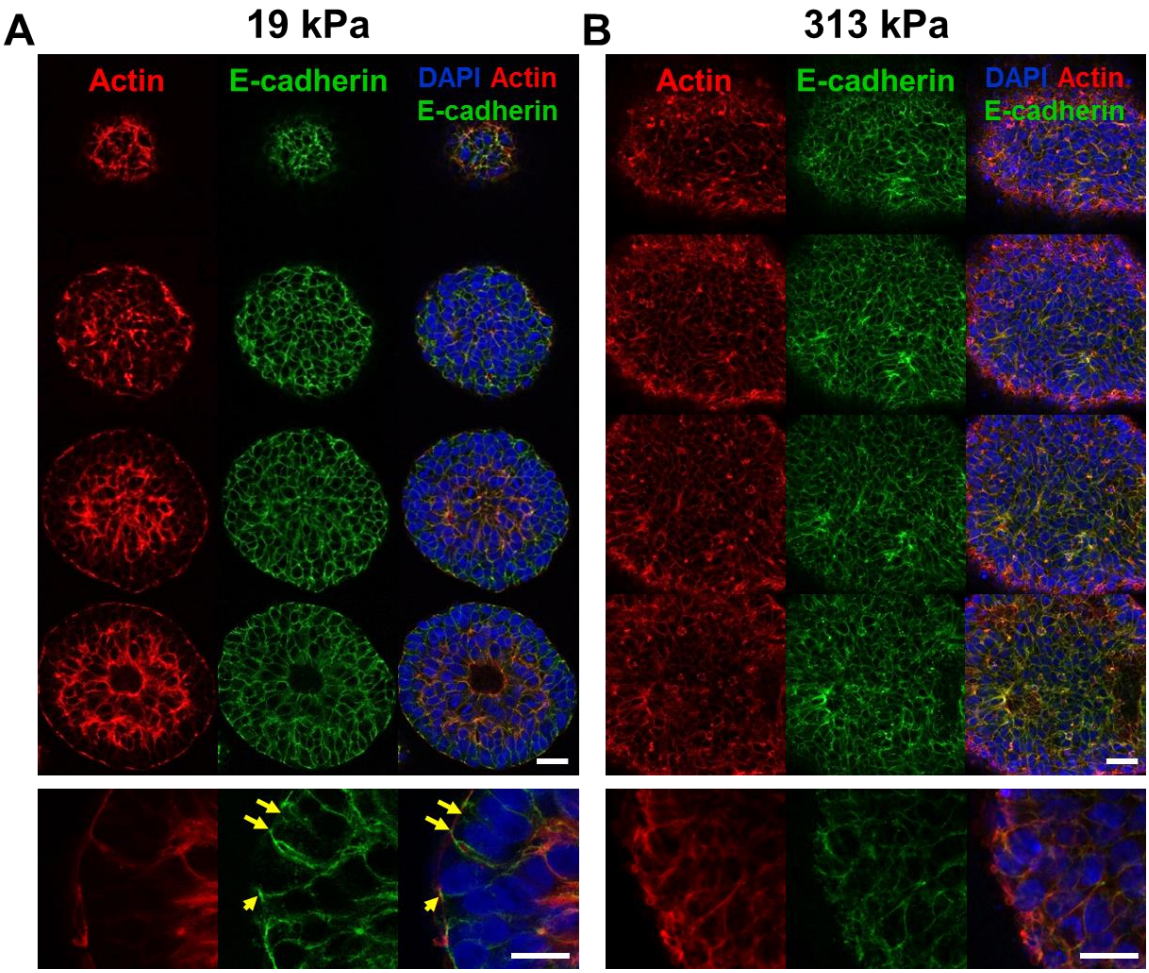

FIGURE 5.2. IPSC COLONY MORPHOLOGY IS MEDIATED BY ACTIN AND E-CADHERIN ORGANIZATION.

(A-B) Confocal images of representative IPSC colonies cultured on soft (19 kPa) or stiff (313 kPa) scaffolds revealed differences in actin and E-cadherin organization. A greater actin bundling was observed in 3D IPSC colonies on 19 kPa scaffolds as compared to the 2D colonies on 313 kPa scaffolds. Greater clustering of E-cadherin (arrows) at the cell-cell junctions near the periphery of the colony in IPSCs cultured on 19 kPa scaffolds was observed (red: actin, green: E-cadherin, blue: DAPI, scale bar: 25 µm). Confocal images were taken every 5 µm intervals but representative images at every 20 µm are shown for the IPSC colony on 19 kPa scaffolds. IPSCs were pre-cultured in proliferation media for 5 days on 19 kPa and 313 kPa scaffolds prior to analysis of protein expression by immunocytochemistry.

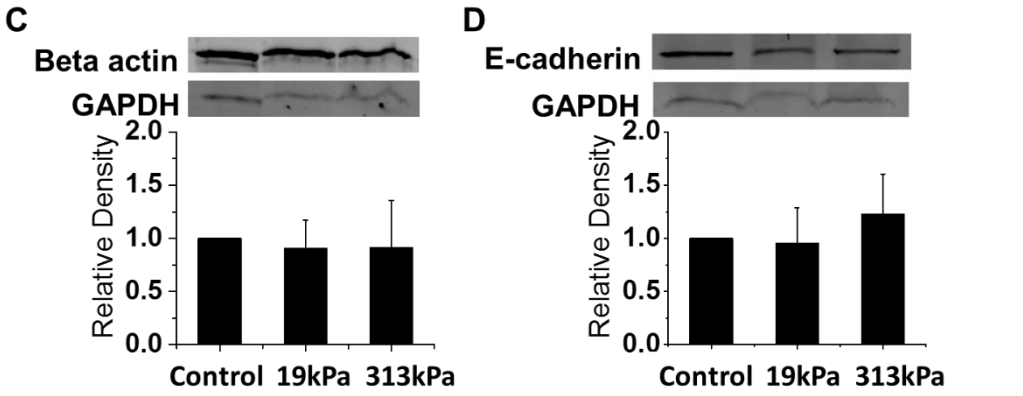

FIGURE 5.3. IPSC COLONY MORPHOLOGY IS MEDIATED BY ACTIN AND E-CADHERIN ORGANIZATION.

(C-D) Insignificant differences in the expression of beta actin and E-cadherin in IPSCs cultured on soft and stiff scaffolds, examined by Western blotting. IPSCs were pre-cultured in proliferation media for 5 days on 19 kPa and 313 kPa scaffolds prior to analysis of protein expression Western blotting. Protein expression values were normalized to IPSCs cultured in proliferation media on tissue culture plastic (Control).

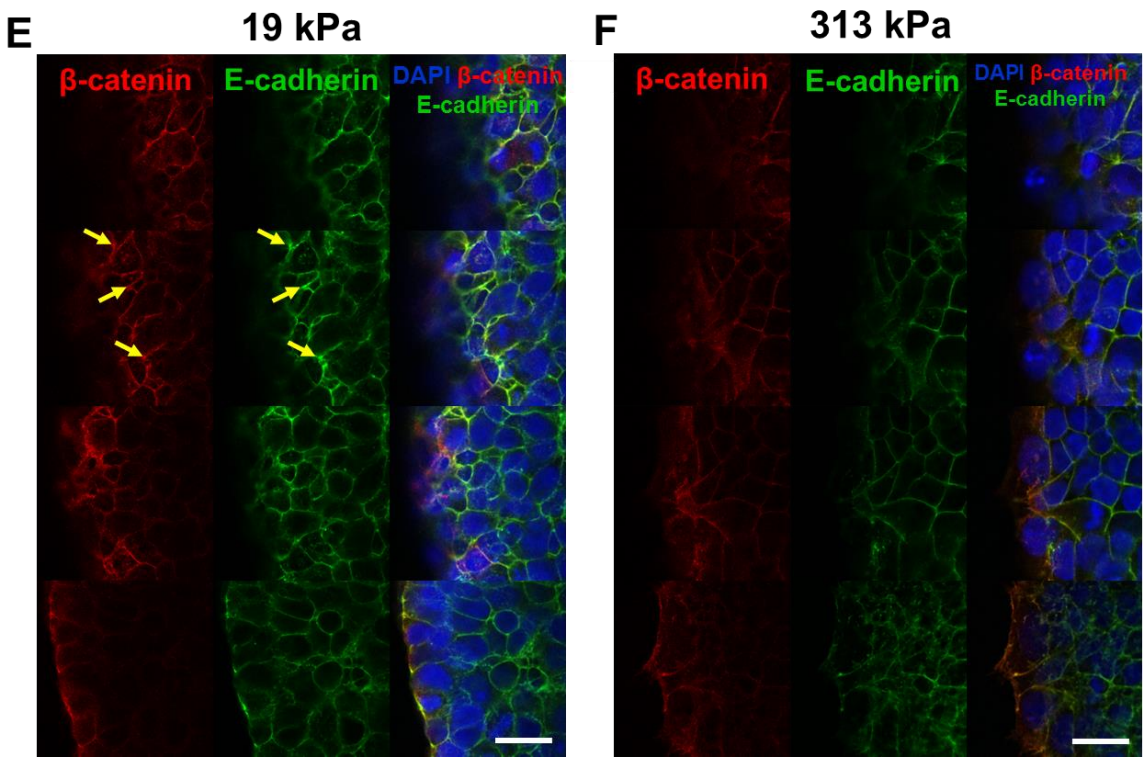

FIGURE 5.4. IPSC COLONY MORPHOLOGY IS MEDIATED BY ACTIN AND E-CADHERIN ORGANIZATION.

(E-F) Localization of beta-catenin was primarily observed at cell-cell junctions as determined by immunocytochemistry, suggesting sequestration of beta-catenin at E-cadherin clusters. Higher beta-catenin intensity was observed at the periphery of 3D IPSC colonies on 19 kPa scaffolds. IPSCs were pre-cultured in proliferation media for 5 days on 19 kPa and 313 kPa scaffolds prior to analysis of protein expression by immunocytochemistry.

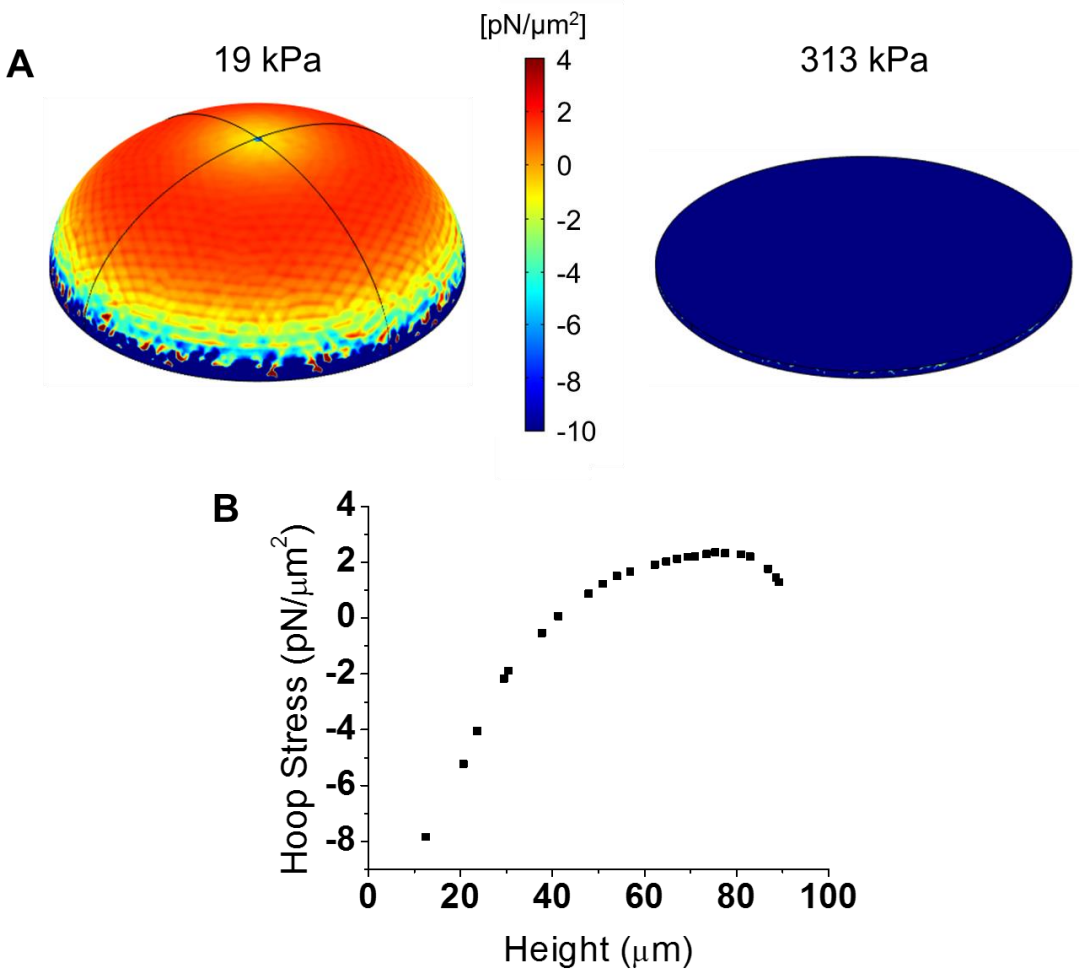

FIGURE 5.5. DISTINCT IPSC COLONY MORPHOLOGIES IMPOSE DIFFERENTIAL STRUCTURAL STRESSES, ON THE CELLS, MEDIATED BY ACTIN AND E-CADHERIN ORGANIZATION.

(A) Structure-dependent hoop stresses due to distinct colony morphology, predicted by COMSOL modeling. A 3D, round colony (19 kPa) experiences tensional hoop forces towards the top of the colony while only compressive forces near the bottom are predicted. A flat, 2D colony (313 kPa) structure experiences relatively uniform compressive hoop forces. (B) Hoop stress values determined from the dimensions of a representative 3D colony on 19 kPa scaffolds. (C) Confocal z-stack images were used to analyze the intensity of actin along the periphery of the colony using ImageJ. (D) Correlation plot of actin and the predicted hoop stress revealed a positive relationship (Pearson's correlation: 0.803, significance: 0.000). (E) E-cadherin intensity at the periphery of the 3D colony. (F) Correlation plot of E-cadherin intensity and the predicted hoop stress values demonstrated a positive relationship (Pearson's correlation: 0.618, significance: 0.008).

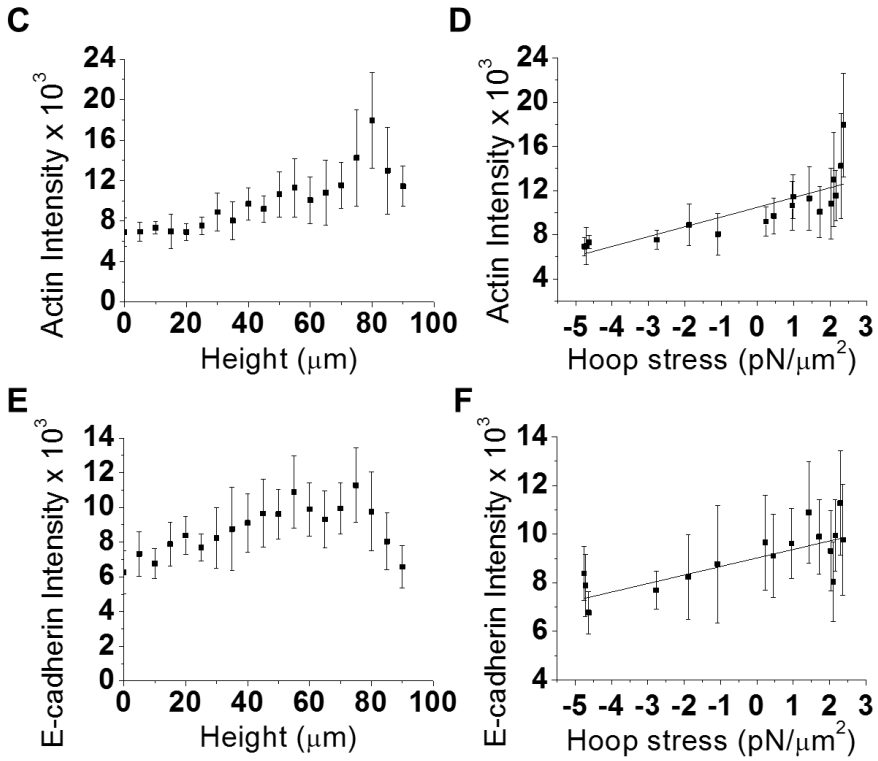

FIGURE 5.6. DISTINCT IPSC COLONY MORPHOLOGIES IMPOSE DIFFERENTIAL STRUCTURAL STRESSES, ON THE CELLS, MEDIATED BY ACTIN AND E-CADHERIN ORGANIZATION.

(A) Structure-dependent hoop stresses due to distinct colony morphology, predicted by COMSOL modeling. A 3D, round colony (19 kPa) experiences tensional hoop forces towards the top of the colony while only compressive forces near the bottom are predicted. A flat, 2D colony (313 kPa) structure experiences relatively uniform compressive hoop forces. (B) Hoop stress values determined from the dimensions of a representative 3D colony on 19 kPa scaffolds. (C) Confocal z-stack images were used to analyze the intensity of actin along the periphery of the colony using ImageJ. (D) Correlation plot of actin and the predicted hoop stress revealed a positive relationship (Pearson's correlation: 0.803, significance: 0.000). (E) E-cadherin intensity at the periphery of the 3D colony. (F) Correlation plot of E-cadherin intensity and the predicted hoop stress values demonstrated a positive relationship (Pearson's correlation: 0.618, significance: 0.008).

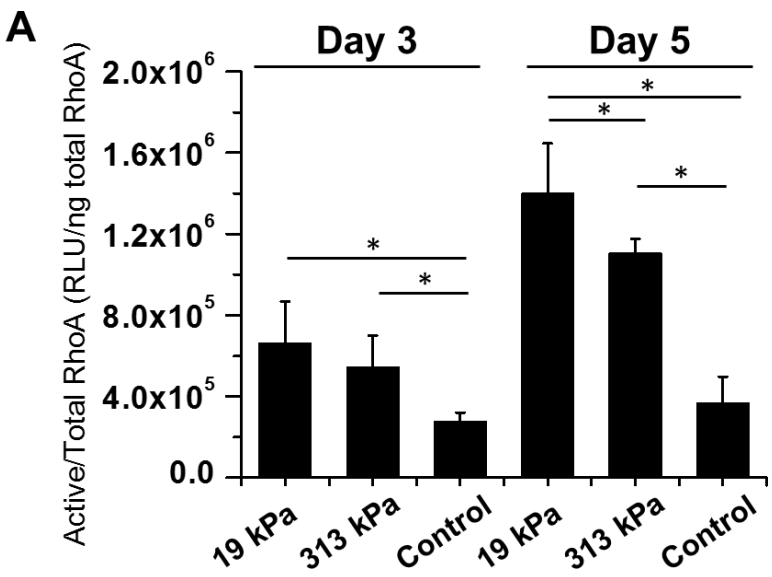

FIGURE 5.7. SCAFFOLD STIFFNESS-DEPENDENT COLONY MORPHOLOGY IS REGULATED BY RHOA.

(A) RhoA activity of IPSCs depends on colony morphology developed by different stiffness of scaffolds and culture duration. IPSCs cultured on softer scaffolds for a longer duration (5 days) resulting in 3D colony formation, exhibited significantly greater RhoA activity as compared to that of IPSCs on 313 kPa scaffolds or tissue culture plates (Control) (* denotes $p < 0.05$). IPSCs were cultured on soft (19 kPa) or stiff (313 kPa) scaffolds in proliferation media for 3 or 5 days.

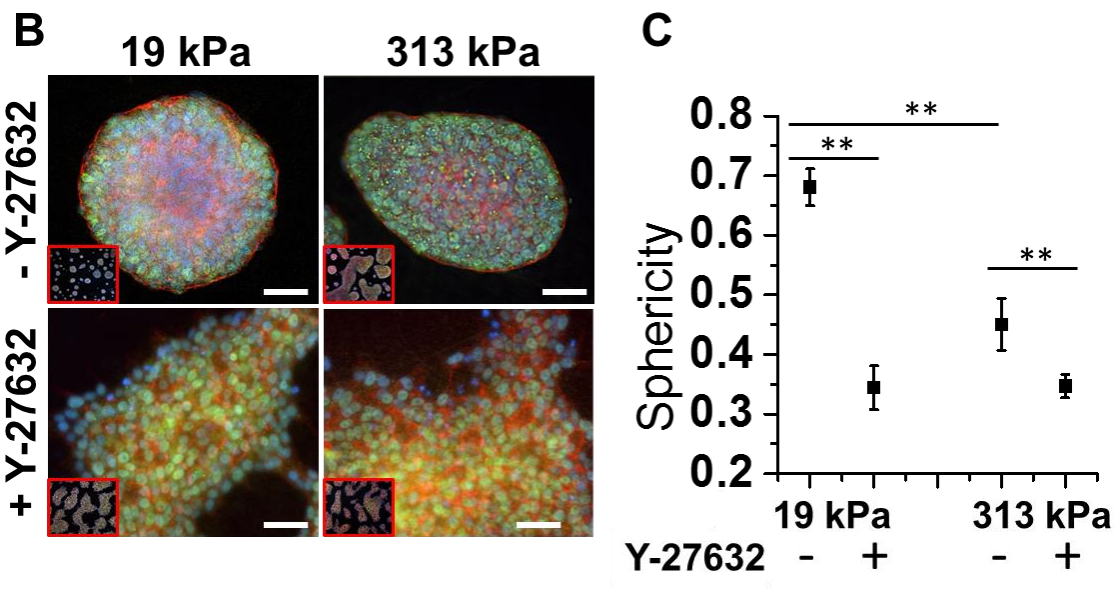

FIGURE 5.8. SCAFFOLD STIFFNESS-DEPENDENT COLONY MORPHOLOGY IS REGULATED BY RHOA.

(B) The application of a ROCK inhibitor (Y-27632) during IPSC culture, for 5 days in proliferation media, abolished the 3D colony formation on 19 kPa scaffolds (bottom panel). IPSCs cultured under all conditions maintained expression of pluripotency marker NANOG (green: NANOG, red: actin, blue: DAPI, scale bar: 100 µm). (C) Colony sphericity was significantly decreased by the supplementation of Y-27632 on both soft and stiff scaffolds. (** denotes $p < 0.01$). IPSCs were cultured on soft (19 kPa) or stiff (313 kPa) scaffolds in proliferation media for 5 days with (+) or without (-) the addition of 40 µM Y-27632.

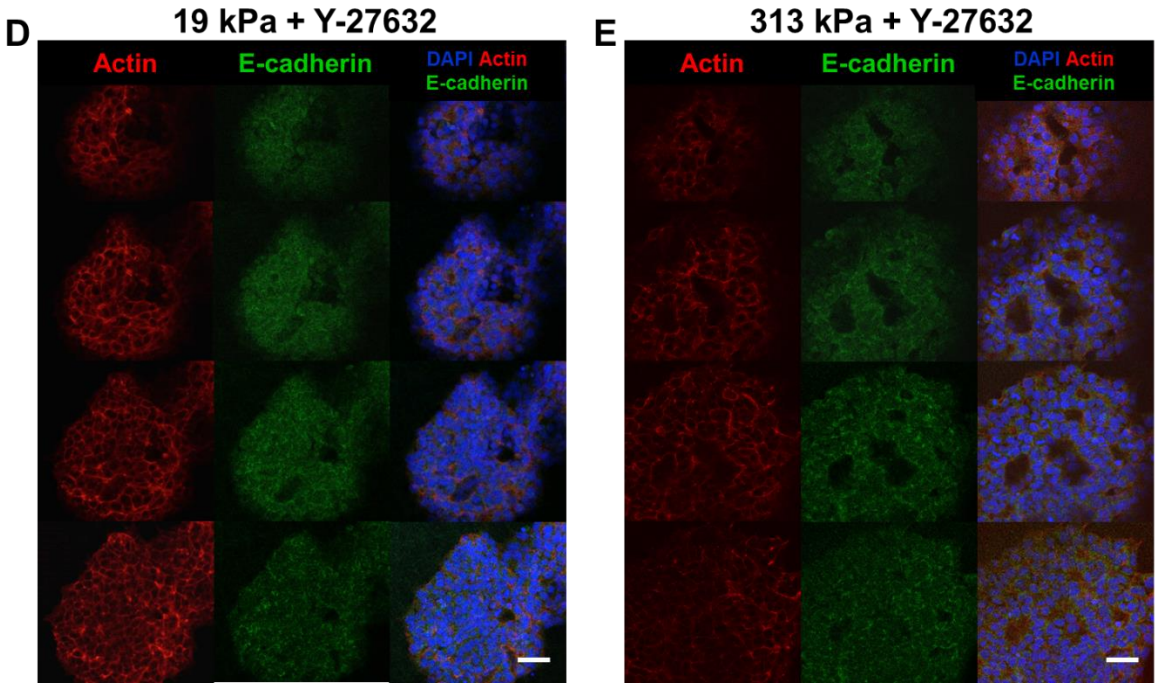

FIGURE 5.9. SCAFFOLD STIFFNESS-DEPENDENT COLONY MORPHOLOGY IS REGULATED BY RHOA.

(D-E) Confocal imaging of IPSCs cultured on 19 kPa and 313 kPa scaffolds in the presence of Y-27632 revealed similar actin organization. Additionally, E-cadherin was not localized to the cell-cell junctions and dispersed within the cytoplasm (red: actin, green: E-cadherin, blue: DAPI, scale bar: 50 µm). IPSCs were cultured on soft (19 kPa) or stiff (313 kPa) scaffolds in proliferation media for 5 days with the addition of 40 µM Y-27632.

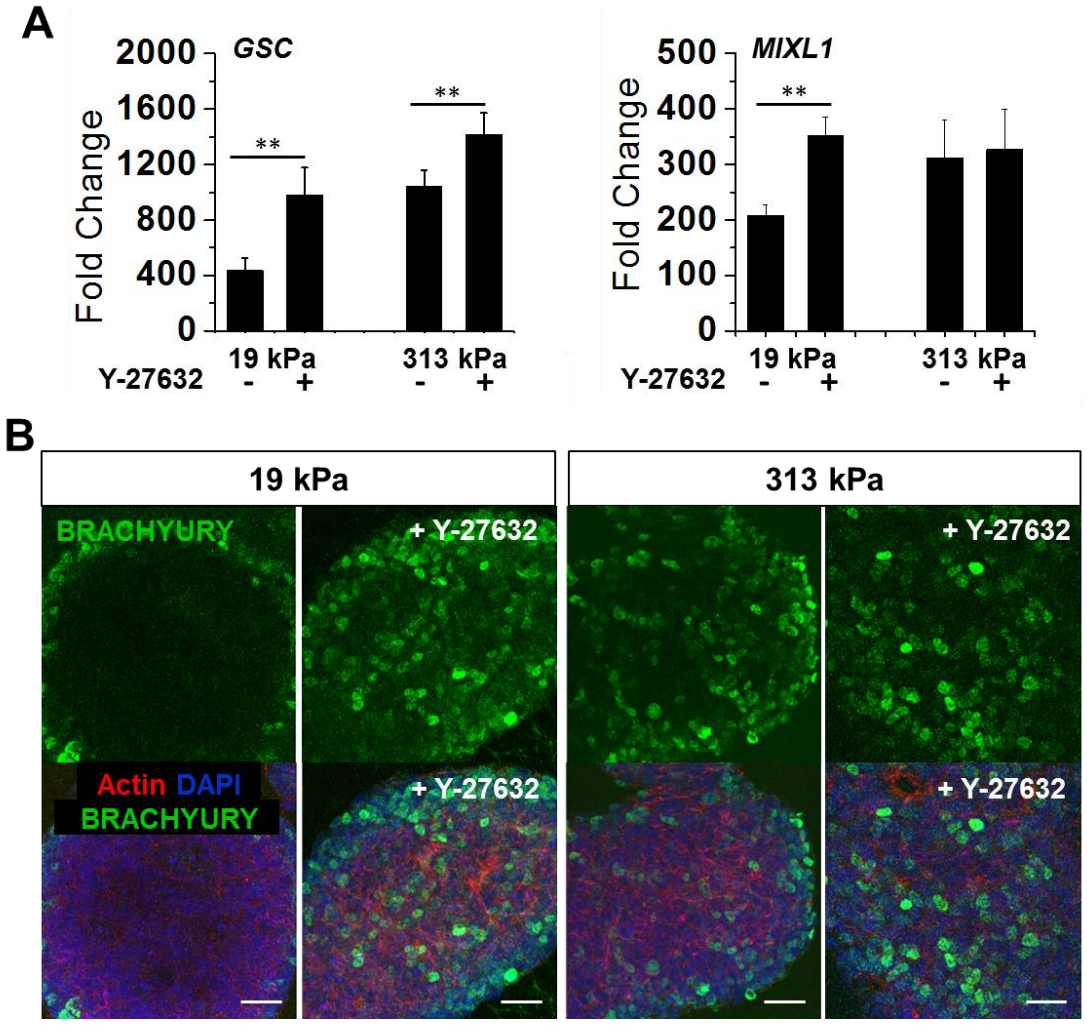

FIGURE 5.10. INHIBITION OF ROCK ABOLISHES SCAFFOLD STIFFNESS-DEPENDENT COLONY FORMATION AND SUBSEQUENT PREFERENTIAL DIFFERENTIATION OF IPSCS TO SPECIFIC LINEAGES.

Induction of a 2D colony morphology via culture on stiffer 313 kPa scaffolds and/or supplementation of Y-27632 during proliferation enhanced mesendodermal differentiation as demonstrated by increased (A) GSC and MIXL1 gene expression and (B) BRACHYURY protein expression. (** denotes $p < 0.01$, green: BRACHYURY, red: actin, blue: DAPI, scale bar: 100 µm). IPSCs were pre-cultured in proliferation media for 5 days with (+) or without (-) the addition of 40 µM Y-27632 on either 19 kPa or 313 kPa scaffolds. After the pre-culture period, the cells were subjected to the respective differentiation media for either (A-B) mesendodermal lineage differentiation. Gene expression of IPSCs cultured in proliferation media on tissue culture plates was used as controls.

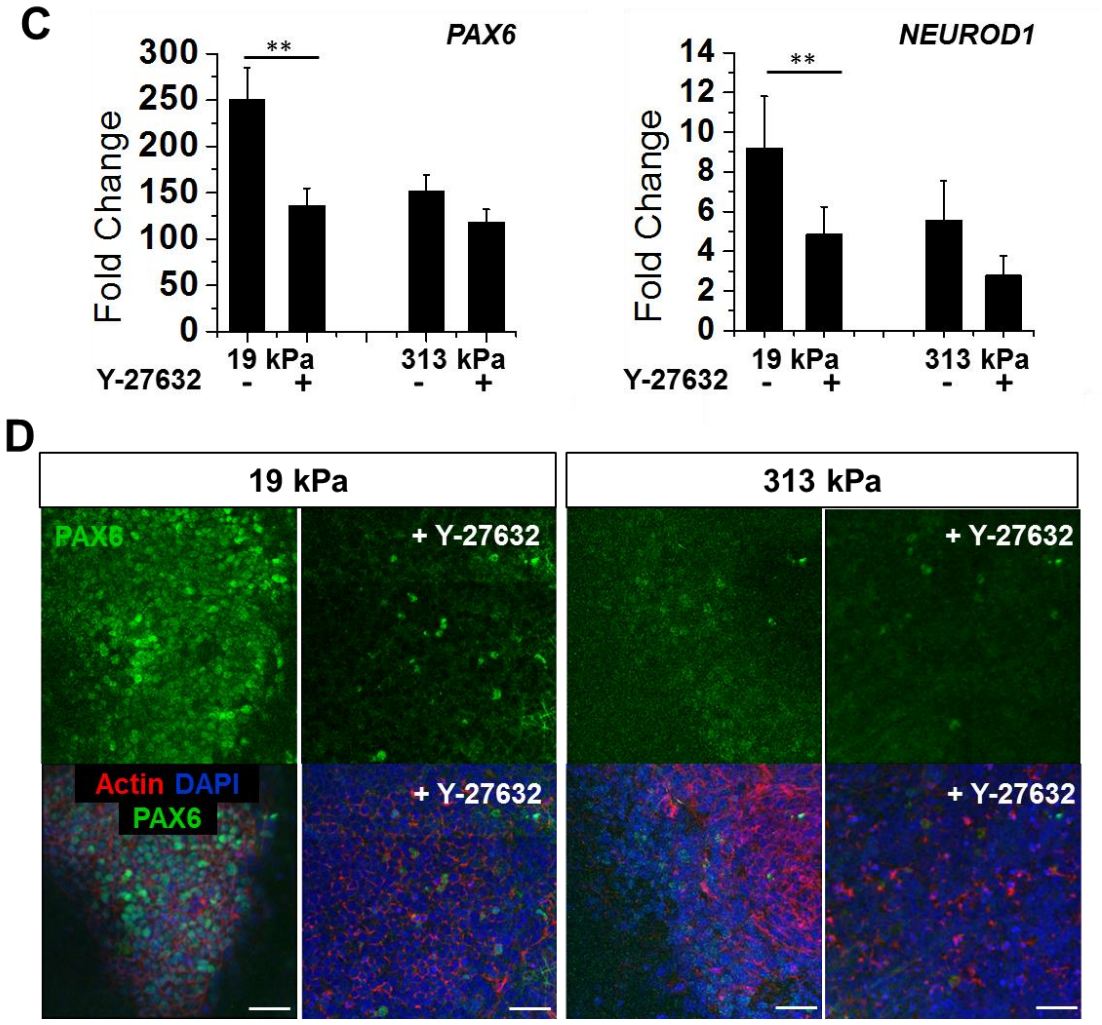

FIGURE 5.11. INHIBITION OF ROCK ABOLISHES SCAFFOLD STIFFNESS-DEPENDENT COLONY FORMATION AND SUBSEQUENT PREFERENTIAL DIFFERENTIATION OF IPSCS TO SPECIFIC LINEAGES.

In contrast, induction of a round, 3D colony morphology prior to differentiation via culture on softer 19 kPa scaffolds enhanced ectodermal differentiation, evident by a significant upregulation of (C) PAX6 and NEUROD1 gene expression and (D) PAX6 protein expression (** denotes $p < 0.01$, green: protein of interest, red: actin, blue: DAPI, scale bar: 100 µm). IPSCs were pre-cultured in proliferation media for 5 days with (+) or without (-) the addition of 40 µM Y-27632 on either 19 kPa or 313 kPa scaffolds. After the pre-culture period, the cells were subjected to the respective differentiation media for either (A-B) mesendodermal or (C-D) ectodermal lineage differentiation. Gene expression of IPSCs cultured in proliferation media on tissue culture plates was used as controls.

CHAPTER 6 – ELECTROSPUN SCAFFOLD STIFFNESS MODULATES STAGE-SPECIFIC DIFFERENTIATION EFFICIENCY OF HUMAN INDUCED PLURIPOTENT STEM CELLS

6.1 – Abstract

The field of mechanobiology has been widely studied for multiple adult stem cell types to enhance their differentiation efficiency. However, little is known about the effects of the mechanical microenvironment on the developmental differentiation of human induced pluripotent stem cells (IPSCs) to adult cell types. In the current proof-of-concept study, we examined how scaffold stiffness affects the differentiation of IPSCs along the developmental stages of differentiation to motor neuron, pancreatic endoderm, or chondrocyte phenotypes. Electrospun polymeric nanofibrous scaffolds with distinct mechanical properties (Reduced Young's Modulus = 19kPa (Soft) or 313kPa (Stiff)) were subjected to Collagen Type I surface conjugation to maintain similar surface chemistries for cell attachment. IPSCs were then seeded onto scaffolds at each developmental stage and samples were analyzed for lineage stage-specific gene and protein expression using rt-PCR and immunocytochemistry, respectively. We demonstrate that a specific stiffness at each stage (soft or stiff) can enhance the differentiation to all three germ layer derivative cell types. Collectively, our results suggest that IPSCs are mechano-responsive and that an optimal mechanical microenvironment can enhance their downstream differentiation for clinical applications.

6.2 – Introduction

The study of human induced pluripotent stem cells has revolutionized the field of personalized medicine by offering a potentially unlimited cell source to treat multiple diseases. Although much efforts have been made to minimize safety concerns of IPSCs by using non-viral techniques for their generation, one inherent risk is their ability to form teratomas in the body [126]. One way to minimize such a risk is to differentiate them to downstream target cell types prior to implantation. IPSCs, which resemble embryonic stem cells, can be differentiated using protocols which mimic embryonic development and trigger specific signaling pathways to maximize their differentiation efficiency [146].

Aside from their clinical potential, IPSCs may also be used to study developmental processes *in vitro*. In this regard, although biochemicals can elicit activation or downregulation of specific signaling cascades, standard culture practices rely on the use of stiff tissue culture plates which are not physiologically relevant. The developing embryo receives many cues, not only through biochemicals, but by the physical extracellular matrix (ECM) that provides structural support and modulates cell behavior. As such, the use of synthetic substrates, such as the electrospun scaffolds used in the current study, can provide an ECM-resembling environment. Additionally, the electrospun scaffolds can be surface-modified using ECM proteins to investigate the effects on cell behavior. Although chemical cues have provided a foundational backbone to guide IPSC

differentiation, the underlying role of the mechanical microenvironment may significantly improve the outcomes of previously published protocols to guide differentiation towards specific lineages.

Our previous studies have discovered the significant role of the mechanical microenvironment on PSC self-renewal and differentiation [106, 121]. Soft electrospun scaffolds result in the development of three-dimensional colonies which enhance ectodermal differentiation whereas stiff scaffolds result in the development of two-dimensional colonies which enhance mesendodermal differentiation. To extend these results further and understand the significant contribution of scaffold stiffness on the developmental stages of differentiation towards three germ layer derivatives, we examined the effects of scaffold stiffness on the biochemically-guided differentiation. Our results demonstrate that depending on the lineage, soft or stiff electrospun scaffolds can enhance the differentiation efficiency of IPSCs at each developmental stage. These results are significant because they establish the mechano-responsiveness of IPSCs and provide a role of the mechanical microenvironment to enhance directed differentiation of IPSCS.

6.3 – Materials and Methods

6.3.1 – Electrospun scaffold synthesis

We previously optimized the electrospinning conditions for 8 wt.% poly(ε-caprolactone (PCL) dissolved in 5:1 trifluoroethanol-water and 5 wt.% PEKK (Oxford Performance Materials, South Windsor, CT) dissolved in 1,1,1,3,3,3-Hexafluoro-2-propanol (HFP) (Oakwood Products Inc., West Columbia, SC) to synthesize nanofibrous scaffolds with approximately 450 nm average fiber diameter [121]. The scaffolds were mechanically characterized to determine a 19 kPa and 313 kPa Reduced Young's Modulus for PCL and PEKK, respectively. Similar to our previous report, to examine the contributions of scaffold mechanics, and not surface chemistry, the scaffolds were air-plasma-treated at 30 W for 5 minutes and further processed for bovine collagen type I conjugation using the zero-length crosslinking agent N-hydroxysuccinimide (NHS)/N-(3-Dimethylaminopropyl)-N'-ethylcarbodiimide hydrochloride (EDAC) [121]. The collagen-conjugated scaffolds were sterilized prior to cell seeding using 70% ethanol and UV.

6.3.2 – Cell culture

An established human induced pluripotent stem line was maintained on Geltrex®-coated tissue culture plates in mTeSR™1 medium (STEMCELL Technologies, Vancouver,

Canada) in a humidified incubator at 37 °C and 5% CO_2 [106]. Cells were passaged from tissue culture plates for each stage of differentiation using 0.25% Trypsin-EDTA (Life Technologies, Grand Island, NY). ROCK inhibitor, Y-27632 (EMD Millipore, Billerica, MA), was used at 10 µM concentration to enhance cell survival after seeding onto electrospun scaffolds. After overnight incubation with defined stage-specific media, the Y-27632 was removed and fresh media supplemented with lineage-specific growth factors was added. Media was exchanged daily unless otherwise noted.

6.3.3 – Differentiation of IPSCs

To study the effects of electrospun scaffold stiffness on the differentiation of IPSCs, defined developmental-stage protocols for motor neuron, pancreatic endoderm, and chondrocytes were utilized. IPSCs were pre-cultured on Geltrex®-coated tissue culture plates (TCPS) according to the protocol recommendations (i.e., motor neuron differentiation required a three day proliferation culture period to reach near confluency prior to the induction of differentiation). Initially, IPSCs were seeded at 70,000 cells/cm^2 on TCPS for propagation and induction of differentiation to stage 2 or stage 3. Alternatively, to analyze the effects of scaffold stiffness at stage 1 differentiation, IPSCs were seeded directly onto electrospun scaffolds at approximately 125,000 cells/cm^2. At the end of each stage of differentiation, samples were either lysed for gene expression analysis or fixed for protein expression analysis. IPSCs differentiated on TCPS through

Stage 1 were seeded onto electrospun scaffolds at a seeding density of 150,000 cells/cm^2 for differentiation through Stage 2. Similarly, cells differentiated on TCPS through Stage 2 were seeded onto scaffolds at a seeding density of 150,000 cells/cm^2 for differentiation through Stage 3.

Differentiation to motor neurons

To differentiate IPSCs towards a motor neuron lineage, a protocol by Chambers et al. was utilized to guide the cells through the ectodermal, neural progenitor, and motor neuron stages [147]. Media was supplemented every other day with stage-specific media and growth factors. For Stage 1 differentiation the cells were cultured in knockout replacement (KO) media (Gibco) supplemented with 10 μM TGF-β inhibitor, SB431542 (Cayman Chemical, Ann Arbor, MI) and 500 ng/ml Noggin (PeproTech, Rocky Hill, NJ) (Days 1-5). Stage 2 differentiation was induced on Days 6-10 using a gradual increase in amount of N2 media from 25%, 50%, and 75%. The media was supplemented with 20 ng/ml BDNF (Peprotech), 0.2 mM ascorbic acid (Sigma), 200 ng/ml sonic hedgehog (Peprotech), and 0.1 μM retinoic acid (Sigma). Stage 3 differentiation was induced on Days 11-19 using N2 media supplemented with 20 ng/ml BDNF, 0.2 mM ascorbic acid, 200 ng/ml sonic hedgehog, and 0.1 μM retinoic acid.

Differentiation to pancreatic endoderm

A protocol by Kroon et al. was utilized to differentiate IPSCs through mesendoderm, posterior foregut, and pancreatic endoderm stages [148]. Media was supplemented every day with stage-specific media and growth factors. For Stage 1 differentiation the cells were cultured in RPMI Glutamax media (Gibco) supplemented with 100 ng/ml Activin A (PeproTech) and 25 ng/ml Wnt3a on Day 1 and RPMI media with 0.2% vol/vol FBS supplemented with 100 ng/mL Activin A for Days 2-4. At the start of Stage 2, the wells were briefly washed with PBS with calcium and magnesium and media was exchanged to RPMI media with 2% vol/vol FBS supplemented with 25-50 ng/ml KGF on Days 5-9. On Days 10-12 the media was changed to DMEM with 1% vol/vol B27 supplemented with 0.25 µM KAAD-cyclopamine (EMD Millipore, Temecula, CA), 2 µM retinoic acid, and 50 ng/ml noggin. Stage 3 was induced on Days 13-16 by DMEM with 1% vol/vol B27 and no addition of growth factors.

Differentiation to chondrocytes

The directed differentiation of IPSCs to chondrocytes was adapted from a protocol by Oldershaw et al. by guiding the cells through a mesendoderm, mesoderm, and chondrocyte stage [109]. Basal media, DMEM:F12 with L-glutamine, ITS, nonessential amino acids, B27, and beta-mercaptoethanol, was exchanged daily with stage-specific

growth factors. Stage 1 was induced by the addition of: 25 ng/ml WNT3A and 50 ng/ml Activin A on Day 1; 25 ng/ml WNT3A, 25 ng/ml Activin A, and 20 ng/ml FGF2 on Day 2; 25ng/ml WNT3A, 10 ng/ml Activin A, 20 ng/ml FGF2, and 40 ng/ml BMP4 on Day 3. Stage 2 was induced by the addition of: 20 ng/ml FGF2, 40 ng/ml BMP4, 100 ng/ml Follistatin, and 2 ng/ml NT4 on Days 4-7; 20 ng/ml FGF2, 40 ng/ml BMP4, and 2 ng/ml NT4 on Day 8. Stage 3 was induced by the addition of: 20 ng/ml FGF2, 20 ng/ml BMP4, 20 ng/ml GDF5, and 2 ng/ml NT4 on Days 9-10; 20 ng/ml FGF2, 40 ng/ml GDF5, and 2 ng/ml NT4 on Days 11-14.

6.3.4 – Gene expression analysis

IPSCs were harvested at each stage of differentiation for total RNA isolation using an RNeasy Micro Kit (Qiagen, Valencia, CA) following manufacturer instructions. Complementary DNA synthesis was performed using an iScript cDNA Synthesis Kit (Bio-Rad, Hercules, CA). Quantitative real-time PCR was used to detect stage/lineage specific markers using custom primers (**Table 6.1**). Gene expression levels were analyzed using the comparative threshold cycle (CT) method with *GAPDH* used as an endogenous control [75].

6.3.5 – Immunocytochemistry

To analyze the protein expression of stage/lineage-specific markers, cells were fixed with 4% paraformaldehyde for 30 minutes. The cell membrane was permeabilized using a 0.1% Triton-X in phosphate buffered saline (PBS) solution. To prevent non-specific binding, samples were incubated with 1% bovine serum albumin (BSA) in PBS for 30 minutes at room temperature. Samples were then incubated at 4 °C with the following stage-specific primary antibodies: mouse anti-PAX6 (Developmental Hybridoma Studies Bank (DSHB), Iowa City, IA), mouse anti-GSC (Abcam, San Francisco, CA), mouse anti-Nestin (DSHB), goat anti-FOXA2 (R&D systems), goat anti-BRACHYURY (R&D Systems), mouse anti-HB9 (DSHB), rabbit anti-PDX1 (Abcam), or mouse anti-Collagen Type II (DSHB). After overnight incubation, the samples were stained with their respective secondary antibodies: donkey anti-mouse 488, donkey anti-goat 488, or goat anti-rabbit 488 (Invitrogen, Waltham, MA)). Samples were counter-stained using mounting medium with 4',6-diamidino-2-phenylindole (DAPI) (Vectashield, Vector Laboratories, Burlingame, CA) to stain nuclei. Images were acquired using an epi-fluorescent microscope (Nikon Eclipse, Melville, NY). Image J software was used to quantify the percent positive cells using the single color images to count total cell number (DAPI images) and the protein-positive cells (green fluorescence images). Briefly, the images were converted to an 8-bit image type and the threshold was adjusted to highlight the cell nuclei. To divide merged cells the image was processed using the Watershed option. The 'analyze particles' function was

used to determine the cell count. If the clarity of the images taken was not sufficient to accurately obtain a cell count the nuclei or positive cells were counted manually. At least 10 images were analyzed from stage-specific stained samples and the data is presented as mean ± standard deviation.

6.3.6 – Statistical analysis

All experiments were conducted with at least triplicate samples and data is represented as means ± standard error of means (SEM) unless otherwise noted. Statistical significance was determined by the one sample student T-test using SPSS (v.23.0) software. A '*p*' value of 0.05 or less was considered statistically significant.

6.4 – Results & Discussion

6.4.1 – Examining the role of scaffold stiffness on the developmental stages of differentiation of human IPSCs towards three germ layer downstream phenotypes.

To fully achieve their therapeutic potential, human IPSCs must be differentiated to end fully functional phenotypes. Many protocols follow developmental signaling pathways and promote differentiation by characterizing the effects of various growth factors/cytokines. In the current study we aimed to examine the role of scaffold stiffness

on the differentiation IPSCs by seeding cells onto soft (19 kPa) or stiff (313 kPa) scaffolds at either Stage 1, 2, or 3 of differentiation to either motor neuron, pancreatic endoderm, or chondrocytes. Cells from the previous stage were seeded onto the scaffolds and after overnight incubation they were subjected to defined growth factors following previously published protocols [109, 147, 148]. Briefly, motor neuron differentiation was performed by initial dual inhibition of SMAD signaling followed by patterning to motor neurons using BDNF, ascorbic acid, SHH, and retinoic acid [147]. Pancreatic endoderm differentiation was performed by high concentrations of activin A followed by primitive gut tube, posterior foregut, and pancreatic endoderm/endocrine precursors using FBS, KAAD-cyclopamine, and retinoic acid [148]. Optimization of this protocol was conducted by testing various concentrations and temporal approaches to mimic the developmental stages by detection of multiple key gene expression markers. Lastly, chondrocyte differentiation was performed by primitive streak induction with Wnt3a/activin A followed by mesoderm induction using BMP4 and FGF2, and chondrogenesis was induced by reducing BMP4 and increasing GDF5 [109]. Each of the protocols was optimized to yield the highest population of cells expressing lineage-specific markers to ultimately enhance the differentiation efficiency. Although the protocols are expected to be highly efficient, inherent differences in cell lines, regardless of origin, may result in inconsistencies in the expected yields [149]. Therefore, although a high differentiation efficiency was expected, further optimization of the differentiation protocol may be necessary to compensate for differences between cell lines.

6.4.2 – Stage 1 differentiation of IPSCs

In many adult stem cell types, matrix elasticity or stiffness has been shown to be an important mediator of lineage specification where soft substrates promote neural phenotypes while more rigid substrates promote muscular phenotypes [110]. We first examined how electrospun nanofibrous scaffold stiffness affects the differentiation of IPSCs to ectodermal lineage (**Figure 6.2**). Consistent with our previous results, the expression of ectodermal markers *FGF5* and *PAX6* was significantly increased on 19 kPa (**Figure 6.2A**). Consistent with gene expression data, the protein expression of PAX6 was significantly enhanced on 19 kPa scaffolds with a 48% increase in %-positive cells as compared to 313 kPa scaffolds (**Figure 6.2B**). In contrast, when IPSCs were differentiated to mesendodermal lineage, expression of mesendodermal markers *GSC* and *MIXL1* was significantly increased on 313 kPa (**Figure 6.3A**). Consistent with gene expression data, protein expression of GSC was significantly enhanced on 313 kPa scaffolds as compared to 19 kPa scaffolds (**Figure 6.3B**). The results presented here further demonstrate the mechano-responsive nature of IPSCs even at the early stages of lineage commitment where neural induction is enhanced on soft scaffolds while the primitive streak/mesendodermal differentiation requires a stiffer substrate.

6.4.3 – Stage 2 differentiation of ectodermal or mesendodermal cells from IPSCs

To further understand how the mechanical microenvironment affects the developmental differentiation of IPSCs, expanded ectodermal or mesendodermal cells were sub-cultured onto electrospun scaffolds. Following attachment, the differentiation was induced through the end of Stage 2 for each cell lineage. Interestingly, the differentiation of ectodermal cells to neural progenitors was enhanced on 313 kPa scaffolds (**Figure 6.4**). The trend was consistent for gene expression of *SOX1* and *VIM* (**Figure 6.4A**) and protein expression of NESTIN (**Figure 6.4B**), although there was no significant difference in %-positive cells regardless of scaffolds stiffness. Additionally, it should be noted that gene expression of *SOX1* was not significantly upregulated (fold change value less than 1). Overall, these results suggest that although neural progenitor differentiation may be enhanced on stiffer substrates, electrospun scaffolds may not be the ideal platform to maximize the differentiation efficiency.

The differentiation of mesendodermal cells to posterior foregut was significantly enhanced on 19 kPa scaffolds (**Figure 6.5**). Gene expression of *HNF6* and *FOXA2* was significantly increased on 19 kPa scaffolds (**Figure 6.5A**). In accordance, protein expression of FOXA2 was significantly increased on 19 kPa evident by a 32% increase in %-positive cells (**Figure 6.5B**). Interestingly, clusters or colony-forming cells did not express FOXA2 suggesting the heterogeneous differentiation possibly to other pancreatic

cell types. Further analysis would need to be conducted to reveal if other early/late lineage-markers are expressed depending on the spreading of the cells. Recently, Dorrell et al. demonstrated different β cell subtypes in human islets which indicates that heterogeneity in pancreatic differentiation may be positive for insulin-production [150].

In contrast to the posterior foregut stage, the differentiation of mesendodermal cells to mesodermal specification is significantly enhanced on 313 kPa scaffolds (**Figure 6.6**). Gene expression of mesodermal markers *KDR* and *PDGFB* are significantly enhanced on 313 kPa scaffolds (**Figure 6.6A**). Additionally protein expression of BRACHYURY is also enhanced with a significant increase of 20% more positive cells on 313 kPa scaffolds as compared to 19 kPa scaffolds (**Figure 6.6B**). Overall, the results suggest that mechanical microenvironment contributes to the divergence of a mesendoderm population where specification of endodermal phenotypes is enhanced on soft scaffolds whereas mesodermal phenotypes are enhanced on stiff scaffolds.

6.4.4 – Stage 3 differentiation of neural progenitors, posterior foregut cells, or mesodermal cells from IPSCs

To determine the final downstream specification of IPSCs, the differentiated neural progenitors, pancreatic endodermal cells, or mesodermal cells on TCPS were passaged and seeded on electrospun scaffolds with distinct stiffness. The cells were further differentiated to either motor neurons, pancreatic endoderm, or chondrocytes.

Interestingly, motor neuron differentiation was significantly enhanced on 313 kPa scaffolds (**Figure 6.7**). Expression of motor neuron markers *NEUROG2* and *ISL1* was significantly increased on 313 kPa scaffolds (**Figure 6.7A**). In agreement, protein expression of HB9 was also significantly enhanced with a 15% increase in positive cells on 313 kPa scaffolds as compared to 19 kPa scaffolds (**Figure 6.7B**). Unlike studies using hydrogel systems, our results indicate specification of neural progenitor cells to motor neurons is enhanced on stiffer substrates. Inherent differences in topography and the pliability of fiber networks, in addition to the tested stiffness range, may contribute to the opposing results. Nonetheless, the 313 kPa electrospun scaffolds used in this study promote enhanced differentiation to motor neurons.

The specification of posterior foregut cells to pancreatic endodermal cells was significantly enhanced on 19 kPa scaffolds (**Figure 6.8**). Gene expression of pancreatic endoderm markers *NKX2-2* and *NKX6-1* was significantly increased on soft scaffolds (**Figure 6.8A**). Protein expression of PDX1 was also significantly enhanced on 19 kPa scaffolds with a 16% increase in positive cells as compared to 313 kPa scaffolds (**Figure 6.8B**). Similarly, the specification of mesodermal cells to chondrocytes was significantly enhanced on 19 kPa scaffolds (**Figure 6.9**). Gene expression of *SOX9* and *COL2A* was significantly increased on 19 kPa scaffolds, with protein expression of Collagen Type II also displaying a similar trend (**Figure 6.9**). A significant 35% increase in positive cells on 19 kPa scaffolds was determined as compared to 313 kPa scaffolds (**Figure 6.9B**). Taken

together, these results suggest that although a divergence in optimal scaffold stiffness is observed for mesendodermal differentiation towards endodermal or mesodermal lineages, the final stage of downstream phenotype differentiation to either pancreatic endoderm or chondrocytes is enhanced on soft scaffolds. Chondrocyte commitment from a mesodermal stage is consistent with our previous work with mesenchymal progenitors where chondrogenesis was enhanced on soft substrates [115].

6.4.5 – Summary

Overall, the results presented in this proof-of-concept study demonstrate the significant role of the mechanical microenvironment on the developmental differentiation of IPSCs to specific lineages (**Figure 6.10**). Neural induction is initially enhanced on soft substrates but as the differentiation progresses stiff scaffolds promote neural progenitor and motor neuron specification. Neural progenitor differentiation on electrospun scaffolds may not be suitable to enhance the efficiency of specification unless an intermediate stiffness is required. Mesendodermal differentiation is enhanced on stiff scaffolds but further specification to posterior foregut requires a soft scaffold while mesodermal specification requires a stiff scaffold. The final specification stages of pancreatic endoderm and chondrocyte lineages are enhanced on soft scaffolds. Due to the distinctive changes in differentiation efficiency based on scaffold stiffness, it is likely

that an optimal stiffness can significantly contribute to enhancing lineage specification possibly saving both time and costs.

6.5 – Conclusions

The mechanical microenvironment significantly contributes to stage- and lineage-specific differentiation of IPSCs. The results presented in this proof-of-concept study demonstrate that an optimal scaffold stiffness can be used to enhance the differentiation efficiency of IPSCs along developmental stages. Thus, optimization of the mechanical microenvironment using electrospun scaffolds may facilitate the clinical application of IPSCs for therapeutic applications by enhancing their directed differentiation to adult cell types.

6.6 – Tables & Figures

Primer	Forward	Reverse
GAPDH	*5′*-GCAAATTCCATGGCACCGT-*3′*	*5′*-TCGCCCCACTTGATTTTGG-*3′*
Ectoderm		
FGF5	*5′*-GTATGTGGCCCTGAATAAAAGAGG-*3′*	*5′*-AAAGTTCTGGCTGCTCCGACT-*3′*
PAX6	*5′*-GAGTTCTTCGCAACCTGGCTA-*3′*	*5′*-CTGCCCGTTCAACATCCTTAG-*3′*
SOX1	*5′*-AACGCCTTCATGGTGTGGT-*3′*	*5′*-TGATCTCCGAGTTGTGCATCTT-*3′*
VIM	*5′*-GGAAGAGAACTTTGCCGTTGAAG-*3′*	*5′*-ACGAAGGTGACGAGCCATTTC-*3′*
NEUROG2	*5′*-CATCAAGAAGACCCGTAGACTG-*3′*	*5′*-TCTCGATCTTGGTGAGCTTGG-*3′*
ISL1	*5′-GCTTACAGGCTAACCCAGTGGAA-3′*	*5′*-TGTCACTCTGCAAGGCGAAGTC-*3′*
Mesendoderm		
GSC	*5′*-GATGCTGCCCTACATGAACGT-*3′*	*5′*-TACTTGGTCTCCTGGAAGAGGTT-*3′*
MIXL1	*5′*-CTTTGGCTAGGCCGGAGATTA-*3′*	*5′*-GGCAGGCAGTTCACATCTACCT-*3′*
Endoderm		
HNF6	*5′*-GCGTCCATCCAAAGAATTGC-*3′*	*5′*-CCTCCTTCTTGCGTTCATGAA-*3′*
PDX1	*5′-GGAGCTGGCTGTCATGTTGAACT-3′*	*5′*-TTGTCCTCCTCCTTTTTCCACTTC-*3′*
NKX2-2	*5′*-ACGCAGGTCAAGATCTGGTTC-*3′*	*5′*-GCGTCACCTCCATACCTTTCTC-*3′*
NKX6-1	*5′*-CCACTTTTTCCGGACAGCA-*3′*	*5′*-CCCCAACGAATAGGCCAAA-*3′*
Mesoderm		
KDR	*5′*-CACCACTCAAACGCTGACATGTA-*3′*	*5′*-CCAACTGCCAATACCAGTGGA-*3′*
PDGFB	*5′*-ATGCAGACATCGAGTCCTCCA-*3′*	*5′*-ATCAAAGTTGCTCGGCAGGTC-*3′*
COL2A	*5′*-CAACACTGCCAACGTCCAGAT-*3′*	*5′*-CTGCTTCGTCCAGATAGGCAA-*3′*
SOX9	*5′*-TGCTCAAAGGCTACGACTGG-*3′*	*5′*-TTGACGTGCGGCTTGTTCT-*3′*

TABLE 6.1. CUSTOM REAL-TIME POLYMERASE CHAIN REACTION (PCR) PRIMERS.

Sequences of forward and reverse primers for lineage-specific genes.

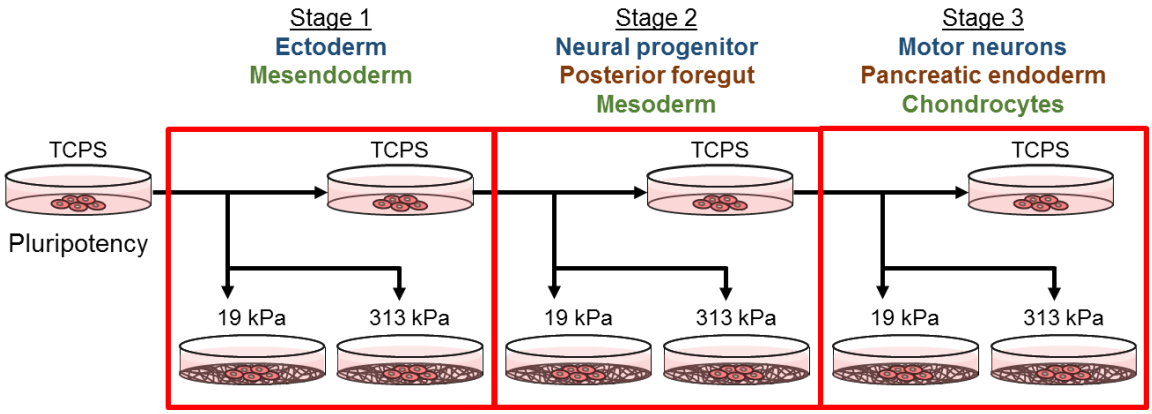

FIGURE 6.1. SCHEMATIC OF THE EXPERIMENTAL DESIGN TO EXAMINE THE EFFECTS OF SCAFFOLD STIFFNESS AT EACH DEVELOPMENTAL STAGE OF DIFFERENTIATION.

Human induced pluripotent stem cells (IPSCs) were differentiated along three germ layer phenotypes following defined developmental protocols (i.e., Stage 1: ectoderm, Stage 2: neural progenitor, Stage 3: motor neurons). IPSCs were cultured on Geltrex®-coated tissue culture plastic (TCPS) prior to passaging for Stage 1 differentiation to either mesendoderm or ectoderm on 19 kPa (soft) or 313 kPa (stiff) electrospun scaffolds. Alternatively, cells were seeded onto TCPS and after Stage 1 of differentiation they were passaged and seeded onto electrospun scaffolds and further differentiated through the end of stage 2. At the end of stage 2 differentiation on TCPS cells were passaged and seeded onto electrospun scaffolds and propagated through the end of stage 3. At each stage of differentiation the samples were analyzed for gene and protein expression of lineage-specific markers.

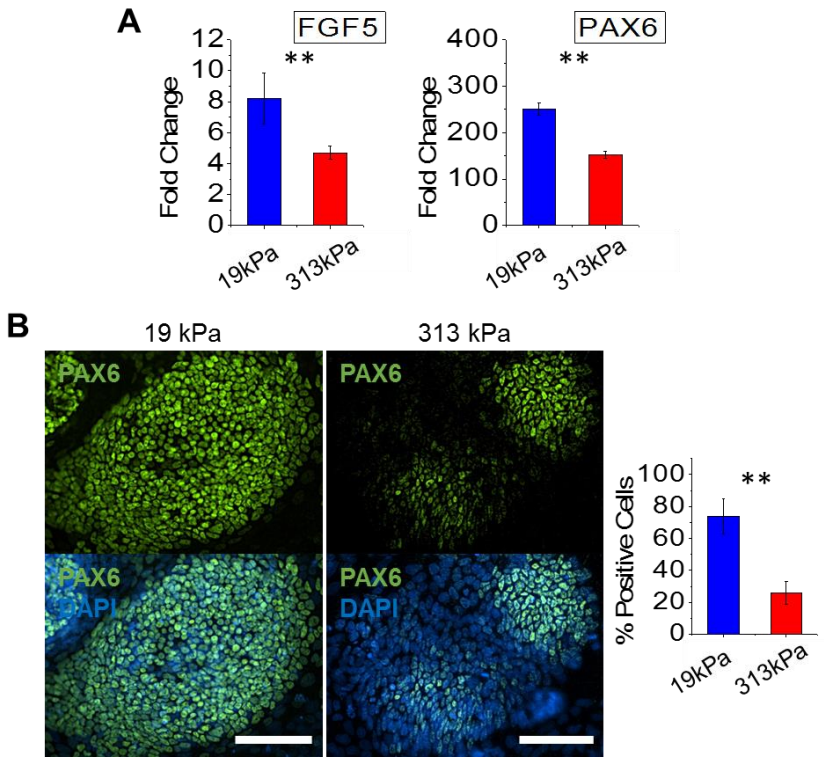

FIGURE 6.2. ECTODERMAL DIFFERENTIATION OF IPSCS IS SIGNIFICANTLY ENHANCED ON SOFT ELECTROSPUN SCAFFOLDS.

(A) Gene expression of ectodermal markers *FGF5* and *PAX6* is significantly upregulated on 19 kPa scaffolds as compared to 313 kPa scaffolds after ectodermal differentiation (Stage 1). Gene expression was normalized to IPSCs without induction of differentiation on TCPS (fold change = 1). (B) PAX6 protein expression is significantly higher on 19 kPa scaffolds after ectodermal induction and this observation is further confirmed by quantitative analysis of percent positive cells (green: PAX6, blue: DAPI, scale bar: 100 μm). ** denotes $p < 0.01$.

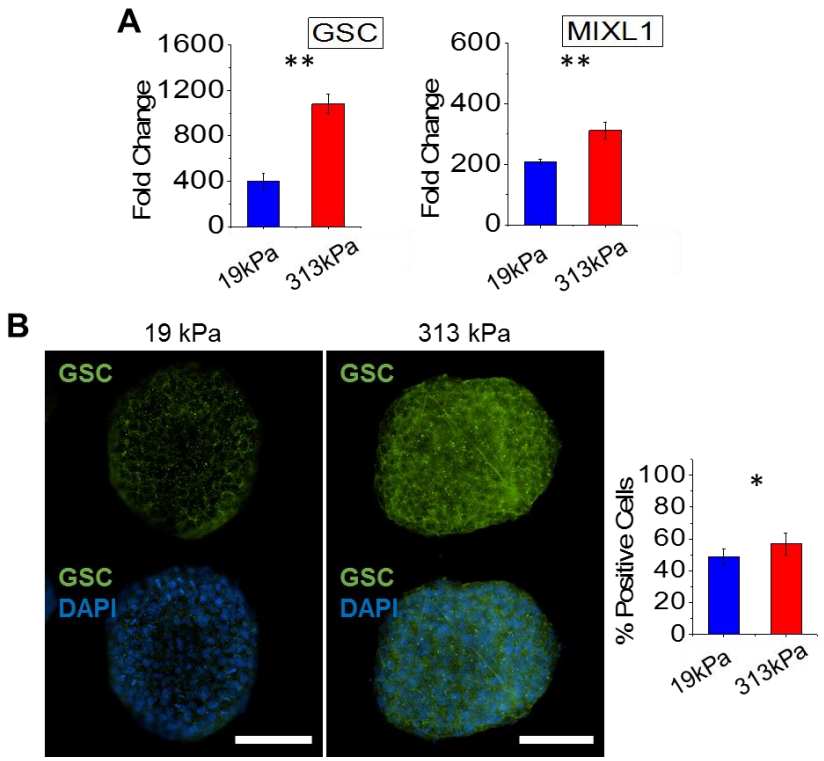

FIGURE 6.3. MESENDODERMAL DIFFERENTIATION OF IPSCS IS SIGNIFICANTLY ENHANCED ON STIFF ELECTROSPUN SCAFFOLDS.

(A) Gene expression of mesendodermal markers *GSC* and *MIXL1* is significantly upregulated on 313 kPa scaffolds as compared to 19 kPa scaffolds after mesendodermal differentiation (Stage 1). Gene expression was normalized to IPSCs without induction of differentiation on TCPS (fold change = 1). (B) GSC protein expression is significantly higher on 313 kPa scaffolds after mesendodermal induction and this observation is further confirmed by quantitative analysis of percent positive cells (green: GSC, blue: DAPI, scale bar: 100 µm). * and ** denote $p < 0.05$ and $p < 0.01$, respectively.

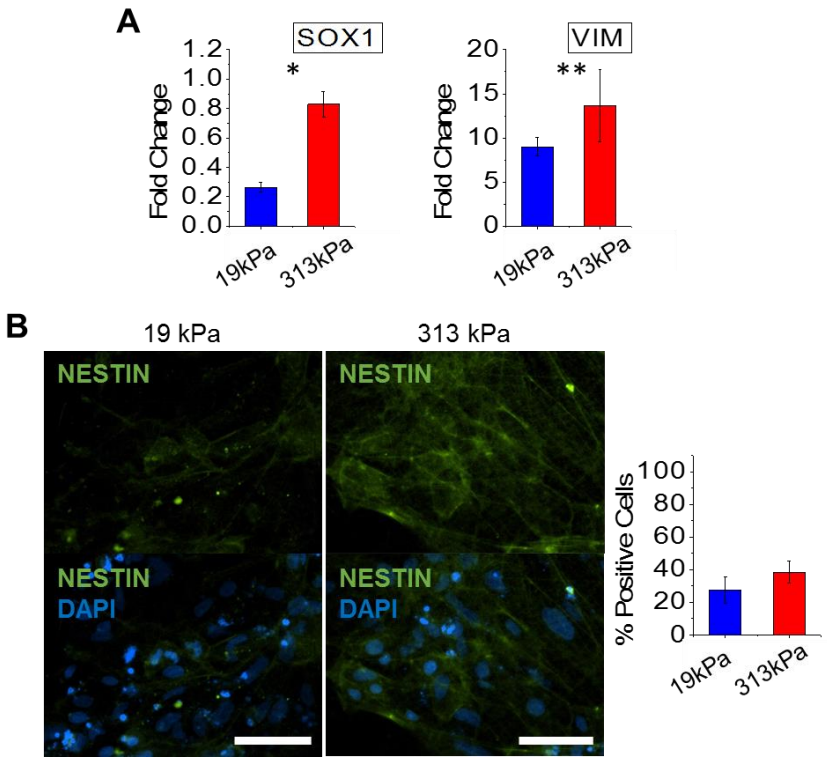

FIGURE 6.4. NEURAL PROGENITOR DIFFERENTIATION OF NEUROECTODERMAL CELLS IS ENHANCED ON STIFF ELECTROSPUN SCAFFOLDS.

IPSCs were differentiated to neuroectodermal cells on TCPS (Stage 1) prior to seeding onto electrospun scaffolds and differentiated to neural progenitors (Stage 2). (A) Gene expression of neural progenitor markers *SOX1* and *VIM* is significantly upregulated on 313 kPa scaffolds as compared to 19 kPa scaffolds after neural progenitor induction. Gene expression was normalized to neuroectodermal cells on TCPS from Stage 1 (fold change = 1). (B) NESTIN protein expression was higher on 313 kPa scaffolds after neural progenitor induction and this observation was confirmed by a slight increase in percent positive cells, although the difference was not considered statistically significant (green: NESTIN, blue: DAPI, scale bar: 100 µm). * and ** denote $p < 0.05$ and $p < 0.01$, respectively.

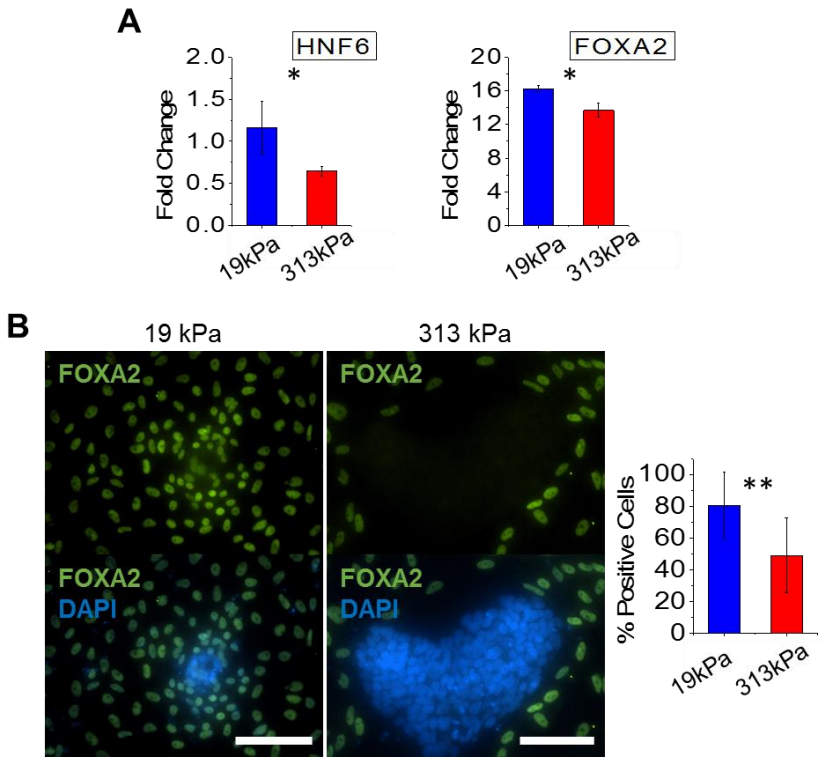

FIGURE 6.5. POSTERIOR FOREFUT DIFFERENTIATION OF MESENDODERMAL CELLS IS SIGNIFICANTLY ENHANCED ON SOFT ELECTROSPUN SCAFFOLDS.

IPSCs were differentiated to mesendodermal cells on TCPS (Stage 1) prior to seeding onto electrospun scaffolds and differentiated to posterior foregut cells (Stage 2). (A) Gene expression of posterior foregut markers *HNF6* and *FOXA2* is significantly upregulated on 19 kPa scaffolds as compared to 313 kPa scaffolds after posterior foregut induction. Gene expression was normalized to mesendodermal cells on TCPS from Stage 1 (fold change = 1). (B) FOXA2 protein expression was significantly higher for cells cultured on 19 kPa scaffolds after mesendodermal induction and this observation was further confirmed by quantitative analysis of percent positive cells (green: FOXA2, blue: DAPI, scale bar: 100 μm). * and ** denote $p < 0.05$ and $p < 0.01$, respectively.

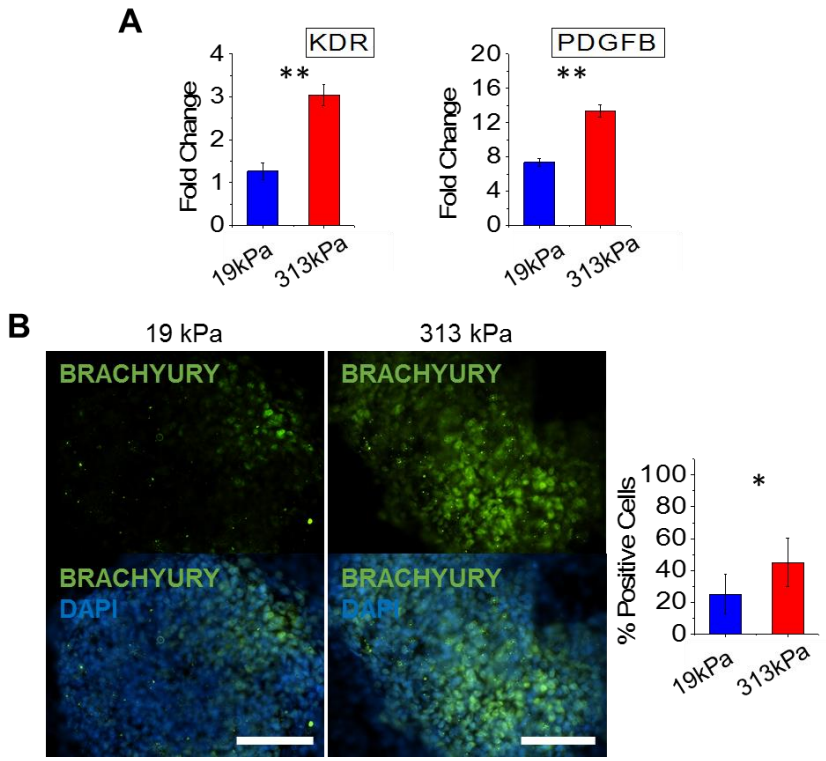

FIGURE 6.6. MESODERM DIFFERENTIATION OF MESENDODERMAL CELLS IS SIGNIFICANTLY ENHANCED ON STIFF ELECTROSPUN SCAFFOLDS.

IPSCs were differentiated to mesendodermal cells on TCPS (Stage 1) prior to seeding onto electrospun scaffolds and differentiated to mesodermal cells (Stage 2). (A) Gene expression of mesoderm markers *KDR* and *PDGFB* is significantly upregulated on 313 kPa scaffolds as compared to 19 kPa scaffolds after mesoderm induction. Gene expression was normalized to mesendodermal cells on TCPS from Stage 1 (fold change = 1). (B) BRACHYURY protein expression was significantly higher on 313 kPa scaffolds after mesodermal induction and this observation was further confirmed by quantitative analysis of percent positive cells (green: BRACHYURY, blue: DAPI, scale bar: 100 µm). * and ** denote $p < 0.05$ and $p < 0.01$, respectively.

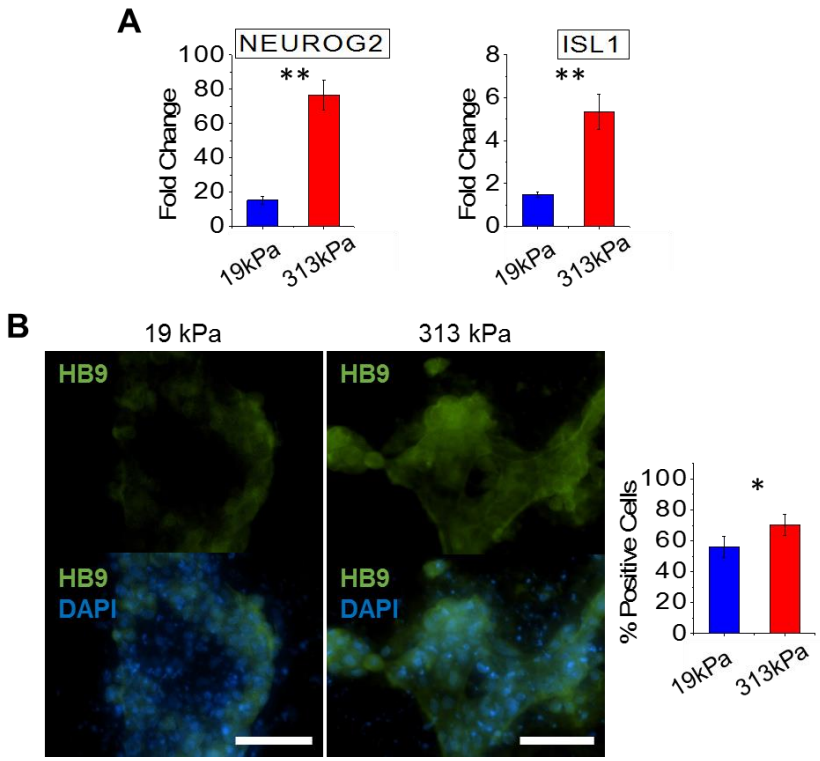

FIGURE 6.7. MOTOR NEURON DIFFERENTIATION OF NEURAL PROGENITOR CELLS IS ENHANCED ON STIFF ELECTROSPUN SCAFFOLDS.

IPSCs were differentiated to neural progenitors on TCPS (Stage 2) prior to seeding onto electrospun scaffolds and differentiated to motor neurons (Stage 3). (A) Gene expression of motor neuron markers *NEUROG2* and *ISL1* is significantly upregulated on 313 kPa scaffolds as compared to 19 kPa scaffolds after motor neuron induction. Gene expression was normalized to neural progenitor cells on TCPS from Stage 2 (fold change = 1). (B) HB9 protein expression was higher on 313 kPa scaffolds after motor neuron induction and this observation was confirmed by a slight but significant increase in percent positive cells (green: HB9, blue: DAPI, scale bar: 100 µm). * and ** denote $p < 0.05$ and $p < 0.01$, respectively.

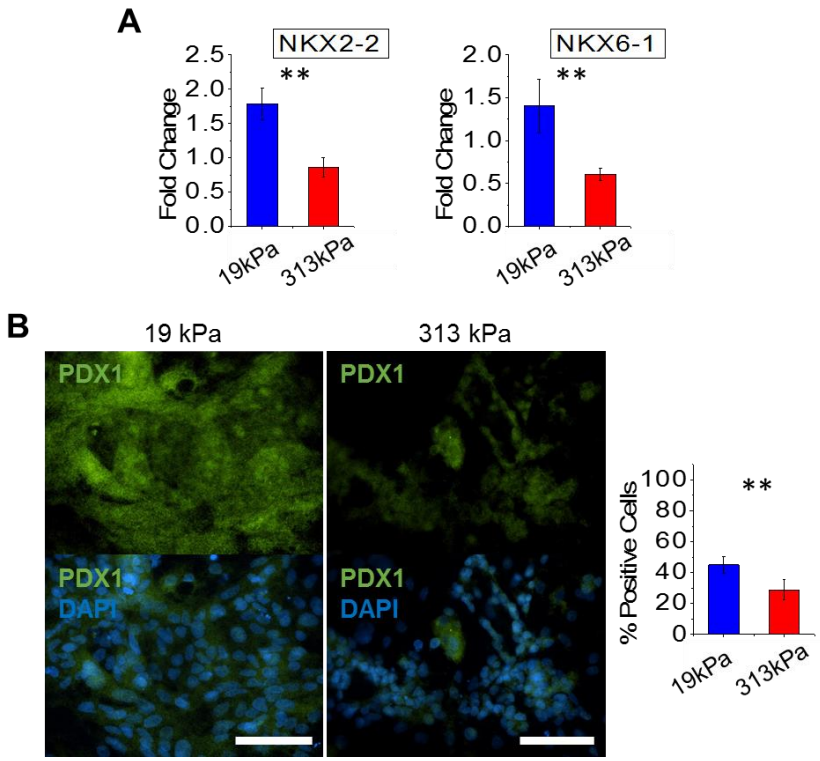

FIGURE 6.8. PANCREATIC ENDODERM DIFFERENTIATON OF POSTERIOR FOREGUT CELLS IS ENHANCED ON SOFT ELECTROSPUN SCAFFOLDS.

IPSCs were differentiated to posterior foregut cells on TCPS (Stage 2) prior to seeding onto electrospun scaffolds and differentiated to pancreatic endoderm cells (Stage 3). (A) Gene expression of pancreatic endoderm markers *NKX2-2* and *NKX6-1* is significantly upregulated on 19 kPa scaffolds as compared to 313 kPa scaffolds after pancreatic endoderm induction. Gene expression was normalized to posterior foregut cells on TCPS from Stage 2 (fold change = 1). (B) PDX1 protein expression was higher on 19 kPa scaffolds after pancreatic endoderm induction and this observation was confirmed by quantitative analysis of percent positive cells (green: PDX1, blue: DAPI, scale bar: 100 µm). ** denotes $p < 0.01$.

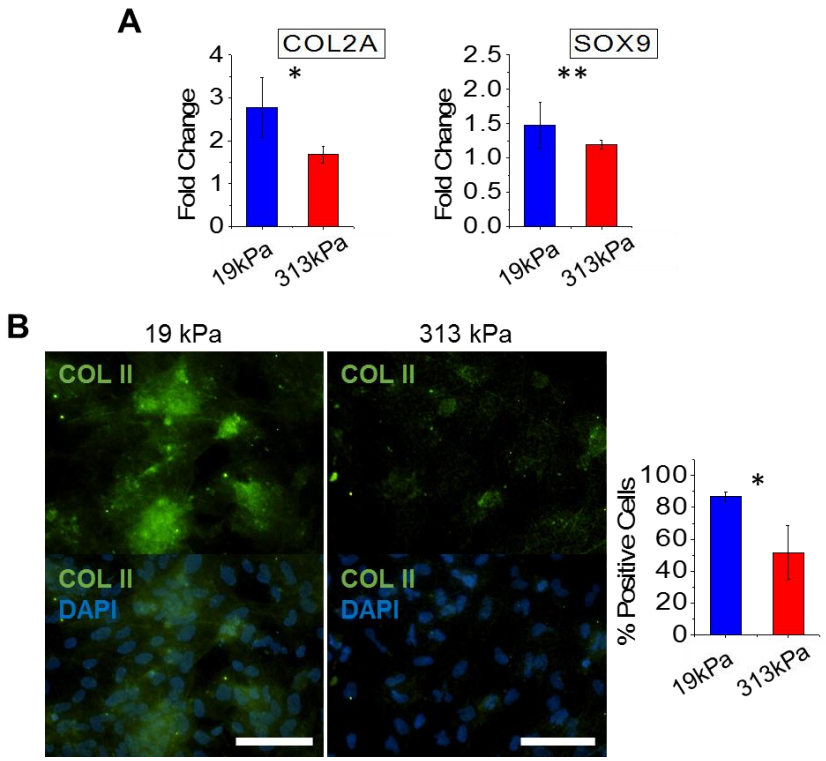

FIGURE 6.9. CHONDROCYTE DIFFERENTIATION OF MESODERMAL CELLS IS SIGNIFICANTLY ENHANCED ON SOFT ELECTROSPUN SCAFFOLDS.

IPSCs were differentiated to mesodermal cells on TCPS (Stage 2) prior to seeding onto electrospun scaffolds and differentiated to chondrocytes (Stage 3). (A) Gene expression of chondrocyte markers *COL2A* and *SOX9* is significantly upregulated on 19 kPa scaffolds as compared to 313 kPa scaffolds after chondrocyte induction. Gene expression was normalized to mesodermal cells on TCPS from Stage 2 (fold change = 1). (B) COLLAGEN II protein expression was significantly higher on 19 kPa scaffolds after chondrocyte induction and this observation was further confirmed by quantitative analysis of percent positive cells (green: COL II, blue: DAPI, scale bar: 100 µm). * and ** denote $p < 0.05$ and $p < 0.01$, respectively.

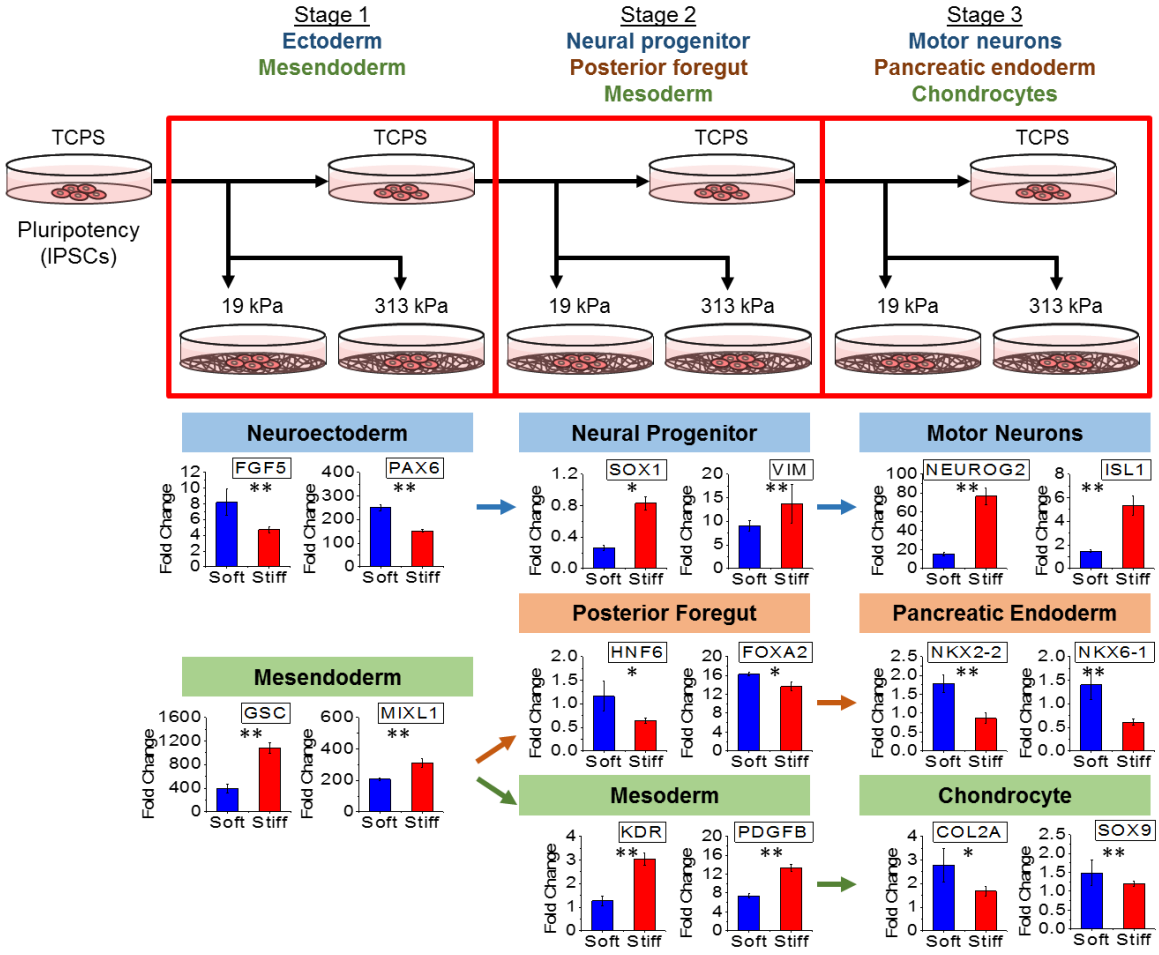

FIGURE 6.10. MODULATION OF ELECTROSPUN SCAFFOLD STIFFNESS ENHANCES LINEAGE-SPECIFIC AND STAGE-SPECIFIC DIFFERENTIATION AT EACH DEVELOPMENTAL STAGE.

IPSCs were differentiated to three germ layer downstream phenotypes following defined developmental protocols. Based on gene and protein expression of lineage-specific markers, an optimal scaffold stiffness can be used to significantly enhance the differentiation efficiency at each developmental stage. Early neuroectodermal differentiation is enhanced on soft scaffolds while downstream differentiation to neural progenitors and motor neurons can be significantly enhanced on stiff scaffolds. Mesendodermal and mesodermal differentiation is enhanced on stiff scaffolds while an intermediate posterior foregut (endodermal) differentiation is enhanced on soft scaffolds. In contrast the final stage to pancreatic endoderm or chondrocyte is enhanced on soft electrospun scaffolds.

CHAPTER 7 – CONCLUSIONS

7.1 – Summary

The work presented in this doctoral dissertation provides insight into the role of the mechanical microenvironment on IPSC behaviors (**Figure 7.1**). Soft electrospun scaffolds induce a three-dimensional IPSC colony morphology which enhances directed differentiation towards ectodermal lineage. In contrast, stiff scaffolds induce a two-dimensional IPSC colony morphology which enhances directed differentiation towards mesendodermal lineage. When the RhoA signaling cascade is modulated via the use of ROCK inhibitor during the pre-culture phase for the development of stiffness-dependent colony morphologies, the differentiation tendencies change towards a mesendodermal cell fate. Additionally, we explored the time-dependent effects of ROCK inhibitor, Y-27632, during proliferation of IPSCs and determined that a prolonged culture results in upregulation of epithelial-to-mesenchymal transition markers. The development of distinct IPSC colony morphologies, depending on scaffold stiffness, results in different structural pre-stresses on the cells and clustering of E-cadherin appears to mediate the differential stresses. Our results suggest that changes in E-cadherin clustering ultimately modulate the Wnt signaling pathway by delaying the release of β-catenin for nuclear translocation. As such, mesendodermal differentiation in 3D colonies is inhibited on soft electrospun scaffolds as compared to 2D colonies on stiff scaffolds. Furthermore, we

demonstrate that there is an optimal scaffold stiffness at each developmental stage to enhance the efficiency of differentiation.

7.2 – Future Directions

The groundbreaking research presented here offers a platform to study the three-dimensional behavior of IPSCs on a two-dimensional substrate. The fibrous nature of electrospun scaffolds better resembles the *in vivo* microenvironment that cells are exposed to. Therefore, the electrospun scaffolds, with distinct mechanical properties, can be used to study developmental processes *in vitro*. Additionally, the development of 3D colonies on soft scaffolds and the subsequent differentiation towards all three germ layers may serve as a model for gastrulation. This model can then be used to study drug development or toxicological studies on developmental processes. Alternatively, there are many researchers exploring the derivation of organoid models to study development [125]. Our soft electrospun scaffolds can also be used to explore the development of organoid models and patterning of cells. The results presented here also offer novel insight into the development of combinatorial protocols for enhancing the directed differentiation of IPSCs along developmental stages using both biochemical and biophysical cues (substrate stiffness). Development of these robust protocols may also help facilitate the therapeutic use of IPSCs for regenerative medicine or to study disease progression.

7.3 – Figures

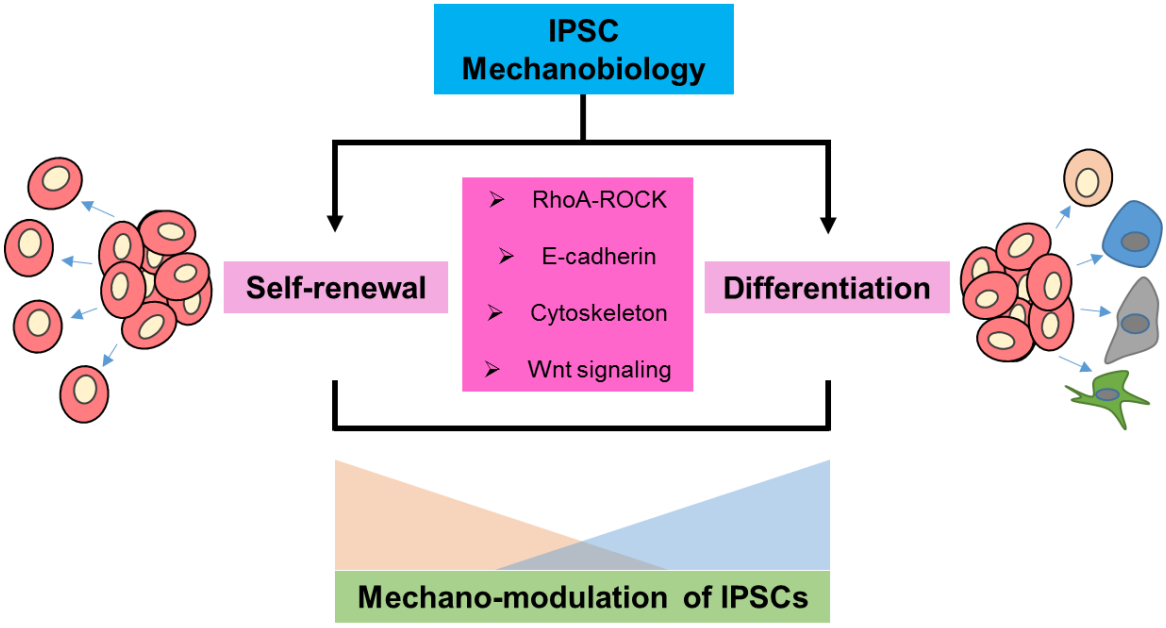

FIGURE 7.1. SUMMARY SCHEMATIC OF THE DISSERTATION STUDIES TO UNDERSTAND IPSC MECHANOBIOLOGY.

To understand IPSC mechanobiology, the work presented here examined the role of electrospun nanofibrous scaffolds on the self-renewal and directed differentiation of IPSCs. Scaffold stiffness modulated IPSC colony morphology/dimensionality which resulted in significant differences in self-renewal or directed differentiation. Such changes in cellular behavior were likely due to changes in RhoA signaling and cell-cell interaction through actin and E-cadherin organization. One potential mechanism by which the cells preferentially differentiate towards a specific lineage is the clustering of E-cadherin and its association with β-catenin to delay the translocation of β-catenin into the nucleus for activation of Wnt target genes. Ultimately, IPSC differentiation can be enhanced by modulating the mechanical microenvironment in a lineage and stage-specific manner.

CHAPTER 8 – REFERENCES

[1] Montero JA, Heisenberg CP. Gastrulation dynamics: cells move into focus. Trends in cell biology 2004;14:620-7.

[2] Biggers JD, McGinnis LK, Raffin M. Amino acids and preimplantation development of the mouse in protein-free potassium simplex optimized medium. Biology of reproduction 2000;63:281-93.

[3] Rauzi M, Krzic U, Saunders TE, Krajnc M, Ziherl P, Hufnagel L, et al. Embryo-scale tissue mechanics during Drosophila gastrulation movements. Nature communications 2015;6:8677.

[4] Krieg M, Arboleda-Estudillo Y, Puech PH, Kafer J, Graner F, Muller DJ, et al. Tensile forces govern germ-layer organization in zebrafish. Nature cell biology 2008;10:429-36.

[5] Beane WS, Gross JM, McClay DR. RhoA regulates initiation of invagination, but not convergent extension, during sea urchin gastrulation. Developmental biology 2006;292:213-25.

[6] Vazin T, Freed WJ. Human embryonic stem cells: derivation, culture, and differentiation: a review. Restorative neurology and neuroscience 2010;28:589-603.

[7] Thomson JA, Itskovitz-Eldor J, Shapiro SS, Waknitz MA, Swiergiel JJ, Marshall VS, et al. Embryonic stem cell lines derived from human blastocysts. Science 1998;282:1145-7.

[8] Turinetto V, Vitale E, Giachino C. Senescence in Human Mesenchymal Stem Cells: Functional Changes and Implications in Stem Cell-Based Therapy. International journal of molecular sciences 2016;17.

[9] Temenoff JS, Mikos AG. Review: tissue engineering for regeneration of articular cartilage. Biomaterials 2000;21:431-40.

[10] Lo B, Parham L. Ethical issues in stem cell research. Endocrine reviews 2009;30:204-13.

[11] Moutos FT, Freed LE, Guilak F. A biomimetic three-dimensional woven composite scaffold for functional tissue engineering of cartilage. Nat Mater 2007;6:162-7.

[12] Takahashi K, Tanabe K, Ohnuki M, Narita M, Ichisaka T, Tomoda K, et al. Induction of pluripotent stem cells from adult human fibroblasts by defined factors. Cell 2007;131:861-72.

[13] Bitton R. The economic burden of osteoarthritis. Am J Manag Care 2009;15:S230-5.

[14] Yelin E, Cisternas M, Foreman A, Pasta D, Murphy L, Helmick C. National and state medical expenditures and lost earnings attributable to arthritis and other rheumatic conditions—United States, 2003. MMWR Morbidity and mortality weekly report 2007;56:4.

[15] Birnbaum H, Pike C, Kaufman R, Marynchenko M, Kidolezi Y, Cifaldi M. Societal cost of rheumatoid arthritis patients in the US. Current medical research and opinion 2010;26:77-90.

[16] Chen KG, Mallon BS, McKay RD, Robey PG. Human pluripotent stem cell culture: considerations for maintenance, expansion, and therapeutics. Cell stem cell 2014;14:13-26.

[17] Jackson RW, Dieterichs C. The results of arthroscopic lavage and debridement of osteoarthritic knees based on the severity of degeneration: a 4- to 6-year symptomatic follow-up. Arthroscopy 2003;19:13-20.

[18] Shannon FJ, Devitt AT, Poynton AR, Fitzpatrick P, Walsh MG. Short-term benefit of arthroscopic washout in degenerative arthritis of the knee. Int Orthop 2001;25:242-5.

[19] Rossant J. Mouse and human blastocyst-derived stem cells: vive les differences. Development 2015;142:9-12.

[20] Niakan KK, Eggan K. Analysis of human embryos from zygote to blastocyst reveals distinct gene expression patterns relative to the mouse. Developmental biology 2013;375:54-64.

[21] Thiery JP, Acloque H, Huang RY, Nieto MA. Epithelial-mesenchymal transitions in development and disease. Cell 2009;139:871-90.

[22] Pauklin S, Vallier L. Activin/Nodal signalling in stem cells. Development 2015;142:607-19.

[23] Oliveira JM, Rodrigues MT, Silva SS, Malafaya PB, Gomes ME, Viegas CA, et al. Novel hydroxyapatite/chitosan bilayered scaffold for osteochondral tissue-engineering

applications: Scaffold design and its performance when seeded with goat bone marrow stromal cells. Biomaterials 2006;27:6123-37.

[24] Erisken C, Kalyon DM, Wang HJ, Ornek-Ballanco C, Xu JH. Osteochondral Tissue Formation Through Adipose-Derived Stromal Cell Differentiation on Biomimetic Polycaprolactone Nanofibrous Scaffolds with Graded Insulin and Beta-Glycerophosphate Concentrations. Tissue Engineering Part A 2011;17:1239-52.

[25] Wang L, Zhao L, Detamore MS. Human umbilical cord mesenchymal stromal cells in a sandwich approach for osteochondral tissue engineering. J Tissue Eng Regen Med 2011;5:712-21.

[26] Rodrigues MT, Lee SJ, Gomes ME, Reis RL, Atala A, Yoo JJ. Bilayered constructs aimed at osteochondral strategies: The influence of medium supplements in the osteogenic and chondrogenic differentiation of amniotic fluid-derived stem cells. Acta Biomaterialia 2012;8:2795-806.

[27] Wang J, Ye R, Wei Y, Wang H, Xu X, Zhang F, et al. The effects of electrospun TSF nanofiber diameter and alignment on neuronal differentiation of human embryonic stem cells. Journal of biomedical materials research Part A 2012;100:632-45.

[28] Mohtaram NK, Ko J, King C, Sun L, Muller N, Jun MB, et al. Electrospun biomaterial scaffolds with varied topographies for neuronal differentiation of human-induced pluripotent stem cells. Journal of biomedical materials research Part A 2015;103:2591-601.

[29] Hoveizi E, Ebrahimi-Barough S, Tavakol S, Nabiuni M. In vitro comparative survey of cell adhesion and proliferation of human induced pluripotent stem cells on surfaces of polymeric electrospun nanofibrous and solution-cast film scaffolds. Journal of biomedical materials research Part A 2015;103:2952-8.

[30] Martin I, Miot S, Barbero A, Jakob M, Wendt D. Osteochondral tissue engineering. Journal of biomechanics 2007;40:750-65.

[31] Prabhakaran MP, Mobarakeh LG, Kai D, Karbalaie K, Nasr-Esfahani MH, Ramakrishna S. Differentiation of embryonic stem cells to cardiomyocytes on electrospun nanofibrous substrates. Journal of biomedical materials research Part B, Applied biomaterials 2014;102:447-54.

[32] Malafaya P, Pedro A, Peterbauer A, Gabriel C, Redl H, Reis R. Chitosan particles agglomerated scaffolds for cartilage and osteochondral tissue engineering

approaches with adipose tissue derived stem cells. Journal of Materials Science: Materials in Medicine 2005;16:1077-85.

[33] Guo X, Park H, Liu G, Liu W, Cao Y, Tabata Y, et al. In vitro generation of an osteochondral construct using injectable hydrogel composites encapsulating rabbit marrow mesenchymal stem cells. Biomaterials 2009;30:2741-52.

[34] Augst A, Marolt D, Freed LE, Vepari C, Meinel L, Farley M, et al. Effects of chondrogenic and osteogenic regulatory factors on composite constructs grown using human mesenchymal stem cells, silk scaffolds and bioreactors. Journal of The Royal Society Interface 2008;5:929-39.

[35] Galois L, Freyria A, Grossin L, Hubert P, Mainard D, Herbage D, et al. Cartilage repair: surgical techniques and tissue engineering using polysaccharide- and collagen-based biomaterials. Biorheology 2004;41:433-43.

[36] Langer R. Selected advances in drug delivery and tissue engineering. Journal of controlled release : official journal of the Controlled Release Society 1999;62:7-11.

[37] Mano J, Silva G, Azevedo HS, Malafaya P, Sousa R, Silva S, et al. Natural origin biodegradable systems in tissue engineering and regenerative medicine: present status and some moving trends. Journal of The Royal Society Interface 2007;4:999-1030.

[38] Green MD, Chen A, Nostro MC, d'Souza SL, Schaniel C, Lemischka IR, et al. Generation of anterior foregut endoderm from human embryonic and induced pluripotent stem cells. Nature biotechnology 2011;29:267-72.

[39] Spence JR, Mayhew CN, Rankin SA, Kuhar MF, Vallance JE, Tolle K, et al. Directed differentiation of human pluripotent stem cells into intestinal tissue in vitro. Nature 2011;470:105-9.

[40] Kobayashi T, Yamaguchi T, Hamanaka S, Kato-Itoh M, Yamazaki Y, Ibata M, et al. Generation of rat pancreas in mouse by interspecific blastocyst injection of pluripotent stem cells. Cell 2010;142:787-99.

[41] Villa-Diaz LG, Ross AM, Lahann J, Krebsbach PH. Concise Review: The Evolution of human pluripotent stem cell culture: From feeder cells to synthetic coatings. STEM CELLS 2013;31:1-7.

[42] Stacey GN, Cobo F, Nieto A, Talavera P, Healy L, Concha A. The development of 'feeder' cells for the preparation of clinical grade hES cell lines: Challenges and solutions. J Biotechnol 2006;125:583-8.

[43] Heng BC, Liu H, Cao T. Feeder cell density - A key parameter in human embryonic stem cell culture. In Vitro Cell Dev-An 2004;40:255-7.

[44] Villa-Diaz LG, Nandivada H, Ding J, Nogueira-De-Souza NC, Krebsbach PH, O'Shea KS, et al. Synthetic polymer coatings for long-term growth of human embryonic stem cells. Nature biotechnology 2010;28:581-3.

[45] Brafman DA, Chang CW, Fernandez A, Willert K, Varghese S, Chien S. Long-term human pluripotent stem cell self-renewal on synthetic polymer surfaces. Biomaterials 2010;31:9135-44.

[46] Li YJ, Chung EH, Rodriguez RT, Firpo MT, Healy KE. Hydrogels as artificial matrices for human embryonic stem cell self-renewal. J Biomed Mater Res A 2006;79A:1-5.

[47] Li ZS, Leung M, Hopper R, Ellenbogen R, Zhang MQ. Feeder-free self-renewal of human embryonic stem cells in 3D porous natural polymer scaffolds. Biomaterials 2010;31:404-12.

[48] Engler AJ, Sen S, Sweeney HL, Discher DE. Matrix Elasticity Directs Stem Cell Lineage Specification. Cell 2006;126:677-89.

[49] Pek YS, Wan ACA, Ying JY. The effect of matrix stiffness on mesenchymal stem cell differentiation in a 3D thixotropic gel. Biomaterials 2010;31:385-91.

[50] Park JS, Chu JS, Tsou AD, Diop R, Tang ZY, Wang AJ, et al. The effect of matrix stiffness on the differentiation of mesenchymal stem cells in response to TGF-beta. Biomaterials 2011;32:3921-30.

[51] Chowdhury F, Li Y, Poh Y-C, Yokohama-Tamaki T, Wang N, Tanaka TS. Soft Substrates Promote Homogeneous Self-Renewal of Embryonic Stem Cells via Downregulating Cell-Matrix Tractions. PLoS ONE 2010;5:e15655.

[52] Guilak F, Cohen DM, Estes BT, Gimble JM, Liedtke W, Chen CS. Control of stem cell fate by physical interactions with the extracellular matrix. Cell stem cell 2009;5:17-26.

[53] McBeath R, Pirone DM, Nelson CM, Bhadriraju K, Chen CS. Cell shape, cytoskeletal tension, and RhoA regulate stem cell lineage commitment. Developmental cell 2004;6:483-95.

[54] Yim EKF, Darling EM, Kulangara K, Guilak F, Leong KW. Nanotopography-induced changes in focal adhesions, cytoskeletal organization, and mechanical properties of human mesenchymal stem cells. Biomaterials 2010;31:1299-306.

[55] Doshi J, Reneker DH. Electrospinning Process and Applications of Electrospun Fibers. Ias 93, Pts 1-3 1993:1698-703.

[56] Subbiah T, Bhat GS, Tock RW, Pararneswaran S, Ramkumar SS. Electrospinning of nanofibers. J Appl Polym Sci 2005;96:557-69.

[57] Li WJ, Tuli R, Okafor C, Derfoul A, Danielson KG, Hall DJ, et al. A three-dimensional nanofibrous scaffold for cartilage tissue engineering using human mesenchymal stem cells. Biomaterials 2005;26:599-609.

[58] McCullen SD, Stevens DR, Roberts WA, Clarke LI, Bernacki SH, Gorga RE, et al. Characterization of electrospun nanocomposite scaffolds and biocompatibility with adipose-derived human mesenchymal stem cells. Int J Nanomed 2007;2:253-63.

[59] Gustafsson Y, Haag J, Jungebluth P, Lundin V, Lim ML, Baiguera S, et al. Viability and proliferation of rat MSCs on adhesion protein-modified PET and PU scaffolds. Biomaterials 2012;33:8094-103.

[60] Zonca MR, Yune PS, Williams JK, Gu M, Unser AM, Imbrogno J, et al. Enhanced Stem Cell Pluripotency in Surface-Modified Electrospun Fibrous Matrices. Macromolecular bioscience 2014;14:215-24.

[61] Hashemi SM, Soudi S, Shabani I, Naderi M, Soleimani M. The promotion of stemness and pluripotency following feeder-free culture of embryonic stem cells on collagen-grafted 3-dimensional nanofibrous scaffold. Biomaterials 2011;32:7363-74.

[62] Chua KN, Chai C, Lee PC, Tang YN, Ramakrishna S, Leong KW, et al. Surface-aminated electrospun nanofibers enhance adhesion and expansion of human umbilical cord blood hematopoietic stem/progenitor cells. Biomaterials 2006;27:6043-51.

[63] Francis MP, Sachs PC, Madurantakam PA, Sell SA, Elmore LW, Bowlin GL, et al. Electrospinning adipose tissue-derived extracellular matrix for adipose stem cell culture. Journal of biomedical materials research Part A 2012;100:1716-24.

[64] Doshi J, Reneker DH. Electrospinning Process and Applications of Electrospun Fibers. J Electrostat 1995;35:151-60.

[65] Yarin AL, Koombhongse S, Reneker DH. Taylor cone and jetting from liquid droplets in electrospinning of nanofibers. J Appl Phys 2001;90:4836-46.

[66] Taylor G. Electrically Driven Jets. Proc R Soc Lon Ser-A 1969;313:453-&.

[67] Nam J, Perera P, Rath B, Agarwal S. Dynamic regulation of bone morphogenetic proteins in engineered osteochondral constructs by biomechanical stimulation. Tissue engineering Part A 2013;19:783-92.

[68] Zhu Y, Chan-Park MB. Density quantification of collagen grafted on biodegradable polyester: Its application to esophageal smooth muscle cell. Analytical Biochemistry 2007;363:119-27.

[69] Babaeijandaghi F, Shabani I, Seyedjafari E, Naraghi ZS, Vasei M, Haddadi-Asl V, et al. Accelerated Epidermal Regeneration and Improved Dermal Reconstruction Achieved by Polyethersulfone Nanofibers. Tissue Eng Pt A 2010;16:3527-36.

[70] Darling EM. Force scanning: a rapid, high-resolution approach for spatial mechanical property mapping. Nanotechnology 2011;22:175707.

[71] Torrez LB, Perez Y, Yang J, Nieden NI, Klassen H, Liew CG. Derivation of Neural Progenitors and Retinal Pigment Epithelium from Common Marmoset and Human Pluripotent Stem Cells. Stem Cells Int 2012.

[72] Green JJ, Zhou BY, Mitalipova MM, Beard C, Langer R, Jaenisch R, et al. Nanoparticles for Gene Transfer to Human Embryonic Stem Cell Colonies. Nano Lett 2008;8:3126-30.

[73] Nam J, Huang Y, Agarwal S, Lannutti J. Improved cellular infiltration in electrospun fiber via engineered porosity. Tissue engineering 2007;13:2249-57.

[74] Wadell H. Volume, shape, and roundness of rock particles. J Geol 1932;40:443-51.

[75] Livak KJ, Schmittgen TD. Analysis of relative gene expression data using real-time quantitative PCR and the 2(-Delta Delta C(T)) Method. Methods 2001;25:402-8.

[76] Shi YC, Kirwan P, Livesey FJ. Directed differentiation of human pluripotent stem cells to cerebral cortex neurons and neural networks. Nat Protoc 2012;7:1836-46.

[77] Oldershaw RA, Baxter MA, Lowe ET, Bates N, Grady LM, Soncin F, et al. Directed differentiation of human embryonic stem cells toward chondrocytes. Nat Biotechnol 2010;28:1221-U80.

[78] Martin MJ, Muotri A, Gage F, Varki A. Human embryonic stem cells express an immunogenic nonhuman sialic acid. Nature medicine 2005;11:228-32.

[79] Jung Y, Bauer G, Nolta JA. Concise review: Induced pluripotent stem cell-derived mesenchymal stem cells: progress toward safe clinical products. STEM CELLS 2012;30:42-7.

[80] Chang JC, Fujita S, Tonami H, Kato K, Iwata H, Hsu SH. Cell orientation and regulation of cell-cell communication in human mesenchymal stem cells on different patterns of electrospun fibers. Biomedical Materials 2013;8.

[81] Shih YRV, Chen CN, Tsai SW, Wang YJ, Lee OK. Growth of mesenchymal stem cells on electrospun type I collagen nanofibers. STEM CELLS 2006;24:2391-7.

[82] Mota A, Lotfi AS, Barzin J, Hatam M, Adibi B, Khalaj Z, et al. Human Bone Marrow Mesenchymal Stem Cell Behaviors on PCL/Gelatin Nanofibrous Scaffolds Modified with A Collagen IV-Derived RGD-Containing Peptide. Cell J 2014;16:1-10.

[83] Nam J, Johnson J, Lannutti JJ, Agarwal S. Modulation of embryonic mesenchymal progenitor cell differentiation via control over pure mechanical modulus in electrospun nanofibers. Acta Biomaterialia 2011;7:1516-24.

[84] Jahani H, Kaviani S, Hassanpour-Ezatti M, Soleimani M, Kaviani Z, Zonoubi Z. The Effect of Aligned and Random Electrospun Fibrous Scaffolds on Rat Mesenchymal Stem Cell Proliferation. Cell J 2012;14:31-8.

[85] Xie JW, Willerth SM, Li XR, Macewan MR, Rader A, Sakiyama-Elbert SE, et al. The differentiation of embryonic stem cells seeded on electrospun nanofibers into neural lineages. Biomaterials 2009;30:354-62.

[86] Carlberg B, Axell MZ, Nannmark U, Liu J, Kuhn HG. Electrospun polyurethane scaffolds for proliferation and neuronal differentiation of human embryonic stem cells. Biomed Mater 2009;4:045004.

[87] Meade KA, White KJ, Pickford CE, Holley RJ, Marson A, Tillotson D, et al. Immobilization of Heparan Sulfate on Electrospun Meshes to Support Embryonic Stem Cell Culture and Differentiation. J Biol Chem 2013;288:5530-8.

[88] Prabhakaran MP, Mobarakeh LG, Kai D, Karbalaie K, Nasr-Esfahani MH, Ramakrishna S. Differentiation of embryonic stem cells to cardiomyocytes on electrospun nanofibrous substrates. J Biomed Mater Res B 2014;102:447-54.

[89] Huebsch N, Arany PR, Mao AS, Shvartsman D, Ali OA, Bencherif SA, et al. Harnessing traction-mediated manipulation of the cell/matrix interface to control stem-cell fate. Nature materials 2010;9:518-26.

[90] Yang K, Jung K, Ko E, Kim J, Park KI, Cho SW. Nanotopographical Manipulation of Focal Adhesion Formation for Enhanced Differentiation of Human Neural Stem Cells. ACS applied materials & interfaces 2013.

[91] Muller P, Langenbach A, Kaminski A, Rychly J. Modulating the actin cytoskeleton affects mechanically induced signal transduction and differentiation in mesenchymal stem cells. PLoS ONE 2013;8:e71283.

[92] Keung AJ, Asuri P, Kumar S, Schaffer DV. Soft microenvironments promote the early neurogenic differentiation but not self-renewal of human pluripotent stem cells. Integrative biology : quantitative biosciences from nano to macro 2012;4:1049-58.

[93] Poh YC, Chen J, Hong Y, Yi H, Zhang S, Wu DC, et al. Generation of organized germ layers from a single mouse embryonic stem cell. Nature communications 2014;5:4000.

[94] Hay DC, Fletcher J, Payne C, Terrace JD, Gallagher RC, Snoeys J, et al. Highly efficient differentiation of hESCs to functional hepatic endoderm requires ActivinA and Wnt3a signaling. Proceedings of the National Academy of Sciences of the United States of America 2008;105:12301-6.

[95] Kim PT, Hoffman BG, Plesner A, Helgason CD, Verchere CB, Chung SW, et al. Differentiation of mouse embryonic stem cells into endoderm without embryoid body formation. PloS one 2010;5:e14146.

[96] Wiles MV, Johansson BM. Embryonic stem cell development in a chemically defined medium. Experimental cell research 1999;247:241-8.

[97] Zavazava N. Progress toward establishing embryonic stem or induced pluripotent stem cell-based clinical translation. Current opinion in organ transplantation 2014;19:598-602.

[98] Bratt-Leal AM, Carpenedo RL, McDevitt TC. Engineering the embryoid body microenvironment to direct embryonic stem cell differentiation. Biotechnology progress 2009;25:43-51.

[99] Carpenedo RL, Sargent CY, McDevitt TC. Rotary suspension culture enhances the efficiency, yield, and homogeneity of embryoid body differentiation. Stem Cells 2007;25:2224-34.

[100] Rungarunlert S, Techakumphu M, Pirity MK, Dinnyes A. Embryoid body formation from embryonic and induced pluripotent stem cells: Benefits of bioreactors. World journal of stem cells 2009;1:11-21.

[101] Moeller HC, Mian MK, Shrivastava S, Chung BG, Khademhosseini A. A microwell array system for stem cell culture. Biomaterials 2008;29:752-63.

[102] Gerecht S, Burdick JA, Ferreira LS, Townsend SA, Langer R, Vunjak-Novakovic G. Hyaluronic acid hydrogel for controlled self-renewal and differentiation of human embryonic stem cells. Proceedings of the National Academy of Sciences of the United States of America 2007;104:11298-303.

[103] Dalton PD, Klinkhammer K, Salber J, Klee D, Moller M. Direct in vitro electrospinning with polymer melts. Biomacromolecules 2006;7:686-90.

[104] Jayasinghe SN. Cell electrospinning: a novel tool for functionalising fibres, scaffolds and membranes with living cells and other advanced materials for regenerative biology and medicine. The Analyst 2013;138:2215-23.

[105] Nisbet DR, Forsythe JS, Shen W, Finkelstein DI, Horne MK. Review paper: a review of the cellular response on electrospun nanofibers for tissue engineering. Journal of biomaterials applications 2009;24:7-29.

[106] Maldonado M, Wong LY, Echeverria C, Ico G, Low K, Fujimoto T, et al. The effects of electrospun substrate-mediated cell colony morphology on the self-renewal of human induced pluripotent stem cells. Biomaterials 2015;50:10-9.

[107] Zhu Y, Chan-Park MB. Density quantification of collagen grafted on biodegradable polyester: its application to esophageal smooth muscle cell. Analytical biochemistry 2007;363:119-27.

[108] Yeung T, Georges PC, Flanagan LA, Marg B, Ortiz M, Funaki M, et al. Effects of substrate stiffness on cell morphology, cytoskeletal structure, and adhesion. Cell motility and the cytoskeleton 2005;60:24-34.

[109] Oldershaw RA, Baxter MA, Lowe ET, Bates N, Grady LM, Soncin F, et al. Directed differentiation of human embryonic stem cells toward chondrocytes. Nature biotechnology 2010;28:1187-94.

[110] Engler AJ, Sen S, Sweeney HL, Discher DE. Matrix elasticity directs stem cell lineage specification. Cell 2006;126:677-89.

[111] Robinton DA, Daley GQ. The promise of induced pluripotent stem cells in research and therapy. Nature 2012;481:295-305.

[112] Lutolf MP, Gilbert PM, Blau HM. Designing materials to direct stem-cell fate. Nature 2009;462:433-41.

[113] Zanatta G, Steffens D, Braghirolli DI, Fernandes RA, Netto CA, Pranke P. Viability of mesenchymal stem cells during electrospinning. Brazilian journal of medical and biological research = Revista brasileira de pesquisas medicas e biologicas / Sociedade Brasileira de Biofisica [et al] 2012;45:125-30.

[114] Levenberg S, Huang NF, Lavik E, Rogers AB, Itskovitz-Eldor J, Langer R. Differentiation of human embryonic stem cells on three-dimensional polymer scaffolds. Proceedings of the National Academy of Sciences of the United States of America 2003;100:12741-6.

[115] Nam J, Johnson J, Lannutti JJ, Agarwal S. Modulation of embryonic mesenchymal progenitor cell differentiation via control over pure mechanical modulus in electrospun nanofibers. Acta biomaterialia 2011;7:1516-24.

[116] Lee LH, Peerani R, Ungrin M, Joshi C, Kumacheva E, Zandstra P. Micropatterning of human embryonic stem cells dissects the mesoderm and endoderm lineages. Stem cell research 2009;2:155-62.

[117] Warmflash A, Sorre B, Etoc F, Siggia ED, Brivanlou AH. A method to recapitulate early embryonic spatial patterning in human embryonic stem cells. Nature methods 2014;11:847-54.

[118] Valamehr B, Jonas SJ, Polleux J, Qiao R, Guo S, Gschweng EH, et al. Hydrophobic surfaces for enhanced differentiation of embryonic stem cell-derived embryoid bodies. Proceedings of the National Academy of Sciences of the United States of America 2008;105:14459-64.

[119] Romito A, Cobellis G. Pluripotent Stem Cells: Current Understanding and Future Directions. Stem cells international 2016;2016:9451492.

[120] Zomer HD, Vidane AS, Goncalves NN, Ambrosio CE. Mesenchymal and induced pluripotent stem cells: general insights and clinical perspectives. Stem cells and cloning : advances and applications 2015;8:125-34.

[121] Maldonado M, Ico G, Low K, Luu RJ, Nam J. Enhanced Lineage-Specific Differentiation Efficiency of Human Induced Pluripotent Stem Cells by Engineering Colony Dimensionality Using Electrospun Scaffolds. Adv Healthc Mater 2016.

[122] Emre N, Vidal JG, Elia J, O'Connor ED, Paramban RI, Hefferan MP, et al. The ROCK inhibitor Y-27632 improves recovery of human embryonic stem cells after fluorescence-activated cell sorting with multiple cell surface markers. PloS one 2010;5:e12148.

[123] Watanabe K, Ueno M, Kamiya D, Nishiyama A, Matsumura M, Wataya T, et al. A ROCK inhibitor permits survival of dissociated human embryonic stem cells. Nature biotechnology 2007;25:681-6.

[124] Richter A, Valdimarsdottir L, Hrafnkelsdottir HE, Runarsson JF, Omarsdottir AR, Ward-van Oostwaard D, et al. BMP4 promotes EMT and mesodermal commitment in human embryonic stem cells via SLUG and MSX2. Stem Cells 2014;32:636-48.

[125] Ader M, Tanaka EM. Modeling human development in 3D culture. Current opinion in cell biology 2014;31:23-8.

[126] Aoi T. 10th anniversary of iPS cells: the challenges that lie ahead. Journal of biochemistry 2016.

[127] Discher DE, Mooney DJ, Zandstra PW. Growth factors, matrices, and forces combine and control stem cells. Science 2009;324:1673-7.

[128] Grover WH, Bryan AK, Diez-Silva M, Suresh S, Higgins JM, Manalis SR. Measuring single-cell density. Proceedings of the National Academy of Sciences of the United States of America 2011;108:10992-6.

[129] Hammerick KE, Huang Z, Sun N, Lam MT, Prinz FB, Wu JC, et al. Elastic properties of induced pluripotent stem cells. Tissue engineering Part A 2011;17:495-502.

[130] Davidson KC, Adams AM, Goodson JM, McDonald CE, Potter JC, Berndt JD, et al. Wnt/beta-catenin signaling promotes differentiation, not self-renewal, of human embryonic stem cells and is repressed by Oct4. Proceedings of the National Academy of Sciences of the United States of America 2012;109:4485-90.

[131] Borghi N, Sorokina M, Shcherbakova OG, Weis WI, Pruitt BL, Nelson WJ, et al. E-cadherin is under constitutive actomyosin-generated tension that is increased at

cell-cell contacts upon externally applied stretch. Proceedings of the National Academy of Sciences of the United States of America 2012;109:12568-73.

[132] Leerberg JM, Gomez GA, Verma S, Moussa EJ, Wu SK, Priya R, et al. Tension-sensitive actin assembly supports contractility at the epithelial zonula adherens. Current biology : CB 2014;24:1689-99.

[133] Wu SK, Gomez GA, Michael M, Verma S, Cox HL, Lefevre JG, et al. Cortical F-actin stabilization generates apical-lateral patterns of junctional contractility that integrate cells into epithelia. Nature cell biology 2014;16:167-78.

[134] Li D, Zhou J, Wang L, Shin ME, Su P, Lei X, et al. Integrated biochemical and mechanical signals regulate multifaceted human embryonic stem cell functions. The Journal of cell biology 2010;191:631-44.

[135] Discher DE, Janmey P, Wang YL. Tissue cells feel and respond to the stiffness of their substrate. Science 2005;310:1139-43.

[136] Zemel A, Rehfeldt F, Brown AE, Discher DE, Safran SA. Optimal matrix rigidity for stress fiber polarization in stem cells. Nature physics 2010;6:468-73.

[137] Ohgushi M, Matsumura M, Eiraku M, Murakami K, Aramaki T, Nishiyama A, et al. Molecular pathway and cell state responsible for dissociation-induced apoptosis in human pluripotent stem cells. Cell stem cell 2010;7:225-39.

[138] Smith AL, Dohn MR, Brown MV, Reynolds AB. Association of Rho-associated protein kinase 1 with E-cadherin complexes is mediated by p120-catenin. Molecular biology of the cell 2012;23:99-110.

[139] Choi YS, Gumbiner B. Expression of cell adhesion molecule E-cadherin in Xenopus embryos begins at gastrulation and predominates in the ectoderm. The Journal of cell biology 1989;108:2449-58.

[140] Soncin F, Ward CM. The function of e-cadherin in stem cell pluripotency and self-renewal. Genes 2011;2:229-59.

[141] Orsulic S, Huber O, Aberle H, Arnold S, Kemler R. E-cadherin binding prevents beta-catenin nuclear localization and beta-catenin/LEF-1-mediated transactivation. Journal of cell science 1999;112 (Pt 8):1237-45.

[142] Chen JW, Xie ZR, Wu YH. Computational Modeling of the Interplay between Cadherin-Mediated Cell Adhesion and Wnt Signaling Pathway. PloS one 2014;9.

[143] Maher MT, Flozak AS, Stocker AM, Chenn A, Gottardi CJ. Activity of the beta-catenin phosphodestruction complex at cell-cell contacts is enhanced by cadherin-based adhesion. The Journal of cell biology 2009;186:219-28.

[144] Cajanek L, Ribeiro D, Liste I, Parish CL, Bryja V, Arenas E. Wnt/beta-catenin signaling blockade promotes neuronal induction and dopaminergic differentiation in embryonic stem cells. Stem Cells 2009;27:2917-27.

[145] Verani R, Cappuccio I, Spinsanti P, Gradini R, Caruso A, Magnotti MC, et al. Expression of the Wnt inhibitor Dickkopf-1 is required for the induction of neural markers in mouse embryonic stem cells differentiating in response to retinoic acid. Journal of neurochemistry 2007;100:242-50.

[146] Murry CE, Keller G. Differentiation of embryonic stem cells to clinically relevant populations: lessons from embryonic development. Cell 2008;132:661-80.

[147] Chambers SM, Fasano CA, Papapetrou EP, Tomishima M, Sadelain M, Studer L. Highly efficient neural conversion of human ES and iPS cells by dual inhibition of SMAD signaling. Nature biotechnology 2009;27:275-80.

[148] Kroon E, Martinson LA, Kadoya K, Bang AG, Kelly OG, Eliazer S, et al. Pancreatic endoderm derived from human embryonic stem cells generates glucose-responsive insulin-secreting cells in vivo. Nature biotechnology 2008;26:443-52.

[149] Narsinh KH, Plews J, Wu JC. Comparison of human induced pluripotent and embryonic stem cells: fraternal or identical twins? Molecular therapy : the journal of the American Society of Gene Therapy 2011;19:635-8.

[150] Dorrell C, Schug J, Canaday PS, Russ HA, Tarlow BD, Grompe MT, et al. Human islets contain four distinct subtypes of beta cells. Nature communications 2016;7:11756.